An Investigation into the Temporal and Spatial Mobility of Leachate Production in a Fly-ash Dam

by

Izak Lukas Marais

A dissertation submitted in accordance with the requirements for the degree

Magister Scientiae

At the

Institute for Groundwater Studies

Faculty of Natural and Agricultural Sciences

University of the Free State

Date

July 2013

Supervisor

Prof. G. Steyl

Acknowledgements

In the name of Jesus Christ, my Lord and Saviour. The Holy Spirit, may its light shine out from within me. All praise to God almighty, gracious Father without whom nothing is possible.

To my parents, for always supporting and encouraging me to realise my academic potential. To my wife, for her inspiration, insight, and comradery. To Prof. Gideon Steyl, for his support and friendship as a mentor.

Thank you.

Izak Lukas Marais

Keywords

Fly ash, ground water, hydraulic conductivity, leaching, matrix response, mobility, porous media, self potential tracer tests, tracer test, transport parameters.

Table of contents

I Izak Lukas Marais declare that the dissertation hereby submitted by me for the degree Magister Scientiae at the University of the Free State is my own independent work and has not previously been submitted by me at another university/faculty. I further more cede copyright of the dissertation in favour of the University of the Free State.

Signed:..... Date:.....

List of abbreviations

BA - Bottom ash

BS - Boiler slag

CCPs - Coal Combustion Products

CEC – Cation exchange capacity

EC - Electroconductivity

ERT - Electrical resistivity tomography

ET - Evapotranspiration

FA - Fly ash

FGD - Flue gas desulfurization residue or synthetic gypsum

ICP- OES - Inductively coupled plasma optical emission spectrometry

SEM - Scanning Electron Microscopy

SPT – Self potential tracer

XRD – X-ray diffraction

List of Figures

List of Tables

Chapter 1

Introduction and objectives of study

1.1 Introduction

Coal combustion products (CCPs) originate from the combustion of coal at power stations and petroleum refineries. Coal remains an abundant and widely dispersed source for energy generation and synthesis gas.[1,2] Fly ash, bottom ash, flue-gas desulphurisation residue (synthetic gypsum) and boiler slag are the predominant residues from these processes.[3] The current worldwide production of the fly ash is more than 700 million tons per annum.[4] This dissertation will mainly focus on fluid transport properties and chemical mobility of selected elements native to or introduced to fly ash from a coal fired station in the Mpumalanga province, South Africa.

Composition

Fly ash is the combustion remnants of mineral impurities in coal such as clay, feldspar, quartz, and shale associated with the coal at its deposition.[5] Impurities rise with the flue-gas and is collected by electrostatic precipitators or bag filters. The ash and trace element concentrations vary according to the type of coal burnt and consist predominantly of silicon dioxide (SiO_2), aluminium oxide (Al_2O_3), iron oxide (Fe_2O_3) and calcium oxide (CaO).The ash is separated into two classes (class C and F) according to the content of these complexes.[6] The composition and flow characteristics of the ash may also be influenced by the handling, treatment and method of disposal.[6] Class F ash is generated by combustion of anthracite and bituminous coal and has less than 20% CaO. Class C ash is generated by combustion of lignite or sub-bituminous coal and has more carbonates and sulphates.[6]

Morphology

Particle size of the ash ranges from 0.1-100 μm and are spherical, although hollow spheres (cenospheres), spheres within spheres and crystalline forms are also found and pose health hazards such as respiratory complications.[7,8] Metal coatings (typically, Se, As, Mo, Zn, Cr, Cd, Pb, Zn and Hg) condense on the surface of the amorphous glass ash particles in concentrations of up to two orders of magnitude higher than that of the parent coal.[8,9,10]

Disposal and Hydrology

At present, the disposal of fly ash is either by wet disposal or dry disposal in landfills or storage lagoons.[6,11] A co-disposal system (fly ash and brine) is used at the discard facility, which is the subject of this study. It involves several discharge points which are used interchangeably to deposit ash slurry and saline brine (ca. 8000 mg/L). During this process the ash interacts with brines.[12] Other constituents may also influence the character of the material, such as CaO which reacts with exposure to CO_2 in the air, forming $CaCO_3$ (limestone) or sulphides inherent to the ash to form gypsum precipitates.[13] Water contained in the ash material at deposition can leach constituents from the ash dump and transport these to the surrounding environment. Rainfall may also supplement the interstitial water and contribute to the leaching of elements. The water migrates through the dump and either daylight along the edge of the ash dump (seepage faces) and enter the surrounding environment as surface water, or migrate to the bottom and enter the soil underlying the dump from where it can recharge into the aquifers.[13]

Beneficial use

Fly ash is now recognised a valuable substance which presents certain desirable characteristics in applications of various construction, waste solidification and stabilisation processes.[4] South Africa has been using fly ash since the 1980's, first only a few thousand tons and lately approaching 2 million tons.[14] In South Africa fly ash has been extensively used as backfill in coal mines and for the treatment of acid mine drainage (AMD).[15] Coal fly ash has also been proven to improve the yield from agricultural land.[16] Fly ash can also be used as a pollution control agent, particularly for soil decontamination, sludge and effluent treatment and in hazardous waste stabilisation.[16]

1.2 The objectives of this dissertation

- Interpret the results obtained from chemical analysis of a fly ash leaching experiment, concerning the mobility of water-soluble major and trace elements native to the weathered ash.
- Obtain information on the flow patterns through ash by evaluating solute transport through the heterogeneous medium at a laboratory and field scale.
- Evaluate the matrix response to the introduction of salts namely saturated solutions of NaCl, KCl, LiCl, LiBr, KBr and NaBr to emulate long term chemical interactions.
- Develop a conceptual understanding of the flow through a fly ash dam and the geochemical characteristics associated with it.

1.3 Outline of subsequent chapters

Apart from chapter one which contains the introduction and aims to this study, this dissertation consists of 5 more chapters which are outlined below.

Chapter 2 – Literature review

This chapter provides insight on selected variables, by reviewing relevant literature. Coal minerals, physical, chemical and mineralogical properties of coal fly ash are investigated in order to characterise the ash from the industrial site. Hydraulic and transport properties of landfills and the self potential method are also discussed. This provides the basis for the methodology employed (Chapter 3) and the interpretation of the results obtained in this study (Chapter 4 and 5).

Chapter 3– Methodology

Experimental and analytical methods used in this study to evaluate the transport and chemical properties associated with the fly ash are presented in Chapter 3. These methods include: Powder X-ray diffraction (PXRD), scanning electron microscopy (SEM), ash permeameter leaching experiments evaluated by inductively coupled plasma mass spectrometry (ICP-MS), cation exchange capacity (CEC), time-lapse electrical resistivity tomography (TERT) and a general description of the electrical resistivity method.

Chapter 4 – Results and discussion

The results for the analysis of the fly ash samples to assess the mobility of elements native to and introduced into the system *via* tracers are considered. Results are also presented in terms of mineralogical, physical and chemical characterisation perspectives. Flow parameters of the fly ash are estimated on a laboratory and field scale as outlined in the methods described in Chapter 3.

Chapter 5 – Self potential tracers and matrix response

This chapter attempts to shed light on the effects of long term chemical interaction of the fly ash in the co-disposal system with constituents native to the ash and that of the natural environment. This is done by comparing the chemical response as well as electrical response along the flow path of the ash by introducing tracers of various chloride and bromide salts that occur in the produced leachate as discussed in Chapter 4 and in the environment (Na, K and Li).

Chapter 6 – Conclusion

Summarises and draws conclusions from the study in order to develop a conceptual understanding of the flow through a fly ash dam and the geochemical characteristics associated with it.

1.4 Conclusion

In the current chapter a general introduction to fly ash has been given, regarding its composition, morphology, beneficial use, disposal and hydrology.

The following chapter (Chapter 2) will review relevant pieces of literature with regards to the chemical and physical factors that play a role in the formation of the waste product fly ash. Coal and the minerals associated with it will be investigated as well as a review of studies using similar techniques to determine the characteristics of fly ash. Also discussed in this chapter are the hydraulic and transport properties of landfills or ash dams and the self potential method.

1.5 References

[1] Van Dyk, J.C., Keyser, M.J. and Van Zyl, J.W., 2001, *Suitability of feedstocks for the Sasol-lurgi fixed bed dry bottom gasification process.*, Gasification technologies.

[2] Sajwan, K.S., Punshon, T. and Seaman, J.C., 2006, *Production of coal combustion products and their potential uses.*,Coal combustion byproducts and environmental issues., Springer, 241.

[3]Kalyoncu, R., 1998, *Coal combustion products*, Mineral year book, USGS.

Available: http://minerals.usgs.gov/minerals/pubs/commodity/coal/.

[4]Lokeshappa, B., Dikshit, A.K., 2011. *Disposal and management of flyash*, in: Ipcbee. Presented at the international conference on life science and technology, IACSIT Press, Singapore.

[5]Özbayoğlu, G. and Özbayoğlu, M.E., 2006, *A new approach for the prediction of ash fusion temperatures: A case study using Turkish lignites,*. Fuel, 85, 545-552.

[6]U.S. Department of Transportation, F. H. A. 1998,*Turner-fairbank highway research centre.* Available: http://www.tfhrc.gov/hnr20/recycle/waste/cfa51.htm

[7]Peng, M., Ruan, X.G., Chen, X.M., Xu, J.W. and Jiang, Z.C., 2004, *Study on both shape and chemical composition at the surface of fly ash by scanning electron microscope, focused ion beam, and field emission-scanning electron microscope.*,Chinese journal of analytical chemistry,32 (9), 1196-1198.

[8] Fisher, G.L., Chang, D.P. and Brummer, M, 1976, *Fly ash collected from electrostatic precipitators: microcrystalline structures and the mystery of the spheres.*, Science. Vol 7, pp. 553-555

[9] Linton, R.W, Loh, A., Natusch, D.F.S., Evans, C.A. and Williams, P., 1976, *Surface predominance of trace elements in airborne particles.*, Science, Vol 191, pp 852-854.

[10]Theis, T.L., Wirth, J.L., 1977, *Sorptive behaviour of trace metals on fly ash in aqueous systems.*, Environmental Science and Technology, Vol 11, no 12, pp. 390-391.

[11]DiGioia, A. M., and Nuzzo, W.L., 1972, *Fly Ash as Structural Fill.*, Proceedings of the american society of civil engineers, Journal of the power division, New York, NY.

[12]Mahlaba, J.S., Kearsley, E.P., Kruger, R.A., 2011, *Physical, chemical and mineralogical characterisation of hydraulically disposed fine coal ash from SASOL Synfuels*, Fuel.

[13]Troskie, K., 2005. *Proposed power station and associated infrastructure Witbank geographical area hydrogeological investigation*. GCS Report reference NIN.05/469.

[14]Kruger, R.A., Krueger, J.E., 2005, *Historical development of coal ash utilisation in South Africa.*, World of coal ash (WOCA), Lexington, Kentucky, USA.

[15]Ward, C.R., French, D., Jankowski, J., Riley, K., Li, Z., 2006, *Use of coal ash in mine backfill and related applications.*, (Research report No. 62). Cooperative research centre for coal in sustainable development, University of New South Wales.

[16]Moolman, D., 2011. *Baseline study of Kendal power station.* (Magister Scientiae).

Chapter 2

Literature Review

2.1 Introduction

The study of fine fly ash as a waste product has given rise to two fundamental problems. Firstly, the chemical retention in the fine fly ash matrix and the subsequent release of retained salt load to the environment. Secondly, the rate of release of the salt to the environment is of critical importance.[1,2]

The following sections of this chapter will review relevant pieces of literature with regards to the chemical and physical factors that play a role in the formation of the waste product fly ash and its possible reaction to the environment. [3,4] Coal and the minerals associated with it will be investigated followed by the various techniques used to determine the characteristics of fly ash. These techniques include: X-ray diffraction, Scanning electron microscopy and Leaching experiments. Also discussed in this chapter are the hydraulic and transport properties of landfills or ash dams and the self potential method.

2.2 Coal

Coal is the starting material for a multitude of processes in power generation and synthetic fuel industries that results in generation of fly ash.[5,6] The chemical properties of fly ash are mainly a product of combusted pulverised coal and is dependent on the grade of coal used in the coal burner.[7] The properties can, however, also be influenced by the handling and storage of the fly ash.[8]

2.2.1 Coal types

Coal grade increases progressively through coalification from brown-coal (lignite) and sub-bituminous coal to bituminous coal and anthracite. The increase in the grade of coal is matched by the increase in the carbon content and calorific value of the coal.[9] The calorific value is the amount of energy released through the burning of one kilogram of coal. Figure 2.1 shows examples of lignite (top), bituminous coal (middle) and anthracite (bottom). Table 2.1 illustrates the classification of coal by calorific value and Figure 2.2 additionally indicates facies.[10,11]

Brown coal / lignite is described as a soft, low rank, earthy brown to black coal. It may contain massive sapropelic forms (generally dark coloured, tough and exhibiting conchoidal fracturing), but is more commonly composed of humic material (heterogeneous organic layers of varying appearance and diverse origin) with wood and plant remains in a finer-grained, organic groundmass.[10]

Sub-bituminous coal is described as a brown intermediate ranking coal, with a calorific value of $< 19.3\ MJ.kg^{-1}$ and a fixed carbon content of 46 – 60 %.[10,12]

Bituminous coal is an intermediate grade coal, containing a mixture of bonded and sapropelic coals and is generally rich in volatile hydrocarbons.[9] Principle chemical components of bituminous coal ash are silica, aluminium, iron and calcium oxide with varying amounts of carbon. Carbon can be measured by the loss of ignition (LOI), a measurement of the unburned carbon in the fly ash.[7]

Anthracite coal is a high ranking coal not commonly burned in utility boilers. This coal is high in carbon content and very low in volatile organic components.[10]

Figure 2.1 Top: Lignite, Middle: Bituminous coal and Bottom: Anthracite.[12]

2.2.2 Coal Mineralogy

Other than the major organic components, coal contains an assortment of inorganic minerals. These minerals may either have originated within the coal particles, or outside during its formation.[8,13] Fly ashes formed in the combustion of lignite and sub-bituminous coal are characterised by higher concentrations of calcium and magnesium oxide and reduced percentages of silica and iron oxide as well as lower carbon content.[7]

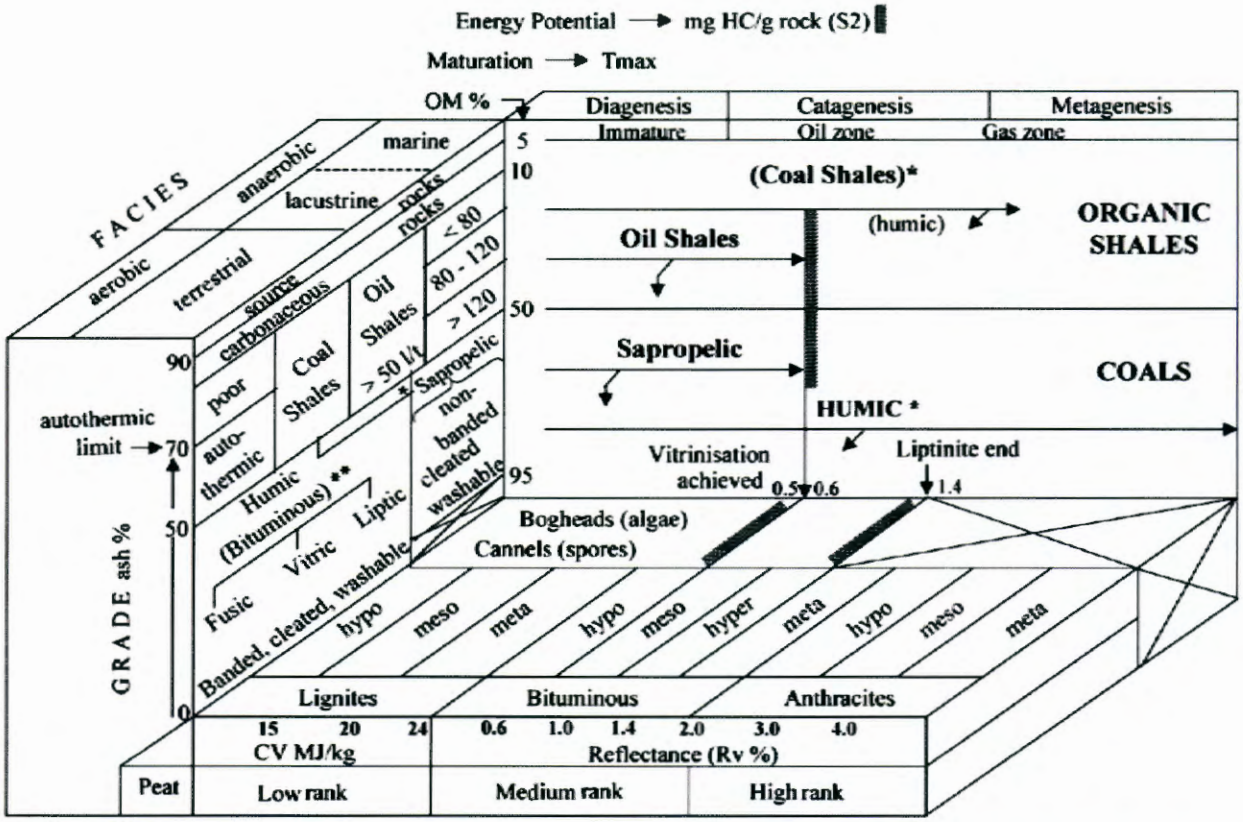

NB:* Coal Shales and Humic coals lines correspond in terms of coalification to the left part of the chart.
**** Petrographic composition, banding and cleating are mainly restricted to Bituminous coals.**

Figure 2.2 Coal classification proposed by *Alpern and de Sousa* for solid sedimentary fossil fuels.[11]

In Table 2.2 a comparison was made between bituminous, sub-bituminous and lignite coal fly ash,[7] which clearly shows that lignite and sub-bituminous coals contain much higher calcium oxide and lower loss on ignition (LOI) than the higher grade coal.

Table 2.1 Classification of coals by American Society for Testing and Materials.

Class	Group	Calorific Value Limits ($MJ.kg^{-1}$)
I. Anthracite	Meta-anthracite	——
	Anthracite	32.5 - 34.0
	Semi-anthracite	26.7 - 32.5
II. Bituminous	Low volatile bituminous	——
	Medium volatile bituminous	——
	High volatile A bituminous	>32.6
	High volatile B bituminous	30.2 - 32.6
	High volatile C bituminous	24.4 - 30.2
III. Subbituminous	Subbituminous A	24.4 - 26.7
	Subbituminous B	22.1 - 24.4
	Subbituminous C	19.3 - 22.1
IV. Lignitic	Lignite A	14.7 - 19.3
	Lignite B	14.7

Table 2.2 Normal range of chemical composition for fly ash produced from different coal types (expressed as percentage by weight).[7]

Component	Bituminous (%)	Sub-bituminous (%)	Lignite (%)
SiO_2	20 – 60	40 – 60	15 – 45
Al_2O_2	5 – 35	20 – 30	10 – 25
Fe_2O_2	10 – 40	4 – 10	4 – 15
CaO	1 – 12	5 – 30	15 – 40
MgO	0 – 5	1 – 6	3 – 10
SO_2	0 – 4	0 – 2	0 – 10
Na_2O	0 – 4	0 – 2	0 – 6
K_2O	0 – 3	0 – 4	0 – 4
LOI	0 – 15	0 – 3	0 – 5

Approximately 30 Mt of bituminous coal is used in South Africa every year as the main feedstock in fixed bed gasification process for the production of synthesis gas (CO and H_2).[6] Petrik *et al.* reported that the coal used in the study area is a low rank

bituminous coal, consisting of a mixture of banded and sapropelic coal generally rich in volatile hydrocarbons.[14] The physical and chemical properties of the coal used in these gasifiers vary to a large extent and is directly related to gasifier behaviour.[15]

The average mineral distribution in the discard matter (those with a relative density larger than 1.9) of the coal used by the fixed bed gasifier in the study area can be seen in Table 2.3. Roof and siltstone samples had high SiO_2 (quartz) and Al_2O_3 (kaolinite) content, whereas floor samples were found to be high in quartz, illite and microline. The carbonates (calcite) were found to have high SiO_2, Fe_2O_3 and CaO contents as well as high sulphur (pyrite) content (12 – 15 %).[16] In Table 2.4 the groups of minerals that have been associated with coal are reported.[17]

Table 2.3 The average mineral yields in the discard material (mass %).

Mineral type	Single coal source (%)	Coal blend (%)
Carbonates	6	6
C-Shale	19	18
Pyrite	15	10
Roof	10	25
Floor	25	21
Siltstone	25	20

Table 2.4 Mineral groups associated with coal.[17]

Group	Minerals
shale	muscovite, illite and montmorillonite (Na, K, Ca, Al, Mg and Fe silicates)
kaolin	kaolinite (Al silicate)
sulphide	pyrite and marcasite (Fe)
carbonate	Calcite, ankerite and sederite (Ca, Fe)
salt	gypsum, sylvite and halite (Na, Ca, K,)

Various coal and sediment samples from the Witbank and Highveld coalfields were analysed using XRD and XRF.[16] It was found that the coal containing higher levels of pyrite, had a higher likelihood of producing acidic conditions, compared to areas with abundant clay minerals and other aluminosilicates.[16] The carbonates found in coal may have a buffering effect; however, insufficient carbonates may be available for long-term neutralisation, especially in areas with high pyrite concentrations. It was also found that the coals from the Highveld had relatively more Na_2O (0.0 to 0.51 wt %) in comparison with the Witbank coals.[16]

Quartz and kaolinite were also the main inorganic minerals in the coals, with varying proportions of calcite, dolomite, pyrite, as well as accessory phosphate phases. Higher K_2O and Na_2O concentrations could be partially attributed to the presence of feldspars and clay minerals such as illite in the sandstones associated with siltstones and carbonaceous shales. The mineral matter distribution of that study can be seen in Table 2.5 and an example of the XRD spectrums for the coal samples are shown in Figure 2.3.[18]

Table 2.5 Mineral matter distribution in coals from the Witbank and Highveld coalfields.[16]

Mineral matter	SiO_2	Al_2O_3	Fe_2O_3	S	CaO	MgO	P_2O_5	K_2O	Na_2O
Mass %	0 – 35	0.5 - 16	0.03 – 10	0.15 - 8	0 – 8	0 - 1	0 - 3.5	0 - 1.3	0 - 0.45

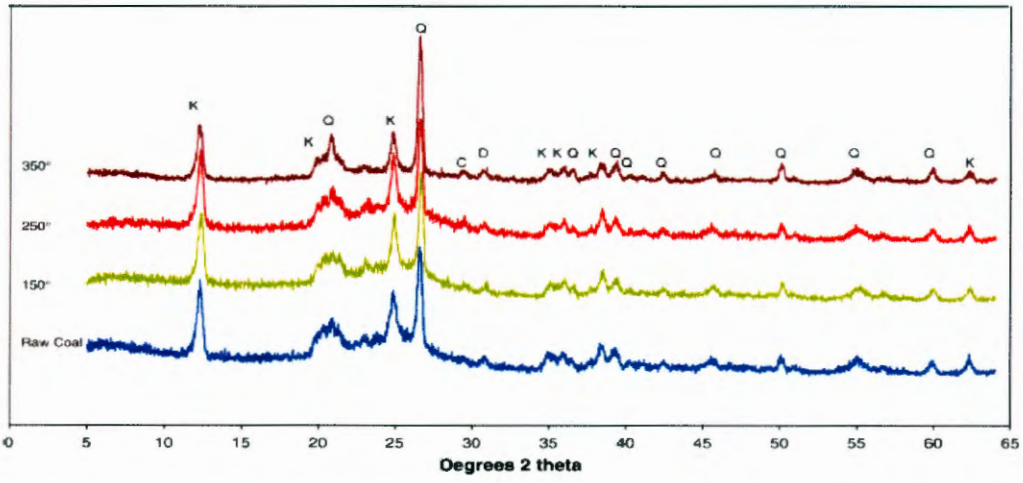

Figure 2.3 X-ray diffraction scans of coal heated to different temperatures. Q = quartz, K = kaolinite, C = calcite and D = dolomite.

2.3 Coal Combustion Products

The burning of pulverised coal in coal-fired boilers to generate heat or synthesis gas causes the production of by-products. The energy released from this process is converted from thermal energy into steam energy which can be used to generate electrical power through steam turbines.[6] In Figure 2.4 the coal combustion process and the associated capture and removal of fly ash from a system is illustrated.[19]

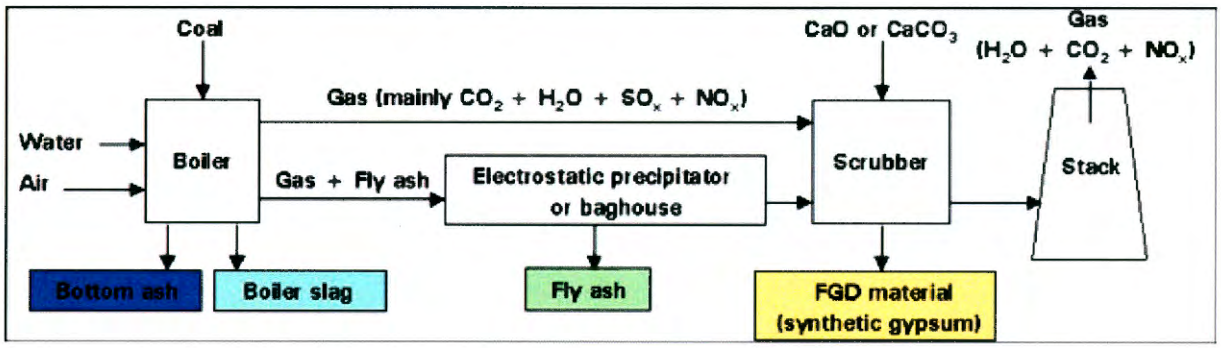

Figure 2.4 The coal combustion process and the associated capture and removal of fly ash from the system.

Approximately 39 % of coal used in South Africa is in the electricity, gas and steam production.[20] The type of by-product produced by a boiler, depends on the type of furnace used to burn the coal.[21] The general electric utility industry makes use of 3 types of boiler furnaces. These boilers differ in fly ash recovery principles and are listed below:

Dry-bottom boilers (most common type)

Dry-bottom boilers recover approximately 80 % of all ash produced or entrained within the flue gas.

Wet-bottom boilers or slag-tap furnaces

The furnaces can retain as much as 50 % of the ash within the boiler, while the remainder leaves the boiler entrained in the flue gas.[7]

Cyclone furnaces (a mechanical collection device)

The mechanical furnaces use crushed coal as fuel. The cyclone system retains 70 to 80 % of the ash within the boiler, as boiler slag, while only 20 – 30 % will leave in the form of dry ash within the flue gas.[7]

Coal Combustion Products (CCPs) mainly consist of: bottom ash; boiler slag; flue gas desulphurisation residue (synthetic gypsum) and fly ash.[22] The relative percentages of these components can be seen in Chart 2.1.[23] The beneficial recycling of these products is becoming a priority as the scale of disposal can no longer be considered feasible. The main environmental hazards associated with CCPs are the content of inherit potentially toxic trace metals and metalloids, from the burnt coal, which may easily be leached out.[24-27]

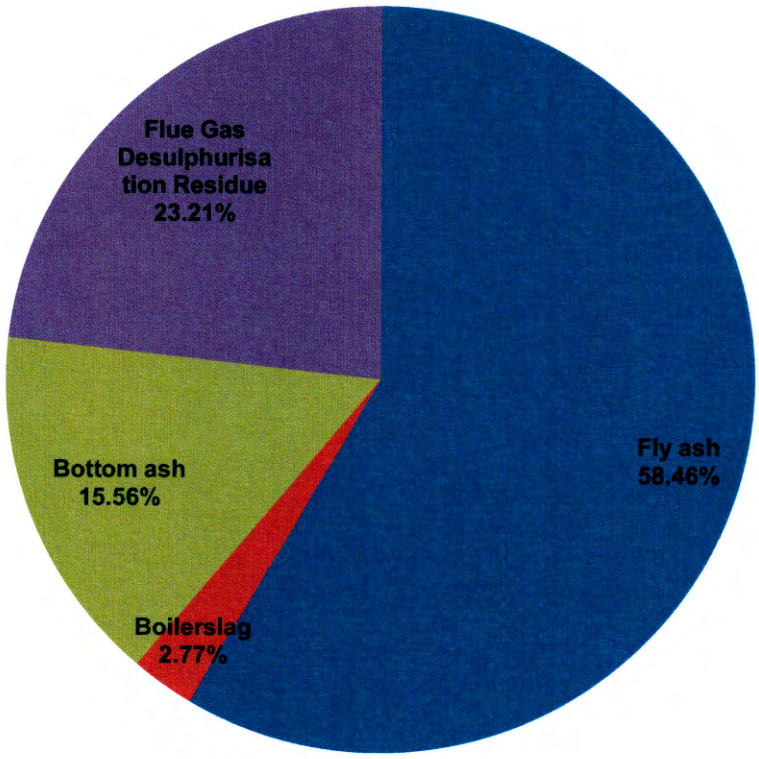

Chart 2.1 Relative average percentages of the various coal combustion products.[23]

2.3.1 Bottom ash and boiler slag

Bottom ash is the fraction of coal that was not burnt and settled to the bottom of the boiler. Bottom ash is granular and is similar to concrete sand.[28] The physical properties, such as grain-size distribution, staining potential and color influence the potential of bottom ash to be reused in construction and often varies.[29,30] The color of the ash is indicative of the amount of unburnt coal which influences durability under freezing and thawing conditions.[31] Boiler slag is also found in the bottom of the combustion chamber when the operating temperature exceeds that of ash fusion and the slag remains molten.[32] Boiler slag is a burnished black granular material that has abrasive properties. It is used as structural embankments, aggregates, grit for snow and ice control and as a road base material.[19] Examples of bottom ash (left) and boiler slag (right) can be seen in Figure 2.5.[6]

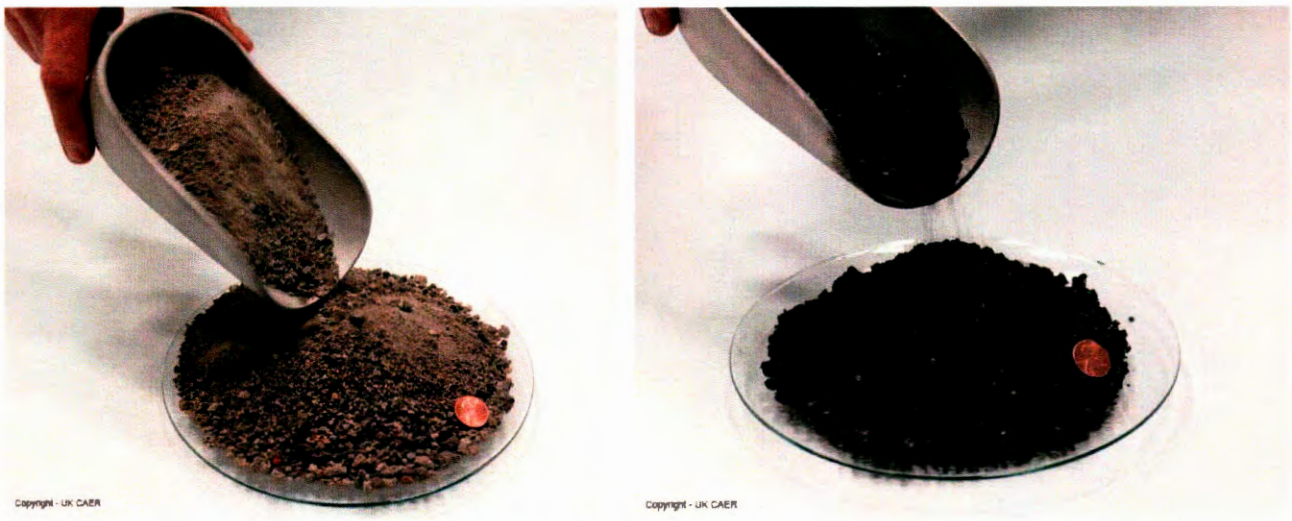

Figure 2.5 Left: Bottom ash and Right: Boiler slag.[6]

2.3.2 Flue gas desulphurisation residue - FGDR (synthetic gypsum)

Flue gas desulphurisation residue is the alkaline waste material produced when SO_x, is removed from power plant and refinery flue gases.[33,34] Legislations aimed at reducing atmospheric pollution and acid rain and subsequent reduction of SO_2 emissions has resulted in this new type of waste.[35] Several extraction technologies are currently in use, these are distinguished by the type of sorbent used (e.g. lime or dolomitic lime) and the method of extraction.[36] Flue gas desulphurisation residue typically consists of

calcium sulphite ($CaSO_3$), calcium sulphate ($CaSO_4$), unreacted sorbent, and fly ash particles. Sodium, magnesium or ammonium sulphites and sulphates may also be found.[22] The properties of the final waste product are determined by the parent coal composition, scrubber efficiency as well as handling and stabilisation procedures prior to deposition.[33] An example of Flue gas desulphurisation residue can be seen in Figure 2.6.[6]

Figure 2.6 Flue gas desulphurisation residue - FGDR (synthetic gypsum).[12]

2.3.3 Fly ash

2.3.3.1 Introduction

Fly ash is a fine-grained, powdery particulate and is carried off in the flue gas (smoke stacks, guiding the smoke/gas up and out of the boiler plants). These particles are collected from the flue gas by means of electrostatic precipitators, bag-houses or mechanical collection devices such as cyclones.[6] Examples of Class C and Class F fly ash can be seen in Figure 2.7.[6]

Figure 2.7 Left: Class C fly ash and Right: Class F fly ash.[12]

2.3.3.2 Processes during coal combustion

During the combustion of coal, the inorganic mineral matter may undergo various processes at temperatures exceeding 1600 °C, yielding an assortment of new phases including mullite, anorthite, cristobalite, diopside and magnetite, in association with an amorphous or glassy component.[37] These processes may include solid-phase interactions and joint reactions with gas, liquid and solid phases. They include: fusion, decomposition, volatilisation, dissolution, oxidation or reduction, dehydration, dehydroxylation, polymorphic transformation, condensation, crystallisation, recrystallisaton and vitrification.[6,37] An example of the transformation of inorganic components during combustion of coal can be seen in Figure 2.8.[38]

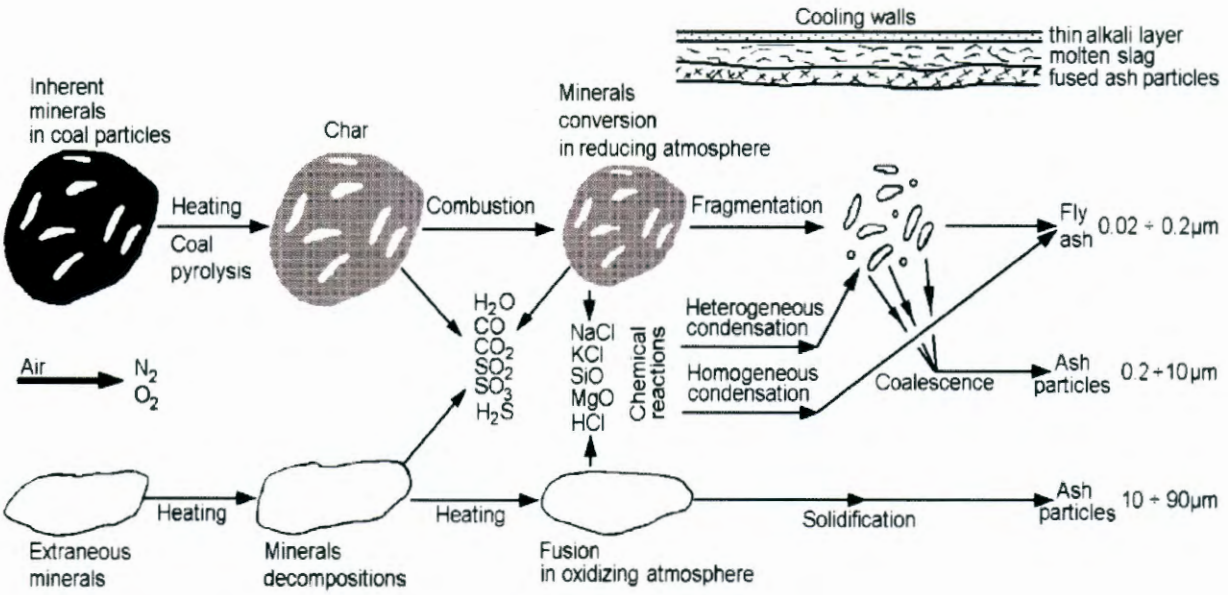

Figure 2.8 Mineral transformation and particle formation pathways during coal combustion.[38]

2.3.3.3 Physical properties

The physical properties of a fly ash particles are controlled by combustion temperature and cooling rate.[39] Fusion and sintering of the particles causes the ash that is formed by gasifiers to be highly heterogeneous.[40] Two types of particle shapes have been identified from fly ash. The more abundant particle morphology is a glassy (amorphous) particle, spherical in shape and is either solid or hollow. In contrast the carbonaceous particles which are more angular in shape and cubic. The particle sizes are comparable to that of silt (0.0039 - 0.063 mm),[41,42] but typically fall within the range of 0.1-1.0 μm.[43]

The Particle size distribution is an important factor influencing the elemental retention and release into the environment.[24] Particles with coarse surfaces have been found to be covered by smaller adhering microspheres and opaque magnetite spheres in electron microscopy studies.[44] The fly ash produced from sub-bituminous coal combustion is generally slightly coarser than that observed for higher grade coals.[12] The specific gravity of fly ash ranges form 2.1 – 3.0. The specific surface area may range from 170 – 1000 m^2/kg.[12] The colour of the fly ash is highly dependent on the source and effectiveness of the coal-fired boiler used. The colour ranges from red and white to various shades of grey.[40] Typically, the darker the ashes, the higher the unburned carbon content, which is a direct indication of boiler efficiency. Lighter shades of gray can be associated with higher quality of ash as found in the study area.[12] Fly ash is pozzolanic in nature and may form cementing compounds in the presence of moisture.[45]

2.3.3.4 Chemical and mineralogical properties

In the order of declining abundance; Si, Al, Ca, C, Mg, K, Na, S, Ti, P and Mn are the main elemental constituents of fly ash.[46] Most of these elements have been found to exist in the core of the fly ash which is relatively stable. This is probably because these elements were not volatilised in the combustion process.[47] The concentrations of trace elements such as Cd, As, Sb, Pb, Cr, Ni, B, Se, Sn, and Zn were found to have increased by factors of 4-10 relative to those in the source coal due to combustion.[48] In Table 2.6, the American Society for Testing and Materials (ASTM) distinguished fly ashes in the following groups based on their CaO content.[49]

Table 2.6 Fly ash classification by ASTM.

	Class		
	N	**F**	**C**
$(SiO_2) + (Al_2O_3) + (Fe_2O_3)$, min, %	70	70	50
(SO_3), max, %	4	5	5
Moisture content, max, %	3	3	3
LOI, max, %	10	6	6

The following methods were used in previous studies to determine the chemical and mineralogical properties of fly ash.

Leaching experiments

A study done on the relative solubility of cat-ions in fly ash at different pH showed cat-ions to be relatively insoluble by naturally occurring fluids such as surface or groundwater. Fe, Ba, Pb, Cd, Sb, and Se were found to be insoluble, while Al, Be, Ca, Co, Cr, Cu, K, Mg, Mn, Na, Ni, and Zn were found to be slightly to moderately soluble in acidic conditions, while only Ca and Na were water soluble and Ca and As were soluble in basic solutions.[50]

A higher degree of dissolution of ions was observed in bituminous coal ash compared to that of anthracite ash. This was thought to be due to the Na and Ca sublimates which are easily dispersed from the surface of the ash particles. Ca and Na (as well as other major elements, including K and Al) were also the main constituents of the alluminiosilicate glass fraction which produced an alkaline leachate (anthracite pH 7.43-9.31 and bituminous pH 10.95-12.01). The leaching behaviour pointed to a slow or long term release of elements associated with the glass fraction.[24]

Leaching has also been found to decrease the specific surface area of the ash, increase roughness on the particle surfaces and shorten, diffuse and broaden peaks in the diffraction spectra compared to ash prior to leaching.[51] The leaching trends of trace impurities in Spanish fly ashes were consistent with the dissolution of small solid particles or outside layer on the surface of the ash solid phases as opposed to the dissolution of a homogeneous glass phase.[52] The leaching rate of the different trace impurities were arranged in decreasing order as B ≥ Mo ≥ Se >Li >Sr ≥ Cr ≥ As = Ba = Cd = V >Sn>Rb= Zn ≥ Cu = Ni = Pb> U > Co >Mn.[52]

X-ray diffraction/absorption/fluoresence

The major phases in fly ashes have been reported as aluminosilicate glass, mullite ($Al_6Si_2O_{13}$), quartz (SiO_2), magnetite (Fe_3O_4), anorthite/albite ($(Ca,Na)(Al,Si)_4O_8$), anhydrite($CaSO_4$), hematite (Fe_2O_3) and lime (CaO).[53]

The mineralogy of sub-bituminous and anthracitic fly ash from Korea was found to be similar, consisting mainly of mullite, quartz and iron oxides, including hematite and magnetite.[21] Figure 2.9 illustrates a comparison of XRD spectra of fly ash, bottom ash and feed coal from Turkey.[54] The chemical composition of ash similar to that of the study area was determined by XRF and can be seen in Chart 2.2.[6]

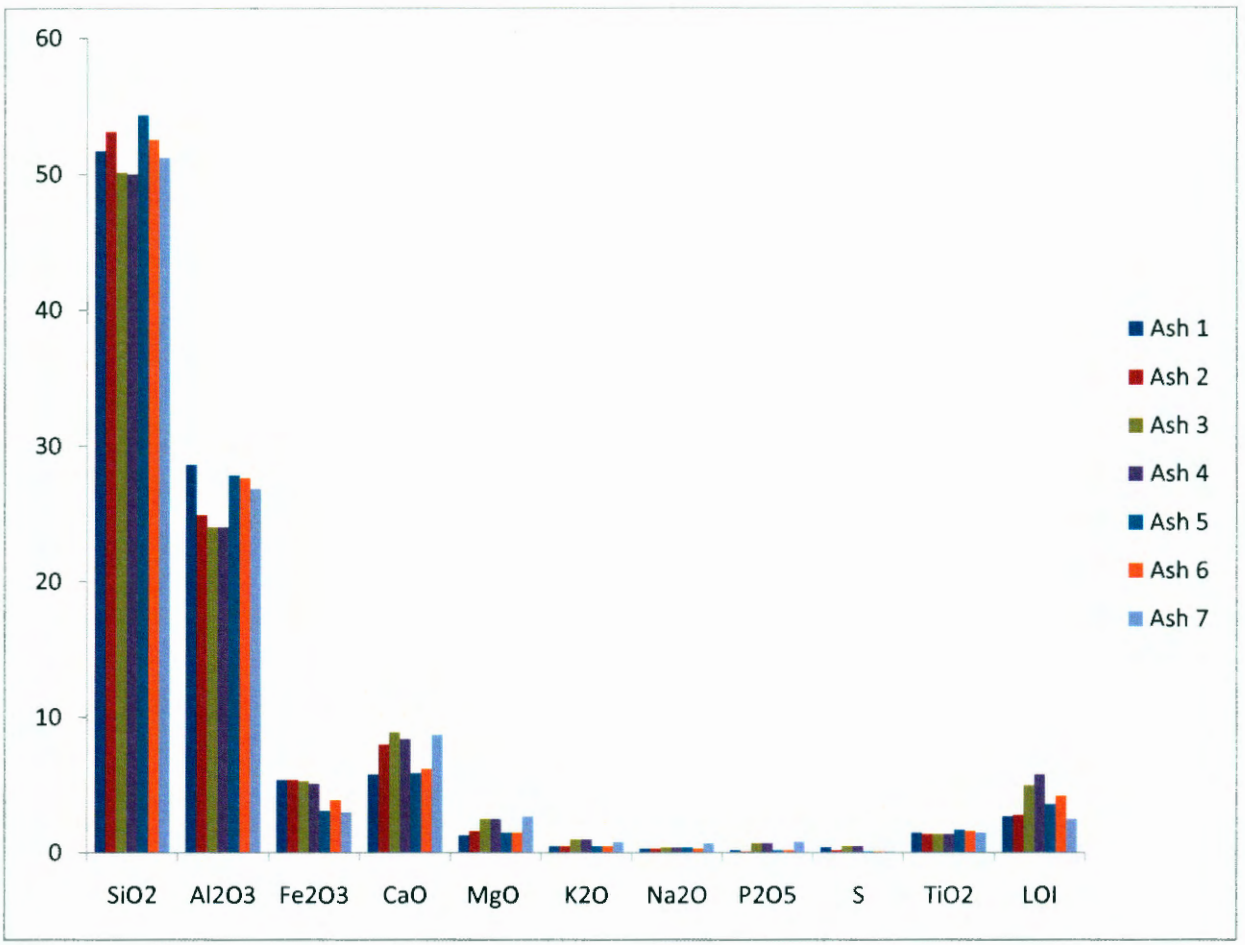

Chart 2.2 Elemental analysis of ashes from the study area determined by XRF.

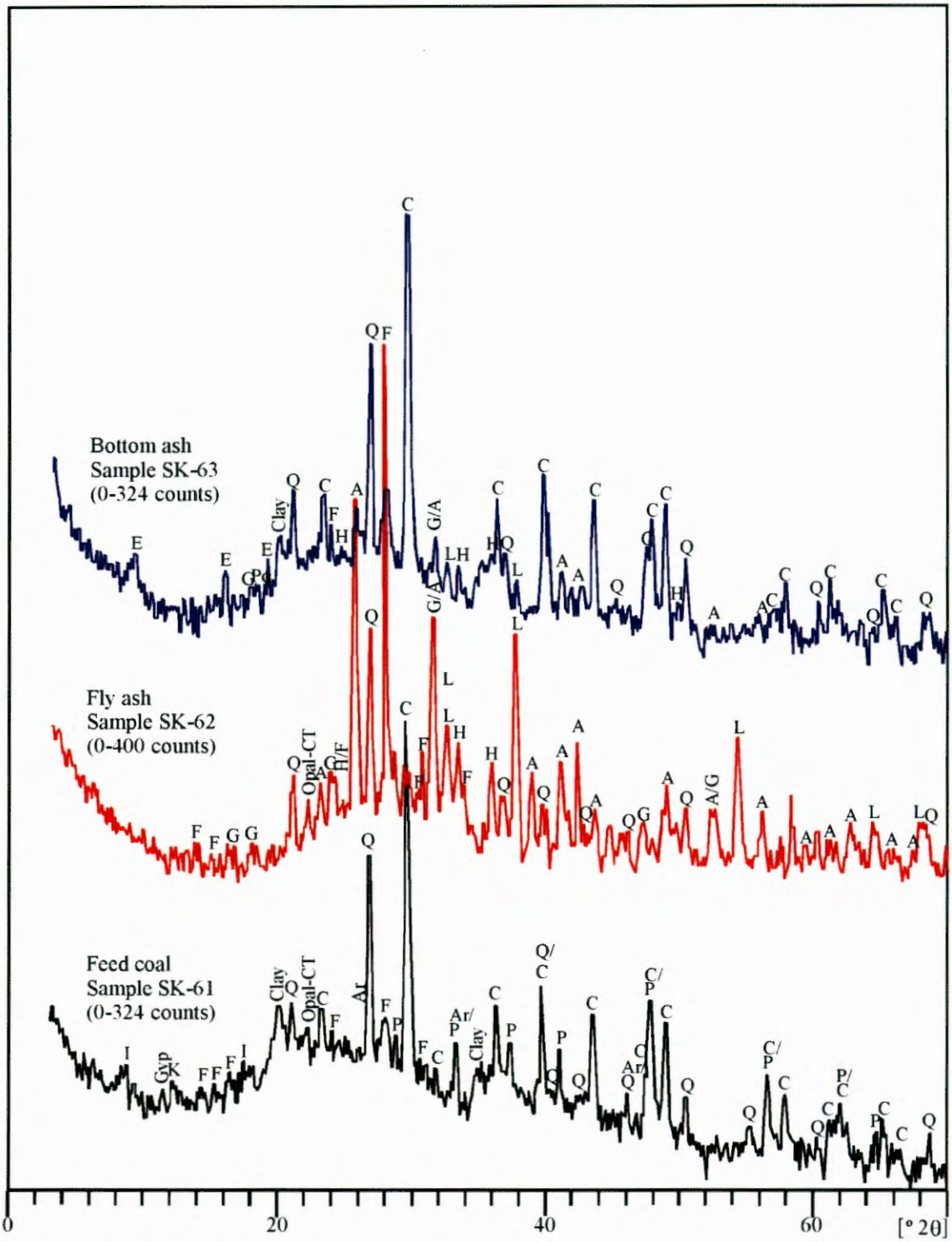

Figure 2.9 Examples of X-ray diffraction spectra of fly ash, bottom ash and feed coal from Turkey. Q=quartz, C=calcite, Ar=aragonite, F=feldspar, I=illite, K=kaolinite, Clay=clay min, P=pyrite, Gyp=gypsum, A=anhydrite, L=lime, H=hematite, E=ettringite, G=gehlenite, Po=portlandite.

Scanning electron microscopy (SEM)

The fact that there is a large proportion of the fly ash material which consists of amorphous glass makes the mineralogical description cumbersome. Amorphous glass, by definition has no crystal structure as well as the lack of a set chemical composition. An investigation using SEM-EDX on fly ash from Turkey showed that the amorphous components included Fe-Ca-Al silicate with trace amounts of Ti, K and Mg and that the crystalline components consisted of the minerals quartz, feldspar, hematite, anhydrite, lime, calcite, opal (hydrated silica) and gehlenite.[54]

In Figure 2.10 an example of a typical EDX spectrum for fly ash can be seen.[55] Examples of SEM images of some of these minerals can be seen in Figure 2.11 as well as components from ash similar to that found in the study area in Figure 2.12.[6,54] SEM images of solid fly ash cenospheres from India showed smoother surfaces prior to leaching compared to post leached samples. Examples of these images can be seen in Figure 2.13.[55]

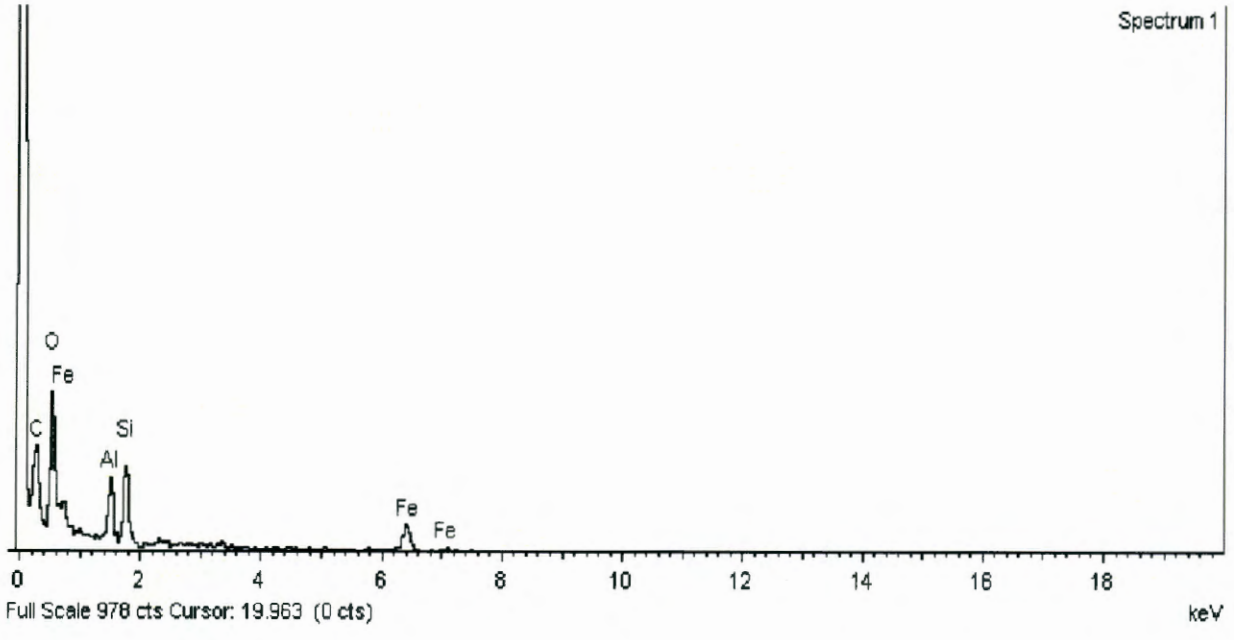

Figure 2.10 An example of a typical SEM-EDX spectrum for fly ash.

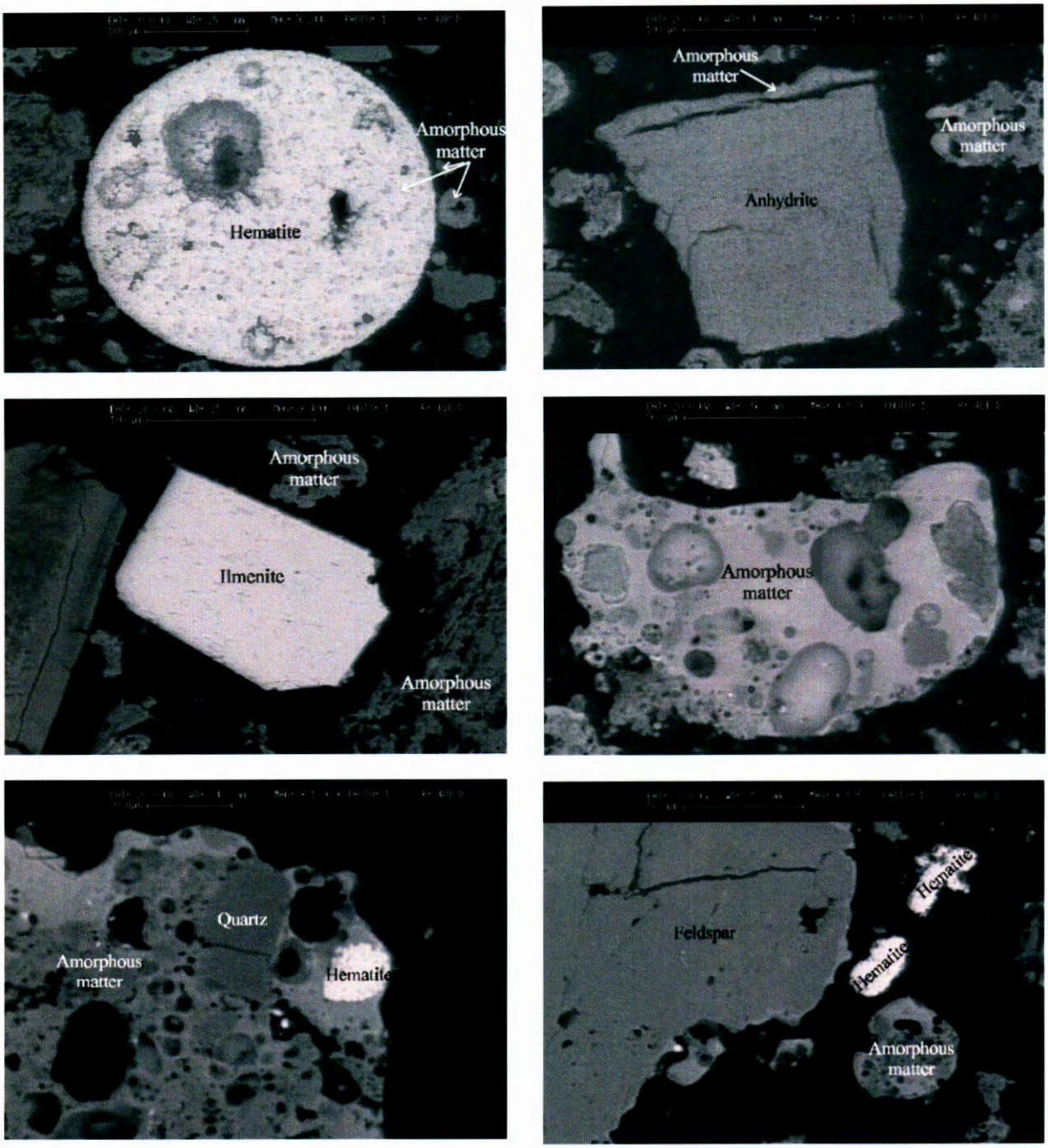

Figure 2.11 SEM-EDX images of components in fly ash from Turkey.

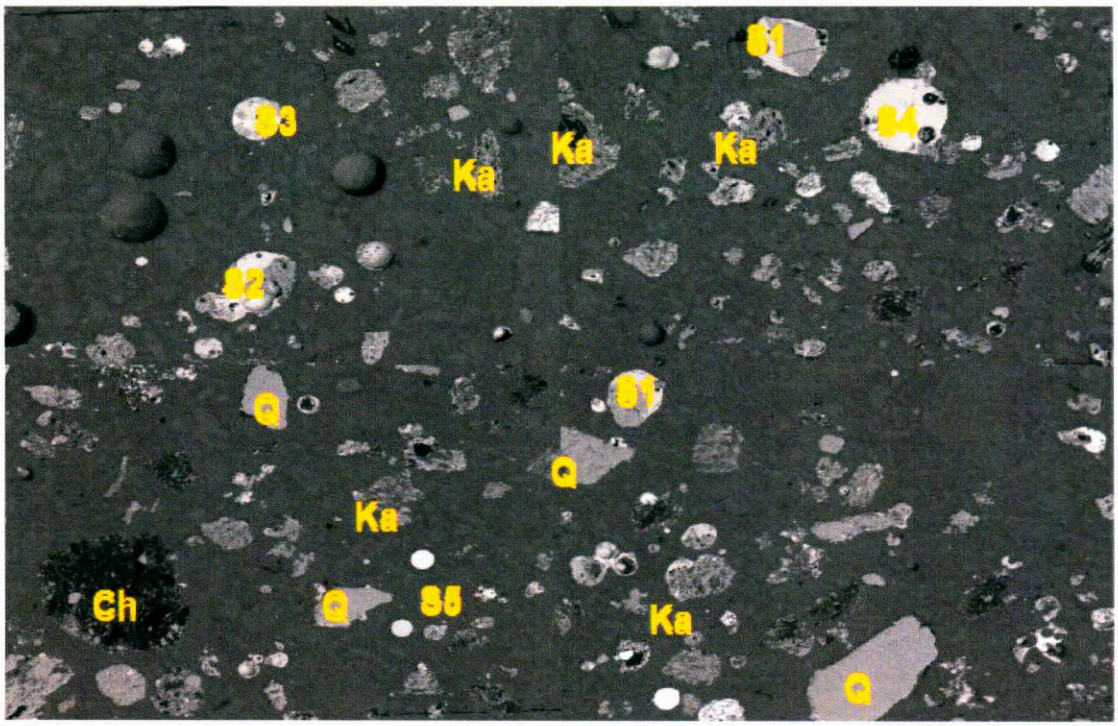

Figure 2.12 SEM image of fly ash.

S1 – Quartz particle (grey) partially surrounded by Ca-Mg-Fe bearing aluminiosilicate glass.

S2 – Aluminio-silicate (dark grey) partially surrounded by Ca-Mg-Fe bearing aluminiosilicate glass.

S3 – Predominantly Ca-Mg-Fe Silica rich glass with minor quartz inclusions.

S4 – Spherical Ca-Mg-Fe aluminiosilicate fly ash particle.

S5 – small (white) spherical Fe bearing aluminiosilicate particle.

Ka – Predominantly "honeycomb" aluminiosilicate particles. Can have small quartz inclusions.

Q – Extraneous quartz particles.

Ch - Predominantly char particle (black) with quartz and aluminiosilicate inclusions (grey).

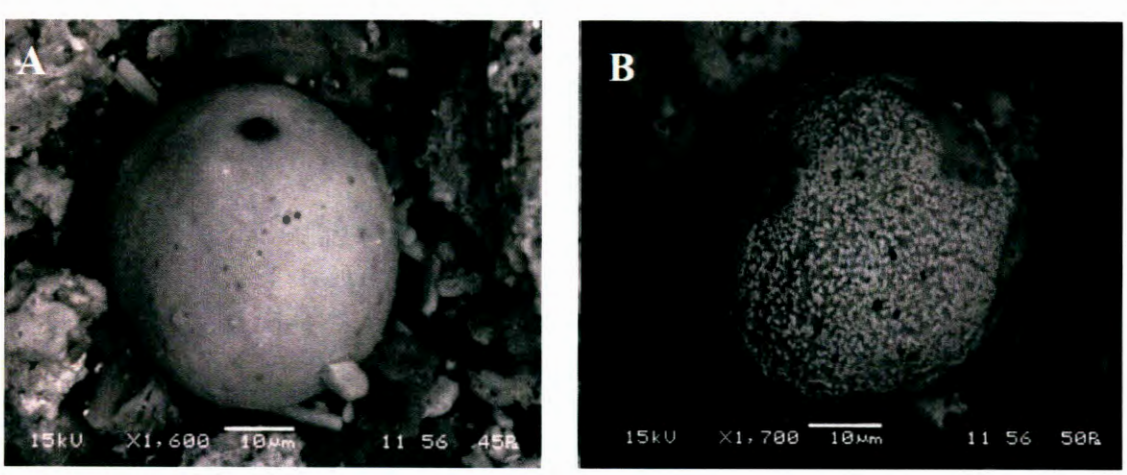

Figure 2.13 SEM images of cenospheres of fly ash before leaching (A) and after leaching (B).

In Figure 2.14 two different compositions have been identified for the amorphous glass component of the fly ash from the study area using QEMSCAN analysis (a computer-controlled scanning electron microscope extension, identifying, mapping and performing a range of different analyses from point-by-point SEM-EDX data by incorporating a high-speed "species identification program" (SIP) on the minerals and other phases in coals, coal ashes and other mineral products).

The first has a calcic nature from which anorthite has crystallised and the other consisting of a more iron rich composition. This was thought to be due to the low fusion temperatures of impure calcareous sediments (calcite, dolomite, kaolinite and quartz) being derived from the mineral matter associated with the coal. The mixture of silicates, carbonates and pyrite could lead to the formation of the two respective calcium rich and iron rich glasses. These are the result of decomposition of the clay minerals and pyrite in associating with the largely unreactive rock fragments. The minerals and inorganic elements in the coal undergo significant transformations at elevated temperatures, probably after the gasification process, the nature of the transformation depends not only on the mineralogy but also the mineral association.[40]

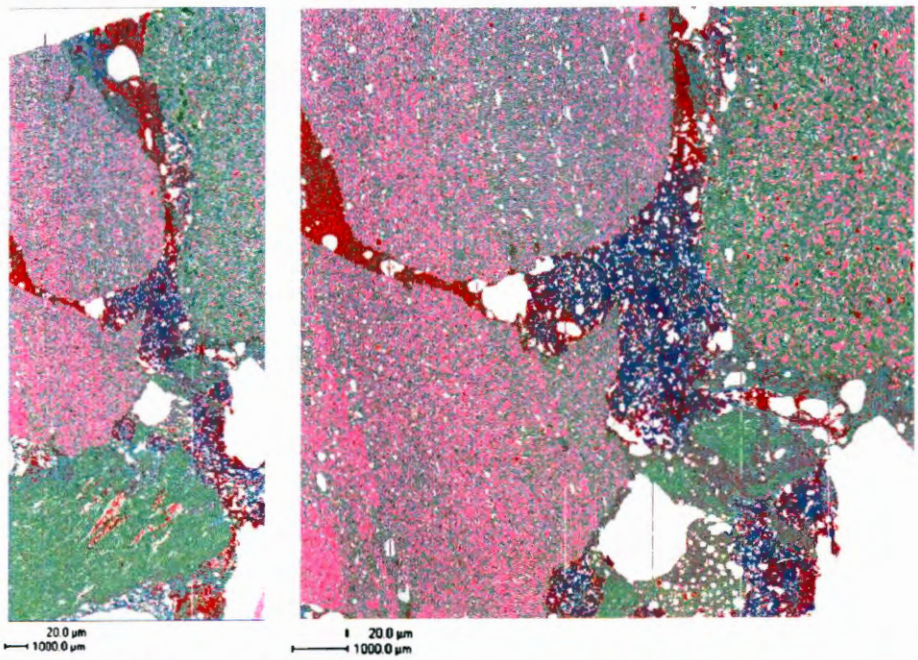

Figure 2.14 QEMSCAN field scan of an ash sample, showing general view (left) and close-up view (right) with rock fragments (sandstone and siltstone) containing quartz (pink) and illitic clay (green) set in a matrix of two glass compositions, one iron-rich (red) and one of calcic composition (blue-green) containing anorthite crystals.

2.3.3.5 Disposal

The fly ash produced has to be disposed of outside the plant grounds so that it causes least interruption to plant operation. Current fly ash management options are based on two strategies, i.e. Disposal and Recycling. Disposal of fly ash in confinement areas remains the most practical and cost effective solution for South African industries.

Approximately 4.75 Mt of fly ash is produced in the study area annually.[56] Typical disposal techniques include the construction of dumps or dams, similar to those employed within the mining sector. Fly ashes can either be dry dumped by means of truck loads or conveyor belts or it can be dumped as slurry in a so-called wet dump facility.[3] Wet dumps are created when fly ash is mixed with a liquid, often also a secondary waste product or brine produced by coal firing facilities to create the slurry.

The slurry is then pumped and discharged onto the wet dump where density settlement separates reusable water from the slurry which is then left to dry over a time period. The water that has separated from the ash is skimmed off and re-circulated to transport more fly ash to the site. Advances in paste technology as a co-disposal option for fly ash and industrial brines have also been reported in recent years.

Process water

Approximately 160Mm^3 of fresh water is used annually in the study area for the production of steam and process cooling.[57] Pre-treatment of this water for utility cooling water and boiler feed in processes such as Electro Dialysis Reversal (EDR), Spiral Reverse Osmosis (SRO) and Tubular Reverse Osmosis (TRO), coupled with the usage of regeneration chemicals (lime, soda ash and polymers) results in the production of highly saline effluents.[2] The desalination process is the main contributor of generated salt and consists of brine produced by process streams of various salinities.

An example of the chemical composition of brine samples can be seen in Table 2.7, however the composition is very unpredictable.[3,58] The brine in co disposal systems may also influence the permeability (especially in clayey soils), soil health and water movement by precipitating as salt barriers.[59]

The site is operated in accordance with the zero liquid effluent discharge (ZLED) policy. This implies that apart from seepage water losses, no saline water is discharged to surface water features. The high saline streams are used for the hydraulic transport of ash (ca. 20 % ash), which results in the ash dumps (dams) acting as a sink for the salts.[60] This is still an issue of concern, as the dam is able to transmit processed water to the surrounding enviroment.[58]

Table 2.7 Example of the chemical composition of brine samples.[3]

Major elements			**Minor elements**		
	A	**B**		**A**	**B**
B	2 ± 0.1	2.2 ±0.2	Al	0.01	0.06 ± 0.03
Ca	91 ± 0.7	90.8 ± 1.2	As	0.007	0.007
K	106.2 ± 3.8	116.7 ± 5.2	Ba	0.06	0.06
Mg	147.5 ± 10.6	157.3 ± 13.7	Cd	BDL	0.0001
Na	4323.2 ± 44.8	4327.7 ± 33.8	Co	0.01	0.01
Si	11.1 ± 0.03	11.1 ± 1.2	Cr	0.02	0.02
Sr	2.6	2.6 ± 0.05	Cu	0.2	0.2 ± 0.02
Cl	2424 ± 17	2436 ± 16.9	Fe	0.1	0.1
SO4	8858 ± 86	8858 ± 86.3	Mn	0.002	0.002
pH	7.89	7.92	Mo	0.04	0.04
EC (mS/cm)	14.63	14.72	Ni	0.1	0.1
			Pb	0.007	0.003
			Se	0.007	0.004
			Ti	0.001	0.003
			V	0.02	0.02
			Zn	0.1	0.1

Ash Pond Effluent Characteristics

A study on the contamination of river water by an ash dams in India showed relatively higher concentrations of S, Al, Fe, Mn, Ba, Zn and Ti, of which Al, Fe, Mn and Pb were the major contaminants in the ash pond effluent at near neutral pH. The other elements found in lesser concentration levels in the effluent are mostly non-leachable from the ash in that area.[61] A study on fly ash-brine co-disposal systems in South Africa showed that hydrolysis within the system rapidly dissolved basic oxides (CaO and MgO) from

the fly ash, contributing to a high alkalinity. It also showed that the fly ashes had the ability to remove some species (Na, Mg, Cl, SO_4, B, As, Cd, Co, Cu, Ni, Pb and Zn) from the brine solution, while other species (Ca, Ba, Sr, Cr, Mo and Se) from the fly ash samples also leached into the brine solution, resulting in an overall decrease in total dissolved solids (TDS).[3]

2.4 Hydraulic and transport properties of landfills

The hydrogeology of waste deposits are complex, but still adhere to the ground rules of contaminant transport. These include the permeability and moisture content of the material within the unsaturated zone, the thickness of the unsaturated zone, as well as the hydraulic conductivity and local hydraulic gradient in the saturated zone. The main processes influencing mass transport are advection, dispersion and concentration gradient. Of these, advection is the main process in mass transport in a porous, permeable systems and diffusion in a low permeability system.[62]

Downward and outward flow of leachate is driven by the increased hydraulic head developed by process fluids and rain water that percolate through a landfill. The fluids often accumulate in lenses or mounds throughout the landfill and the extent of their influence on the surroundings may be seen in monitoring boreholes and seepage faces.[63] The seepage faces reflect a temporal nature of the fluids in a landfill, often being visible during the wet seasons and absent during the dry seasons. The potential for groundwater pollution from older capped landfills may be even higher than from younger, open landfills as the leachate may be highly concentrated and extremely hazardous to the environment.[4]

Preferential flow paths may be the result of various processes that occur at or after deposition of waste material. Physically, compaction or consolidation may reduce permeability whilst layering may be caused by the application of a topsoil cover after the deposition of waste to landfills.[4] Chemical and physical weathering may also be driven by salt cracking (a chemical process where dissolved salts crystallise, exerting considerable force, resulting in a mechanical widening of cracks or even fracturing rock) or exfoliation (a type of pressure release fracturing, caused by the formation of clay

minerals by hydrolysis of feldspar and other silicate minerals, setting off a mechanical fracturing through swelling and shrinking).[64] Fractures and joints in the subsurface as well as faults or holes in liners may increase leachate flow considerably, but contaminant plumes hardly ever extend more than a few hundred metres from a landfill, only the most persistent contaminants are fully distributed.[4]

The leachate plume undergoes continuous transition in the direction of groundwater flow. Chemically, reduced species such as methane and ammonia disappear, and aqueous nitrogen and sulphur convert into oxidised forms of nitrate and sulphate respectively.[4] Iron and organic carbon are oxidised and are converted to hydrous iron oxide and CO_2, respectively. In contrast, manganese remains in solution longer and travels further with the produced leachate plume.[4]

2.5 Self potential method

Preferential adsorption of ions produces a self potential of ground water in motion under a pressure gradient through a porous media. The self potential is caused by the electric double layer of ions associated with the interface between the mineral grains and the pore fluid (ground water) in natural systems. Unoccupied sites (bonds) at the surface of mineral grains adsorb ions from solution, positive ions being attracted to the surface and negative ions being repelled. Thus, the direction of flow is characterised by an overall increase of negative ions in the solution.[65]

Changes in hydraulic head correlate to self potential fluctuations when monitored over seepage zones, indicating that flow rate also affects self potential.[66] For a given set of material properties, the only variables are self potential and drop in pressure along the flow path, which are proportional and the relationship is constant.[67,68] This relationship is known as the electrokinetic coupling coefficient. This coefficient is difficult to calculate because little is known about the behaviour of other fluid properties in the pores of rocks and soil.[69]

Although the fill of the conduits are of importance, the geometry of flow has been found to be relatively unimportant in its effect on self potential in fissured flow and decreases self potential as salinity of the electrolyte (pore fluid) increases.[68,70] When performing

self potential studies in the field and in particular in areas of consolidated bedrock, the complex nature of groundwater flow through fractures and channels needs to be understood to properly interpreted their results. This is due to site conditions and variables such as: Local relief; climatic and seasonal parameters; lithology; variations in water and soil chemistry; bedrock structure and deformation; degree of karstification (extent of subsurface drainage) and depth to the water table or major conduits.[65]

2.6 Concluding remarks

This concludes the literature review highlighting previous research conducted by independent laboratories and institutions in focus areas of the current study. These include properties of fly ash, environmental concerns as well as analytical techniques which will be utilised to achieve the objectives laid out in Chapter 1. In the following chapter the methods used to determine the results discussed in Chapter 4 will be considered.

2.7 References

[1]Wang, H., Ban, H., Golden, D. and Ladwig, K., 2002, *Ammonia release characteristics from coal combustion fly ash,* Fuel chemistry division preprints, 47(2), 836.

[2]Muntingh, Y., Mahlaba, J.S. and Pretorius, C., 2009, *Utilising fly ash as a salt sinking media through pasting with industrial brine.*, Proceedings of the world congress on engineering, Vol 1.

[3]Fatoba, O.O., 2010, *Chemical interactions and mobility of species in fly ash-brine co-disposal systems.*, UWC.

[4]Taylor, R. and Allen, A.R., 2006, Waste disposal and landfill: Information needs. Schmoll, O., Howard, G., Chilton, J., Chorus, I. (eds). *Protecting groundwater for health: managing the quality of drinking-water sources*, WHO drinking water quality series monograph, IWA Publishing.

[5]Twardowska, I. and Stefaniak, S., 2006, *Coal and coal combustion products: prospects for future and environmental issues*, Coal combustion byproducts and environmental issues., Springer, 241.

[6]Matjie, R. H., Ginster, M., van Alphen, C. and Sobiecki, A., 2005, *Detailed characterisation of sasol ashes. In:* LTD., S. T. P. (ed.). Sasolburg, South Africa.

[7]U.S. Department of Transportation, F. H. A., 1998, *Turner-fairbank highway research centre* [Online]. Available: http://www.tfhrc.gov/hnr20/recycle/waste/cfa51.htm.

[8]Chen, H., Li, B. and Zhang, B., 1999, *Effects of mineral matter on products and sulphur distributions in hydropyrolysis.*, Fuel, 78, 713-719.

[9]Kearey, P., 2001, *The new penguin dictionary of geology,* England, Penguin Books.

[10]ASTM: D388-99, 2004, e1 *Standard classification of coals by rank.*

[11]Alpern, B. and Lemos de Sousa, M.J., 2002, *Documented international enquiry on solid sedimentary fossil fuels; coal: definitions, classifications, reserves-resources, and energy potential.*, International journal of coal geology, 50

[12]*Coal combustion by-products.*, 2013, Centre for applied energy research, University of Kentucky. Available: http://www.caer.uky.edu/kyasheducation/glossary.shtml#subcoal.

[13]Lee, B.C. and Sloss, L.L., 1992, *Trace element emissions from coal combustion and gasification.*, London: IEA coal research.

[14]Petrik, L., Gitari, W., Etchebers, O., Nel, J., Kumar Vadapalli, V. R. and Fatoba, O., 2007,*Towards the development of sustainable salt sinks: Fundamental studies on the co-disposal of brines within inland ash dams*. Cape Town: University of the Western Cape.

[15]Van Dyk, J.C., Keyser, M.J. and Van Zyl, J.W., 2001, *Suitability of feedstocks for the Sasol-lurgi fixed bed dry bottom gasification process.*, Gasification technologies.

[16]Van Dyk, J.C. and Keyser, M.J., 2005, *Characterization of inorganic material in Secunda coal and the effect of washing on coal properties.*, The journal of the South African institute of mining and metallurgy, 6.

[17]Özbayoğlu, G. and Özbayoğlu, M.E., 2006, *A new approach for the prediction of ash fusion temperatures: A case study using Turkish lignites,*. Fuel, 85, 545-552.

[18]Pinetown, K.L., Ward, C.R. and Van der Westhuizen, W.A., 2006, *Quantitative evaluation of minerals in coal deposits in the Witbank and Highveld Coalfields, and the potential impact on acid mine drainage*, Int. Journal. of coal geology, 70, 166-183.

[19]Usgweb, 2011, *Synthetic gypsum.*, Securock roofing solutions.

Available: http://securockroofboardsblog.usg.com/2011/11/12/synthetic-gypsum/

[20]Statistics South Africa, 2005, *Energy accounts for South Africa, 1995 – 2001.*, Natural resource accounts.

[21]U.S. Department of transport, Federal highway administration., 2012, *User guidelines for waste and byproduct materials in pavement construction.,* (No. FHWA-RD-97-148).

[22]Kalyoncu, R., 1998, *Coal combustion products*, Mineral year book, USGS.

Available: http://minerals.usgs.gov/minerals/pubs/commodity/coal/.

[23]ACAA, 2010, *Coal combustion product (CCP) production & use survey report.*

Availible: http://acaa.affiniscape.com/displaycommon.cfm?an=1&subarticlenbr=3

[24]Sajwan, K.S., Punshon, T. and Seaman, J.C., 2006, *Production of coal combustion products and their potential uses.*,Coal Combustion byproducts and environmental issues., Springer, 241.

[25]Choi, S.K., Lee, S., Song, Y.K. and Moon, H.S., 2002, *Leaching characteristics of selected Korean fly ashes and its implications for the groundwater composition near the ash disposal mound.*,Fuel,81, 1083-1090.

[26]Stewart, B.R., Daniels, W.L. and Jackson, M.L., 1997, *Evaluation of leachate quality from codisposed coal fly ash and coal refuse., J. Environ Qual.*,26, 1417-1424.

[27]Ugurlu, A., 2004, *Leaching characteristics of fly ash.*, Environmental geology 46(6-7): 890-895.

[28]Keefer, R.F., 1993, Coal ashes-Industrial wastes or beneficial byproducts. *Trace elements in coal and coal conbustion residues.,* R.F. Keefer and K.S. Sajwan, Editors. Lewis Publishers: Ann Arbor., 3-9.

[29]Kula, I., Olgun, A., Sevine, V. and Erdogan, Y., 2002, *An investigation on the use of tincal ore waste, fly ash and coal bottom ash as portland cement replacement materials.*, Cement and concrete research, 32, 227-232.

[30]Bethanis, S., Cheeseman, C.R. and Sollars, C.J., 2004, *Effect of sintering temperature on the properties and leaching of incinerator bottom ash.*, Waste management & research, 22(4), 255-264.

[31]Ramme, B.W., Ficher, B.C. and Naik, T.R., 2001. *Three new ash beneficiation processes for the 21st century*, Seventh CANMET/ACI International Conference on Fly Ash, Silica Fume, Slag, and Natural Pozzolans in Concrete, Chennai (Madras), India (No. CBU 2001-28).

[32]BluedornII, D.C., 2001, *Recent environmental regulation of coal combustion wastes-revised., Proceedings of conference on unburned carbon (UBC) on utility fly ash.,* National energy technology laboratory.

[33]Punshon, T., Knox, A.S., Adriano, D.C., Seaman, J.C. and Weber, T.J., 1999, *Flue gas desulfurization residue (FGD): Potential applications and environmental issues. Biochemistry of trace elements in coal and coal combustion byproducts.*,K.S. Sajwan and R.F. Keefer, Editors. Lewis publishers: Boca Raton, FL., 7-28.

[34]Punshon, T., Seaman, J.C. and Adriano, D.C., 2002, The *effect of flue gas desulfurization residue on corn (Zea mays L.) growth and leachate salinity: Multiple season data from amended mesocosms.*, Chemistry of Trace Elements in Fly Ash, K.S. Sajwan, A.K. Alva, and R.F. Keefer, Editors. Kluwer Academic/Plenum Press: New York, NY. In press.

[35]Kalyoncu, R., 1998, *Coal combustion products.*, Minerals year book, 1, 1057.

[36]Punshon, T., Seaman, J.C. and Sajwan, K.S., 2003, *The production and use of coal combustion products.* Chemistry of trace elements in fly ash, K.S. Sajwan, A.K. Alva, and R.F. Keefer, Editors. Kluwer Academic/Plenum Publishers, New York., 1-1, 1.

[37]Závodská, L. and Lesný, J., 2006, *Recent development in lignite investigation*, Hungarian electronic journal of sciences, Manuscript no: ENV-061026-A,HU ISSN 1418-7108

[38]Tomeczek, J. and Palugniok, H., 2002. *Kinetics of mineral matter transformation during coal combustion.* Fuel 81.

[39]Kutchko, B.G. and Kim, A.G., 2006, *Fly ash characterization by SEM–EDS.*, Fuel, 85, 2537–2544.

[40]Matjie, R.H., French, D., Ward, C.R., Pistorius, C.P. and Li, Z., 2011, *Behaviour of coal mineral matter in sintering and slagging of ash during the* gasification process., Fuel processing technology,1-8.

[41]Hendricks, N.R., 2005, *The application of high capacity ion exchange adsorbent material, Synthesized from fly ash and acid mine drainage, for the removal of heavy and trace metals from secondary co-disposed process waters* (Megastar scientiae in the department of chemistry).

[42]Cairncross, B., 2004, *Field guid to rocks and minerals of Southern Africa,* Cape Town, South Africa, Struik publishers.

[43]Peng, M., Ruan, X.G., Chen, X.M., Xu, J.W. and Jiang, Z.C., 2004, *Study on both shape and chemical composition at the surface of fly ash by scanning electron microscope, focused ion beam, and field emission-scanning electron microscope.,* Chinese journal of analytical chemistry,32 (9), 1196-1198.

[44]Mattigod, S.V., Rai, D., Eary, L.E. and Ainsworth, C.C., 1990, *Geochemical factors controlling the mobilization of inorganic constituents from fossil fuel combustion residues: I. Review of the major elements.,* J. Environ Qual.,19, 188-201.

[45]Manz, O.E., 1999, *Coal fly ash: a retrospective and future look.*,Fuel,78, 133-136.

[46]Lokeshappa, B. and Dikshit, A.K., 2011, *Disposal and management of fly ash*, in: Ipcbee. Presented at the international conference on life science and technology, IACSIT Press, Singapore.

[47]El-Mogazi, E., Lisk, D. and Weinstein, L., 1988, *A review of physical, chemical and biological properties of fly ash and effects on agricultural ecosystems*., Journal of the science of the total environment, 74, 1-37.

[48]Fernandez-Turiel, L.J., de Carvalho, W., Cabanas, M., Querrol, X. and Lopez-Soler, A., 1994, *Mobility of heavy metals from coal fly ash.* Environmental geology 23, 264-270.

[49]ASTM C618-92a, 1994, *Standard specification for fly ash and raw or calcinated natural pozzoland for use as mineral admixture in Portland cement concrete.*, American society for testing and materials, Annual book of ASTM Standards, vol. 04.02, Pennsylvania.

[50]Kim, A.G., Kazonich, G. and Dahlberg, M., 2003, *Relative solubility of cations in class f fly ash*, Environ. Sci. Technol, 37, 4507-4511.

[51]Praharaj, T., Powell, M.A., Hart, B.R. and Tripathy, *S.*, 2002, *Leachability of elements from sub-bituminous coal fly ash from India*. Environment international, 27 (8), 609-615.

[52]Querol, X., Omana, J.C., Alastuey, A., Ayora, C., Lopez-Soler, A. and Plana, F., 2001, *Extraction of soluble major and trace elements from fly ash in open and closed leaching systems*., Fuel, 80.

[53]Moreno, N., Querol, X., Andre´s, J.M., Stanton, K., Towler, M., Nugteren, H., Janssen-Jurkovicova and Jones, M.R., 2005, *Physico-chemical characteristics of European pulverized coal combustion fly ashes*, Fuel, 84, 1351–1363.

[54]Karayigit, A.I. and Gayer, R.A., 2001, *Characterisation of fly ash from the Kangal power plant, Eastern Turkey*., International ash utilization symposium, Centre for applied energy research, University of Kentucky, Paper 4. Available: http://www.flyash.info

[55]Kumar, S., 2010, *Leaching behaviour of elements from sub-bituminous coal fly ash.* B.Tech thesis, Department of mining engineering, National institute of technology, Rourkela.

[56]Krüger, J.E., 2003, South *African fly ash: a cement extender.*

[57]Sasol sustainable development report, 2006.

Availible: http://sasolsdr.investoreports.com/sasol_sr_2006/downloads/sasol_sr_2006_full.pdf.

[58]October, A., Nel, J.M., Reynolds, K., Lasher, C. and Dlamini, L., 2009, *Hydraulic and transport properties of ash dumps.,* World of coal ash (WOCA) conference., Lexington, KY, USA.

[59]Nyamhingura, A., 2009, *Characterization and chemical speciation modelling of saline effluents at Sasol synthetic fuels complex-Secunda and Tutuka power station* (Master of science in chemistry).

[60]Valerio, P. and Water, V., 2012, *Integrated systems reclaim cooling tower blowdown*. World oil 233.

Availible:http://www.worldoil.com/October-2012-Integrated-systems-reclaim-cooling-tower-blowdown.html\

[61]Tripathy, S. and Praharaj, T., 2006, Delineation of water and sediment contamination in river near a coal ash pond in Orissa, India, *Coal Combustion byproducts and environmental Issues*. Springer, NY, 241.

[62]Fetter, C.W., 1999, *Contaminant hydrogeology*, 2nd Ed., Prentice Hall, 458.

[63]Spencer, L.L. and Drake, L.D., 1987, *Hydrogeology of an alkaline fly ash landfill in eastern Iowa*, Groundwater, 25, No. 5.

[64]Thompson, G.R. and Turk, J.,1997, *Introduction to physical geology*., Thompson learning.

[65]Erchul, R.A. and Slifer, D.W., 1989, *Geotechnical applications of the self potential (SP) method.,* (Technical Report REMR-GT-6 Report 2 of a series No. OMS p.0704-O188).Department of civil engenering, Virginia military institute Lexington, VA 24450.

[66]Warriner, J.B. and Taylor, P.A., 1982, *Modeling of electrokinesis*, miscellaneous paper GL-82-13, US army engineer waterways experiment station, Vicksburg, MS.

[67]Cooper, S.S., Koester, J.P. and Franklin, A.G., 1982, *Geophysical investigation at gathright dam*, Miscellaneous Paper GL-82-2, US army engineer waterways experiment station, Vicksburg, MS.

[68]Ahmad, M., 1964, *Laboratory study of streaming potential*, Geophysical prospecting, 12, 49-64.

[69]Corwin, R.G. and Hoover, D.B., 1978, *The self-potential method in geothermal exploration*, Geophysics, 44, 226-245.

[70]Bogoslovsky, V.A. and Ogilvy, A.A., 1973, *Deformations of natural electric fields near drainage structures*, Geophysical prospecting, 21, 716-723.

Chapter 3

Methodology

3.1 Introduction

The following sections of this chapter contain the procedures followed and technical specifications of the instruments used to evaluate the chemical and transport properties of the fly ash from the industrial site. Mineral identification was done by powder X-ray diffraction (PXRD) and scanning electron microscopy (SEM). Chemical analysis was performed on the leachate using inductively coupled plasma - optical emission spectrometry (ICP-OES) to evaluate the mobility of selected elements leached from the ash and to determine the matrix response to other salts introduced to the matrix. A constant head permeameter with tracer and self potential tracer using a fraction collector are some of the apparatus that were improvised or manufactured in house for the purposes of this study. Also described in this section is a geophysical survey conducted on the ash dam in the industrial complex by time-lapse electrical resistivity tomography (ERT)

3.2 Mineral identification

X- ray diffraction (XRD)

Fresh ash samples were analysed using a Bruker D8 Advance powder defractometer with Cu radiation source, a göbel mirror and a Vantec-1 detector. Samples were prepared by grinding fly ash with a mortar and pestle and placed in a cruisible, ensuring a uniform dispersivity. The spectra was then matched with the crystallographic open database on EVA.DIFFRAC.SUITE ™(EVA) Software. The 9 leached samples were also analysed to compare to the fresh samples and to results found in literature.

Scanning electron microscopy (SEM)

Samples were prepared for electron microscopic analysis on a polished section of fresh ash in resin and on a sprinkled sample of leached ash. This analysis was done using a JEOL JSM-6610 scanning electron microscope with a Thermo Scientific Ultra dry EDS detector and an accelerating voltage of 20 kV and a live time of 60 seconds per analysis. The polished sample was carbon coated to ensure good sample conductivity and image quality.

3.3 Chemical analysis

3.3.1 Cation exchange capacity (CEC)

The cation exchange capacity (CEC) of a soil is simply a measure of the quantity of sites on soil surfaces that can retain cat-ions by electrostatic forces.
The experimental procedure was adopted from published procedures,[1] using $BaCl_2$ and $MgSO_4$. This procedure was chosen because it is highly reproducible and does not require a centrifuge.

Sample preparation

2.00 g Fly ash was weighed into a funnel containing medium grade filter paper. The ash was then washed with 20 ml (2X10 ml) 0.1 *M* $BaCl_2 \cdot 2H_2O$ solution, allowing each addition to soak into the ash, followed by 60 ml (6X10 ml) of a 2 mM $BaCl_2 \cdot 2H_2O$ solution. The pH was then determined for later calibration. The filter paper and ash was then transferred to a flask and 10 ml of a 5 mM $MgSO_4$ solution was added before the mixture was agitated for an hour. Distilled water was then added until the mixture had the same electro conductivity as a 1.5 mM $MgSO_4$ solution (~300 μS). The solution pH and conductivity were alternately adjusted using 0.05 M H_2SO_4 and 0.1 M $MgSO_4$ solutions respectively until the endpoints were reached. The final weight was then recorded for calculations. The experiment was performed in triplicate on the 9 sample sections.

3.3.2 Permeameter leaching

Leaching tests are used to estimate potential concentration or amount of waste constituents that can leach from a waste to ground water.[2] This method is used as it can simulate conditions in actual land fill or ash dam conditions. Deionised water was used to emulate the synthetic groundwater leaching procedure (SGLP), as it is used to determine the leachability of constituents from combustion residues, and for any wastes likely to undergo hydration reactions upon contact with water.[3] The flow through leaching test method can be used to simulate the leaching process of stabilised or solidified waste that has degraded under various environmental stresses to a state that groundwater can flow through the waste *via* the porosity system of the waste matrix.[4] When the leachant (deionised water) flows through the waste, it carries away the mobile fraction of the contaminants with it, causing a

contaminant concentration gradient, accelerating the leaching process.[4] At the same time, the immobile fraction is continuously solubilised to restore the equilibrium. Due to this acceleration, the flow through leaching test method can be used to study the long term leaching performance of solidified waste.[4]

Sample preparation

A 958 ml permeameter cylinder was fully packed with fly ash and compacted, using an 800 g sliding hammer, between two filter papers. Compaction was done using three samples, within a 3 m range, in three layers, in reverse order so as to have the deeper sample at the bottom. Each layer was compacted three times in a circular manner. The permeameter was then leached under constant head, using deionised water and the leachate collected in 500 ml intervals. The leachate samples were then shaken and the electro conductivity measured before being sent for further analysis. A schematic representation of the experiment setup can be seen in Figure 3.1.

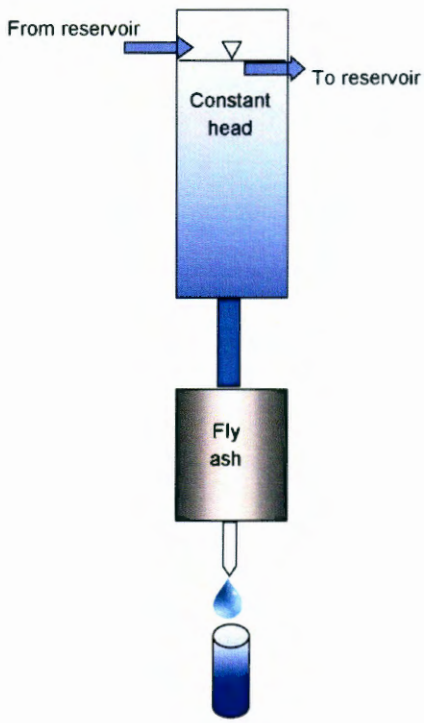

Figure 3.1. Constant head permeameter leaching experimental setup.

3.3.3 Leach solutions chemical analysis ICP/OES

Leach solutions were analysed by ICP-OES on a *Perkin Elmer 3000DV* (Merck IV & VI ICP multi element standard) and ion chromatography by *Dionex DX120 Ion Chromatograph* (AG14 and AS14 Columns).

Inductively coupled plasma/optical emission spectrometry (ICP/OES) is a powerful tool for the determination of metals in a variety of different sample matrices. Liquid samples were injected into a radiofrequency (RF)-induced argon plasma. The sample mist reaching the plasma was quickly vaporized, and energized through collisional excitation at high temperature. The atomic emission emanating from the plasma could be viewed in either a radial or axial configuration, collected with a lens or mirror and imaged onto the entrance slit of a wavelength selection device. Single element measurements can be performed cost effectively with a simple monochromator/photomultiplier tube (PMT) combination, and simultaneous multi-element determinations are performed for up to 70 elements with the combination of a polychromator and an array detector.[5]

3.4 Transport parameters

Permeameter tracer tests

The permeameter experiments were used to simulate the hydraulic and transport properties of the ash dump systems. The first step in conducting the tracer tests is the selection of an appropriate tracer. An ideal tracer is conservative, easily dissolves in water, moves at the same rate as the medium and no adsorption of the substance to the material must take place.[6] Based on these parameters NaCl was determined to be an appropriate conservative tracer.

The residual fly ash from the leaching experiment was dried and repacked into a permeameter. Compensating for any volume lost during the leaching, the cell was then leached again overnight, under constant head, using deionised water. A 5 %, 10 % and 20 % (w/w) solution of sodium chloride (NaCl) was then injected and the leachate collected in 50 ml intervals over time, until the electric conductivity (EC) value was relatively close to the background EC value prior to injection of the NaCl

solution. A schematic representation of the experiment setup can be seen in Figure 3.2.

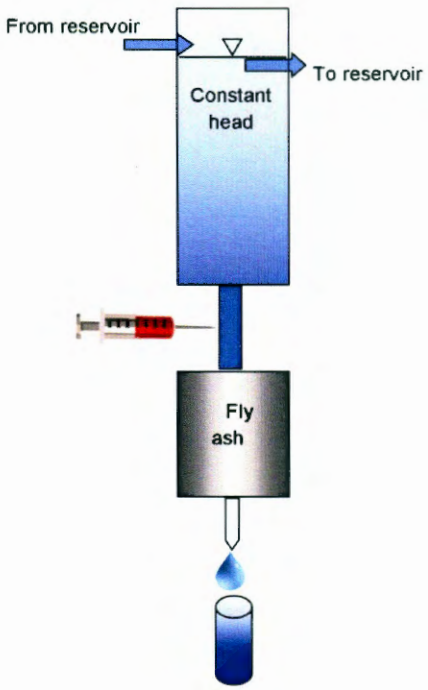

Figure 3.2. Constant head tracer setup.

3.5 Electrical self potential tracer tests and matrix response

Additional tracer tests were performed using saturated solutions of various chloride and bromide salts (Na, K and Li). The self potential was monitored throughout the experiment at five different depths in the permeameter. The chemical response of the matrix of one of the sample series (30 – 34.5 m) during the tracer was also evaluated by ICP-OES. A schematic representation of the experiment setup can be seen in Figure 3.3. The experiment was repeated three times and then followed by a tracer of half the saturated concentration to determine if the behaviour remained consistent. The experiment was done under constant head, to avoid self potential variation due to pressure differences in the carrier fluid. The resulting electrical activity is therefore the result of the electrolyte and interaction with the sample matrix.[7,8]

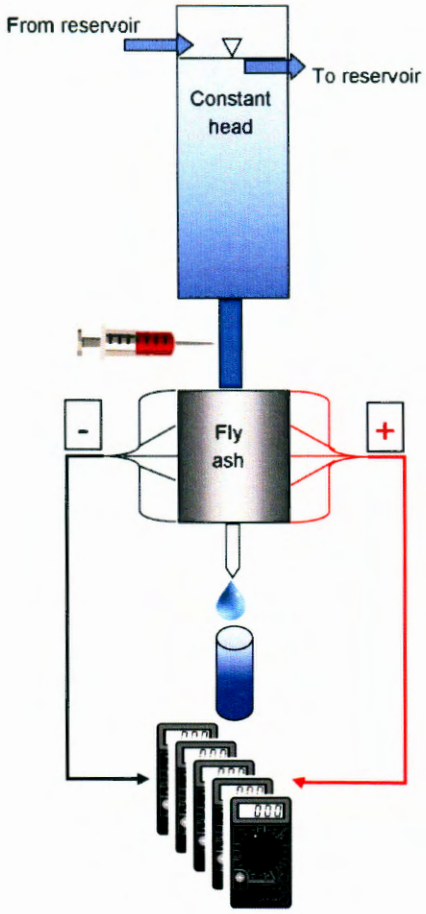

Figure 3.3. Constant head electrical tracer setup.

3.6 Time-lapse electrical resistivity tomography

3.6.1 Introduction

The purpose of the electrical resistivity tomography (ERT) surveys on the Ash Dam at the site was to obtain information on the flow patterns through ash by evaluating the resistivity changes in the subsurface over the time spanned by the surveys. The recorded time-lapse ERT data was used to estimate the horizontal and vertical flow rates.

A brief description of the DC resistivity technique and its two-dimensional application ERT follows:

3.6.2 General description of the electrical resistivity method

The resistivity method is a non-invasive geophysical tool that can provide cost-effective answers to geological questions. The method is based on the fact that different subsurface materials are less or more resistive to electrical current flow. A DC or slowly varying AC current is injected into the earth by means of pairs of grounded current electrodes. The voltage drops between pairs of grounded potential electrodes are then measured at selected positions. These voltage drops are dependent on the resistivities of the materials through which the electrical currents are flowing.

By assuming that the earth is homogeneous and isotropic, measurements of the injected electrical current and measured voltage drops, as well as the distances between the different electrodes, may be used to calculate an apparent resistivity for the earth at a specific position and (pseudo-)depth. The apparent resistivity is an averaged resistivity of the specific resistivities of the subsurface materials through which electrical current flow takes place.

To obtain a model of the resistivity distribution within the subsurface, the calculated apparent resistivity values need to be inverted. During inversion the subsurface is divided into discreet units with distinct resistivities. By means of a mathematical process, the resistivities of the units are adjusted in such a way that the difference between the modelled apparent resistivities and the recorded apparent resistivities are reduced in an iterative process. The modelled resistivity distribution may now be interpreted in terms of the local subsurface conditions by incorporating known information on the site conditions.

3.6.3 Electrical resistivity tomography (ERT)

During ERT surveys resistivity data was recorded along selected profiles at different electrode separations, corresponding to different depths of investigation in order to get a two-dimensional (2D) pseudo-section of the subsurface. The apparent resistivity data was then inverted to obtain two-dimensional models of the resistivity distribution in the subsurface. During 2D inversion, the subsurface was divided into discreet two-dimensional blocks, each with a distinct resistivity. The resistivities of these blocks were adjusted iteratively to minimise the difference between the modelled and observed apparent resistivities.

By repeating the survey along a specific profile after a certain time period, changes in the subsurface resistivity distribution could be identified by comparing the initial and final resistivity sections. This technique is referred to as time-lapse ERT.

3.6.4 Survey geometry and methodology

The survey geometry employed during the time-lapse ERT surveys on the Ash Dam is depicted graphically in Figure 3.4.

An injection pit was dug into the ash at a selected position. Time-lapse ERT data were recorded along two profiles (west/east and north/south), both centred at the injection pit. The time-lapse ERT survey on the ash dam was conducted using the Lund Imaging System with a Wenner geometry and a standard electrode spacing of 1 m in order to record resistivity data with a high spatial resolution.

Due to surface constraints (an embankment and an access road) the north/south profile was limited in its length, extending 12 m to the north and 14 m to the south as measured from the centre of the injection pit. The west/east profile extended 20 m in each direction from the centre of the injection pit. The maximum separation of 40 m between the electrodes on this profile allowed a maximum depth of investigation of approximately 7.5 m (compared to approximately 4.3 m on the north/south profile). Photographs of the survey setup are shown in Figure 3.5 and 3.6.

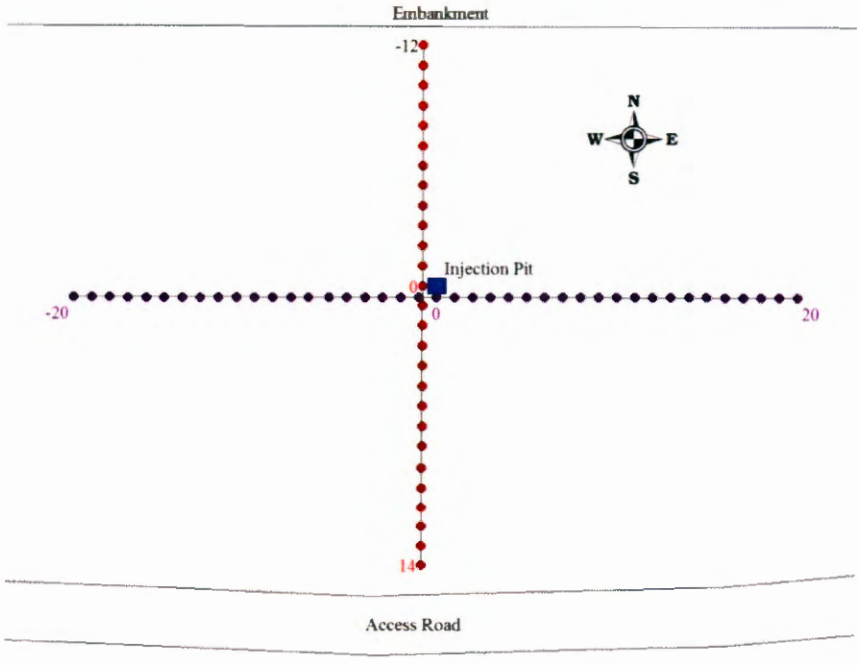

Figure 3.4 Survey geometry employed during the ERT investigations.

Figure 3.5. Photograph of the survey setup (view towards the north-east).

Figure 3.6 Photograph of the survey setup (view towards the east).

The time-lapse ERT survey was conducted over three phases, namely a background investigation phase, and a constant head injection phase followed by a recovery phase. The background investigation phase consisted of ERT surveys on both the west/east and north/south profiles prior to brine injection. The purpose of the background investigation phase was to yield models of the resistivity sections along the two profiles against which the constant head and recovery profiles could be evaluated to investigate the fluid flow patterns through the ash. During the constant head injection phase, the brine level in the injection pit was kept constant at the surface level of the ash by continuous injection of brine (see Figure 3.7). The constant head injection phase lasted 282 minutes (4 hours, 42 minutes).

Figure 3.7 Photograph of the survey setup (view towards the south-east). A constant head level with the ash surface is maintained in the injection pit during the injection phase.

The recovery phase commenced after brine injection was terminated. Sixteen sets of ERT data were recorded along each of the west/east and north/south profiles. The recovery phase of the investigation lasted 2,880 minutes (48 hours).

After acquisition, the recorded ERT data were inverted to obtain models of the subsurface resistivity distribution. Model blocks with widths of half the standard electrode spacing were employed during inversion to model the spatial distribution of resistivities.

3.7 Geological setting

The site is underlain by rocks belonging to the Vryheid Formation of the Ecca Group and Karoo Supergroup. These rocks primarily consist of sandstones, shales and coal beds and are extensively intruded by dolerites of the Jurassic age. The dolerites occur both as sills and linear dyke structures that may extend over tens of kilometres. The ash dam is predominantly underlain by Karoo sediments overlying a dolerite sill in some areas with a large lateral extent.[9] Alluvial deposits of Tertiary and Quaternary age also occur to the east and north of the ash dam where a number of non-perennial rivers are located. No major fault zones or linear, dyke-like intrusions have been mapped in the vicinity of the ash dam.

3.8 Conclusion

The methods discussed in the previous sections of this chapter were used to attempt to develop a conceptual understanding of the geochemical and flow characteristics of fluids moving through a fly ash dam. This was done in field and laboratory scale experiments, producing an estimation of susceptibility to change. The mineral identification as well as the mobility of elements in the ash and flow parameters will be discussed in Chapter 4. The results from the self potential tracers and subsequent matrix response will follow in Chapter 5.

3.9 References

[1]Ross, D., 1995, *Recommended soil testing procedures for the northeastern United States*, 2nd Ed., Northeastern regional publication No. 493, 95.

[2] USEPA - *Guide for industrial waste management, Chapter 2 – Characterizing waste.*

[3] USEPA, 1999, *Announcement of public meeting on the development of new waste leaching procedures under the RCRA program*, Federal register, Vol. 64, No. 100.

[4] Poon, C.S. and Chen, Z.Q., 1999, *Comparison of the characteristics of flow-through and flow-around leaching tests of solidified heavy metal wastes.*, Chemosphere, vol 38, No. 3.

[5]Xiandeng, H., and Jones, B.T., 2000, I*nductively coupled plasma/optical emission spectrometry. Encyclopedia of analytical chemistry.*, R.A. Meyers (Ed.), 9468–9485.

[6]Käss, W., 1998, *Tracing technique in geohydrology*. A.A Balkema Publishers, Rotterdam, 581.

[7] Cooper, S. S., Koester, J. P. and Franklin, A. G., 1982, *Geophysical investigation at Gathright dam*, Miscellaneous paper GL-82-2, US army engineer waterways experiment station, Vicksburg, MS.

[8] Ahmad, M., 1964, *Laboratory study of streaming potential*, Geophysical prospecting, 12, 49-64.

[9] The Council for Geoscience, classified map.

Chapter 4

Results and discussion

4.1 Introduction

In this chapter the results from the various experiments in Chapter 3 are presented and discussed. The sample volume of the fly ash from the study area was limited, therefore the experiments were done in 9 sections of increasing depth. In the following sections of this chapter the chemical composition of the ash (Section 4.2), leaching characteristics and the mobility of elements native to the ash (Section 4.3) are discussed. Transport parameters were obtained through tracer tests in the laboratory (Section 4.4) and a geophysical study in the field (Section 4.5).

4.2 Mineral identification

4.2.1 X-ray diffraction (XRD)

The fly ash was found to consist of the mineral assemblages, mullite ($Al_{4.75}Si_{1.25}O_{9.63}$), alpha quartz ($SiO_2$), calcite ($Ca(CO_3)$), ferroan-dolomite ($Ca(Mg,Fe)(CO_3)_2$) and muscovite ($KAl_3Si_3O_{10}(OH)_2$). Mullite may be present as a high temperature decomposition product of muscovite originating from an alkali-poor peraluminous melt (kaolinite).[1,2,3] The calcite and dolomite found may be present as a weathering product of lime (CaO) interacting with carbon dioxide.[4,5] Figure 4.1 shows the XRD spectrum for crystalline minerals identified in the ash.

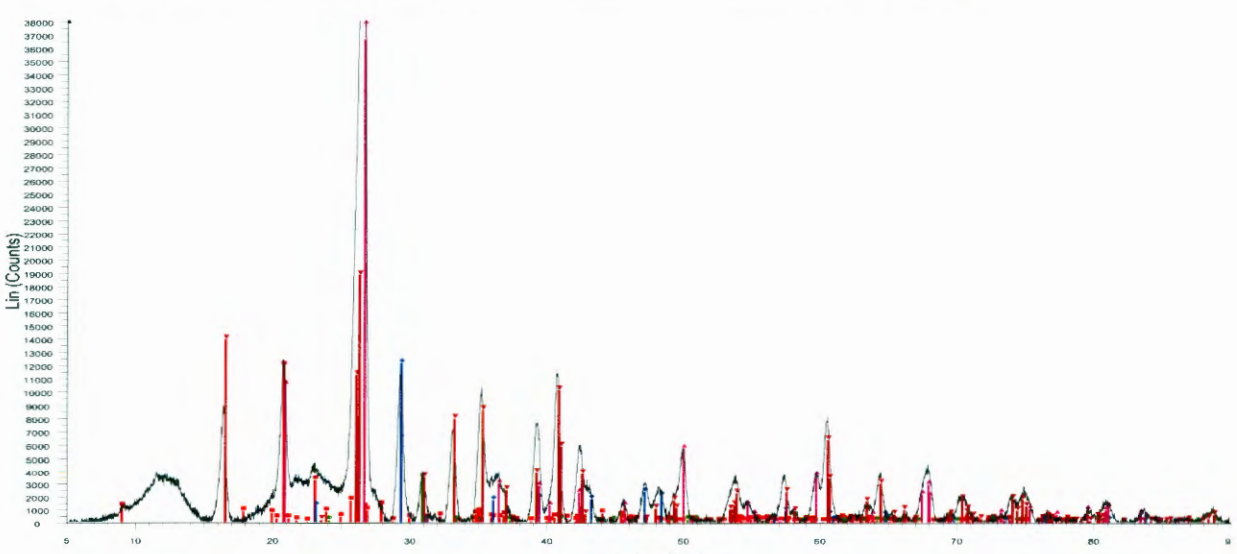

Figure 4.1 Mineral identification of a fly ash sample by XRD with mineral assemblages indicated by colour. Red = muscovite, green = dolomite ferroan, blue = calcite, brown = mullite and pink = quartz.

In Figure 4.2 a comparison of the different samples can be seen before leaching. Figure 4.3 shows the XRD spectra of the 9 depth groups after leaching.

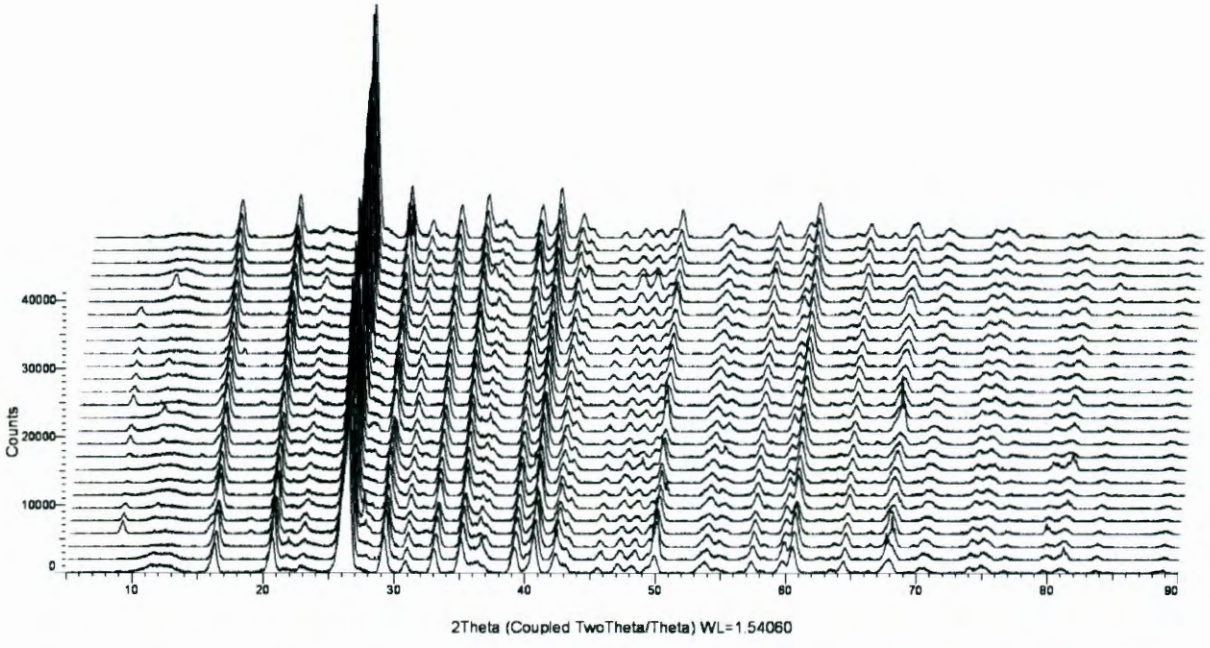

Figure 4.2 XRD spectra of the fly ash samples from different depths, before leaching, with increasing depth from the front to the back.

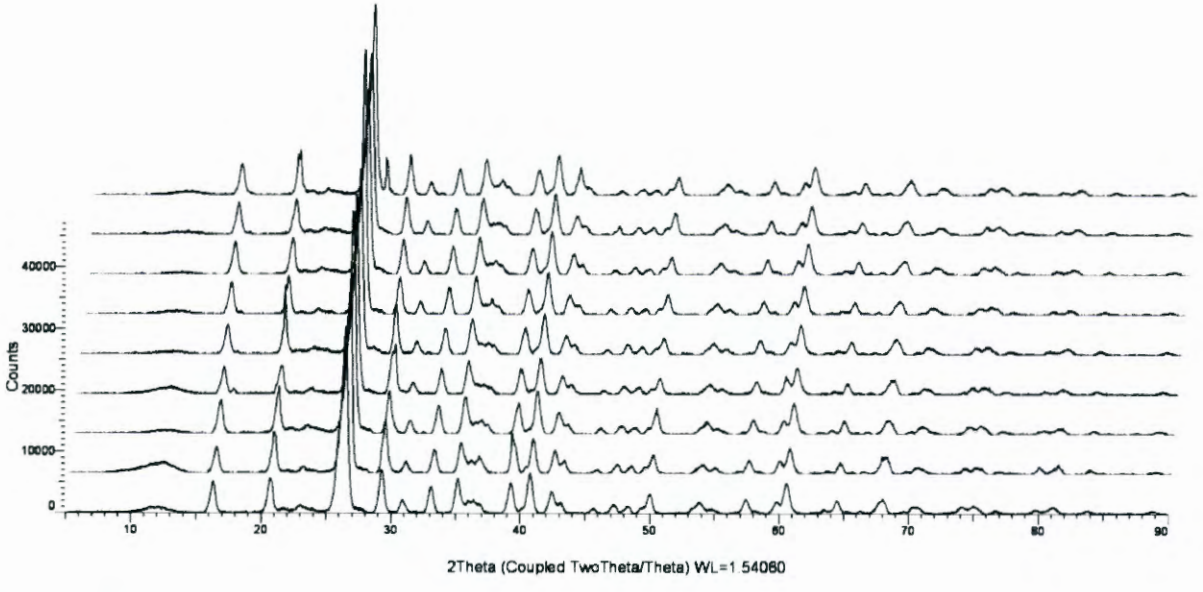

Figure 4.3 XRD spectra of the fly ash samples from the 9 different depth groups, after leaching, with increasing depth from the front to the back.

Figure 4.4 shows the XRD spectra, comparing a selected sample of the fly ash before and after leaching. It is clear that there is little to no change in the ash composition during leaching and that it is fairly mature, indicated by the presence of carbonates.

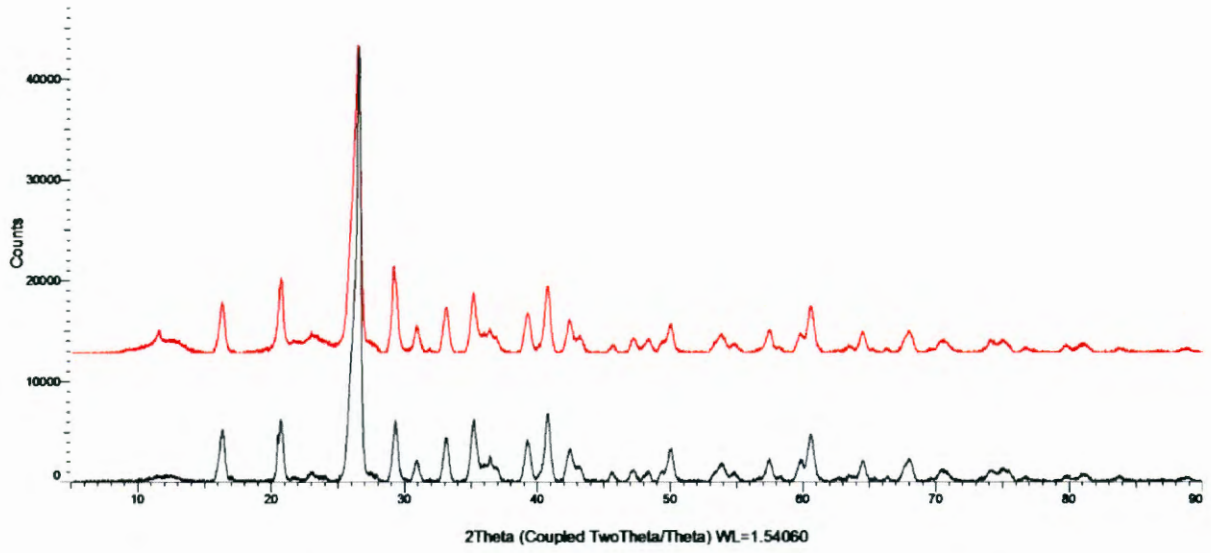

Figure 4.4 XRD spectra, comparing a selected sample of the fly ash before (red) and after (black) leaching.

It should also be noted that fly ash may consist of a large component of amorphous glass which does not have regular arrays of atoms that produce definitive peaks in XRD patterns.[6,7] This amorphous glass component may also be a major host within the ash for adsorbed trace elements, which may be leached to the surrounding environment.[7] Several ash properties, including particle density and particle surface area affect the glass composition.

Although not done in this study, the relative abundance of the glass fraction in addition to its composition is important for evaluating interactions with water at ash disposal sites, but this usually ranges between 40 - 60 %.[7,8] Since the structure did not significantly change during leaching, the crystalline fraction of the ash consists of species in equilibrium with the environment, which may either be newly formed or remnants of minerals in the parent coal.

4.2.2 Scanning electron microscope (SEM) investigation

The scanning electron micrograph of fly ash showed the presence of solid spheres, cenospheres (Fe-Ca-Al silicate glass with trace amounts of Ti, K and Mg) as well as porous structures (coal remnants) and crystalline material (quartz and clay minerals). From these studies it was found that the chemical composition of the fly ash particles were similar to that found in literature,[9] consisting mainly of the oxides of Si, Al, Ca, Mg, Fe, and minor P, Na, K and Ti.[10] Figure 4.5 and 4.6 shows SEM images of the 21 – 24 m depth section before and after leaching respectively.

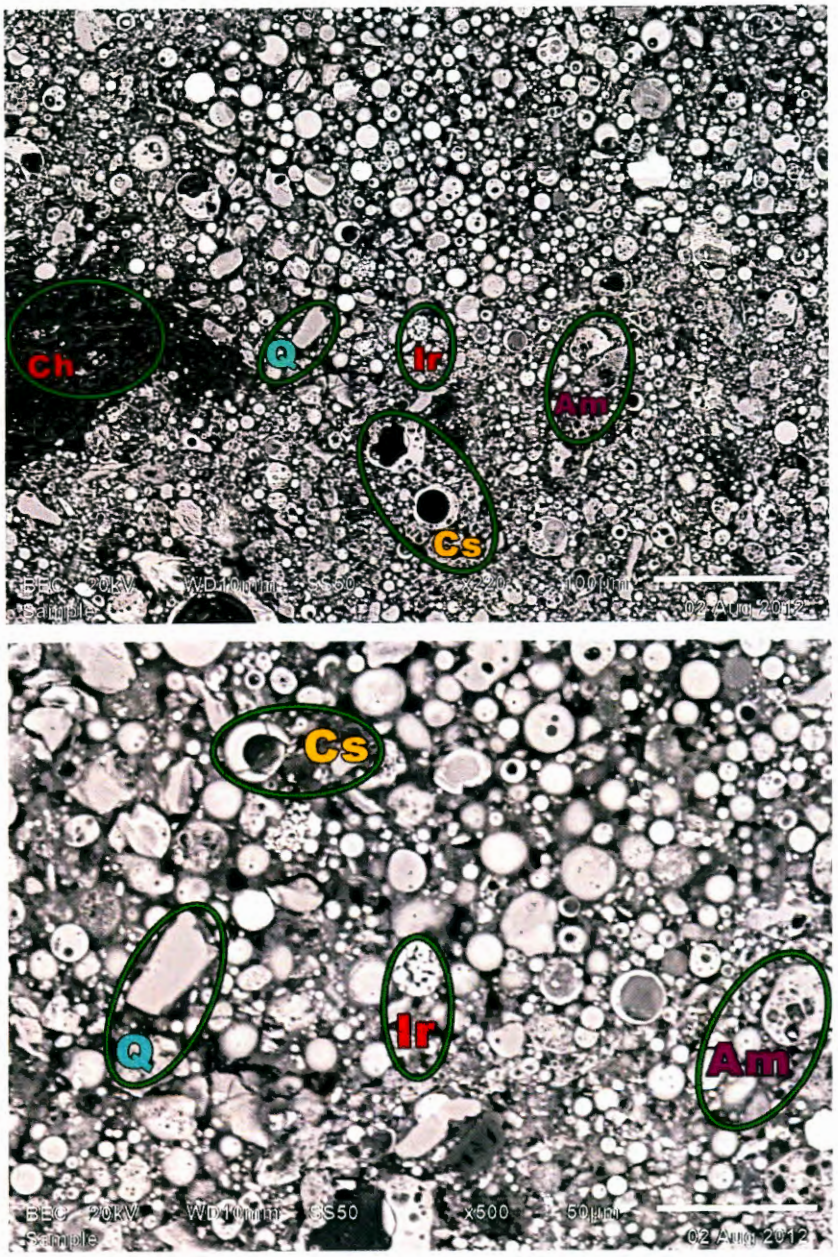

Figure 4.5 Scanning electron microscope images of a fly ash sample of the 21-24 m depth section prior to leaching white bar = 100 µm (top) and 50 µm(bottom). Ir = iron rich spheres, Cs = cenospere, Q = quartz, Am = amorphous material and Ch = char particle.

It was also found that there was a relative decrease in CaO and MgO, accompanied by a relative increase of SiO_2, Al_2O_3 and Fe_2O_3 during leaching. This may be due to the dissolution of the CaO and MgO or decomposition carbonates thereof from the surface of the particles, as well as the simultaneous increase of more resistant species like SiO_2 and Al_2O_3.[11,13] It was also clear that the particles retained the same distinct spherical shape after leaching.

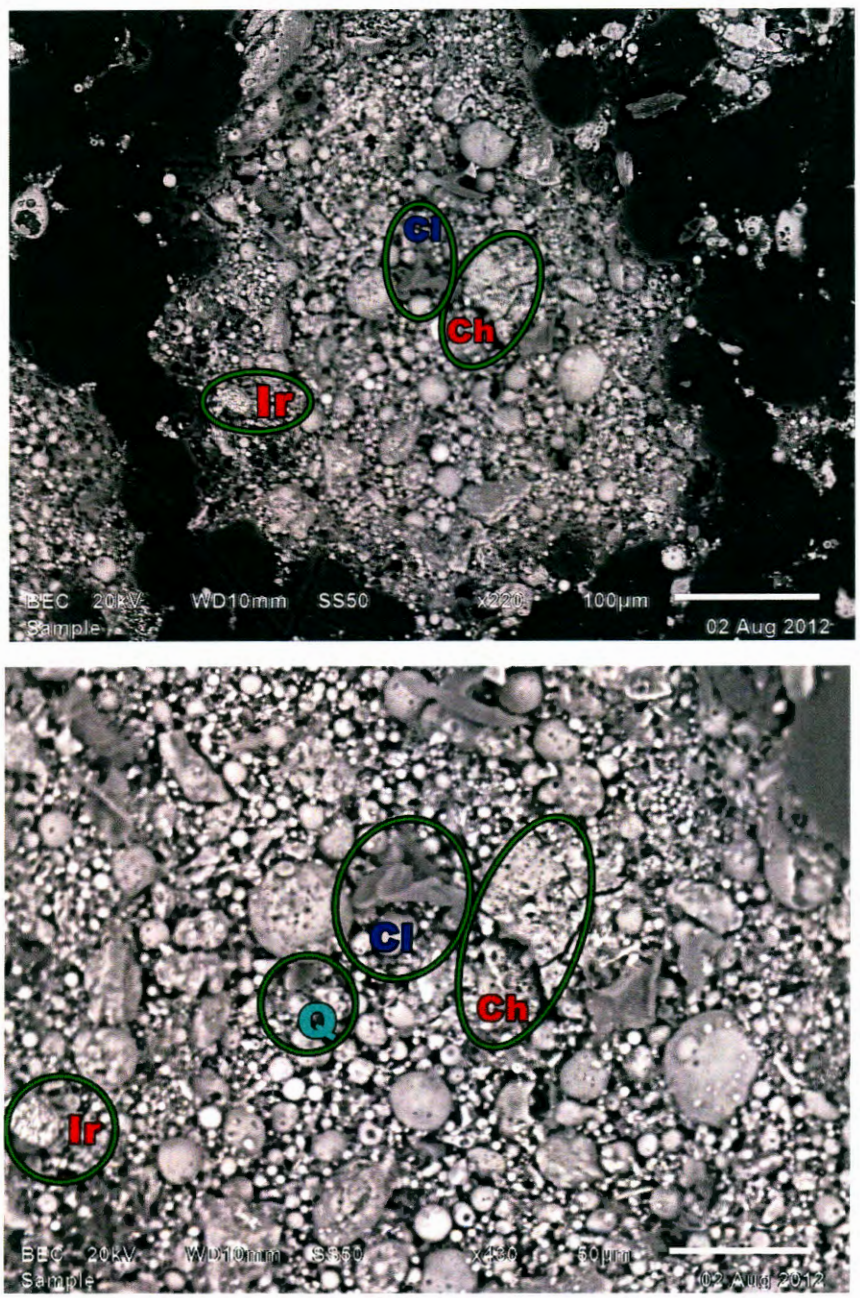

Figure 4.6 Scanning electron microscope images of a fly ash sample of the 21-24 m depth section after leaching white bar = 100 µm (top) and 50 µm(bottom), with Q = quartz, Cl = clay particle, Ir = iron rich spheres and Ch = char particle.

The change in composition for the investigated depth section evaluated by SEM can be seen in Figure 4.7 (top section) compared to the composition of fresh ash found in literature,[6] determined by XRF (bottom section). Although these are two different methods, the results correlate.

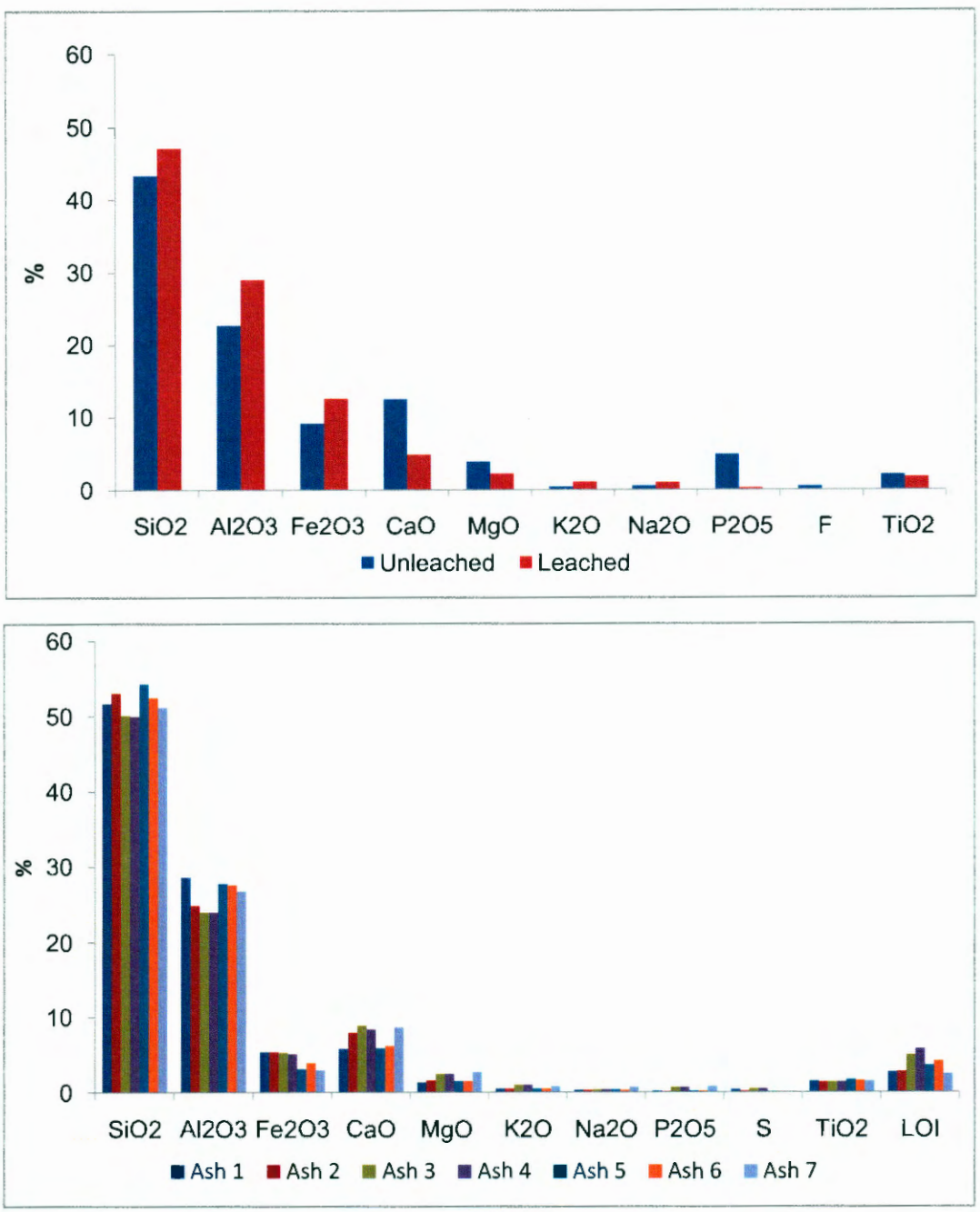

Figure 4.7 Top: Chemical composition of a fly ash sample before (blue) and after leaching (red) analysed by SEM. Bottom: Chemical composition of similar fly ash analysed by XRF.

4.3 Chemical analysis

4.3.1 Cation exchange capacity (CEC)

The cation exchange capacity experiment was done to determine the amount of exchangeable cations available at the surface of the raw fly ash samples. The results of the experiment can be seen relative to depth in Figure 4.8 and accompanied Table 4.1. Due to the limited sample volume, the CEC for the sample series 0 – 3 m could not be determined. The results indicate that the upper part of the profile has a lower cation exchange capacity than the deeper parts. There is however a slightly lower cation exchange capacity in the 18 – 21 m depth section. This may be the result of a relatively lower amount of magnesium found in this section or that more carbonate minerals have formed in this area, reducing the CEC.[12]

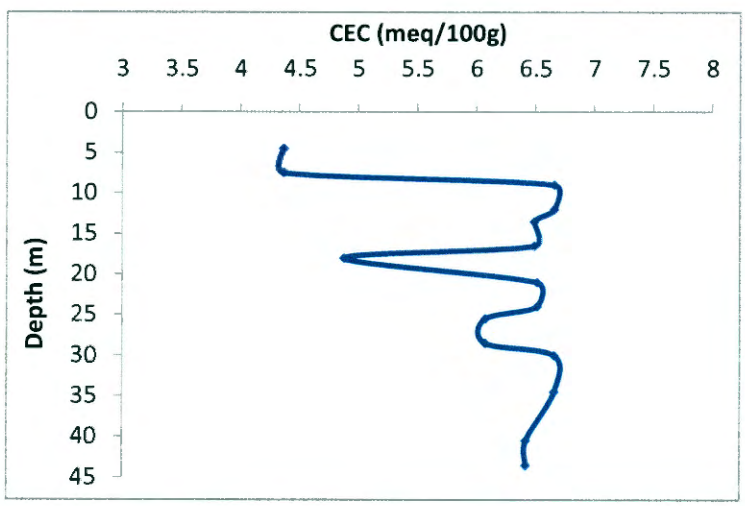

Figure 4.8 Cation exchange capacities relative to depth.

Table 4.1 Cation exchange capacities of the fly ash samples.

Depth (m)	Avg CEC (meq/100g)	Avg CEC (mmol/kg)
0 – 3	-	-
4.5 - 7.5	4.4	43.7
9 - 12	6.7	66.6
13.5 - 16.5	6.5	64.9
18 - 21	4.9	48.8
21 - 24	6.5	65.1
25.5 - 28.5	6.1	60.8
30 - 34.5	6.7	66.6
40.5 - 43.5	6.4	64.2

4.3.2 Leaching characteristics

4.3.2.1 Elemental concentration and mobility variation with depth

In this section, the elemental concentration of the major constituents of the leachate and its variation with depth may be observed. Those elements not detected were taken as half the detection limit. The relative mobility with depth of these elements is illustrated by showing the comparative difference in concentration of the first and last leachate samples taken, indicating the average elemental concentration before (blue) and after leaching (red) in the 9 sample depths (0 - 3 m, 4.5 - 7.5 m, 9 - 12 m, 13.5 - 16.5 m, 18 - 21 m, 21 - 24 m, 25.5 - 28.5 m, 30 - 34.5 m, 40.5 - 43.5 m). Thus, those elements with major differences are more mobile than those with minor differences in concentration in the first and last leachate. Figure 4.9 illustrates the data for SO_4 as an example of the typical leaching behaviour observed.

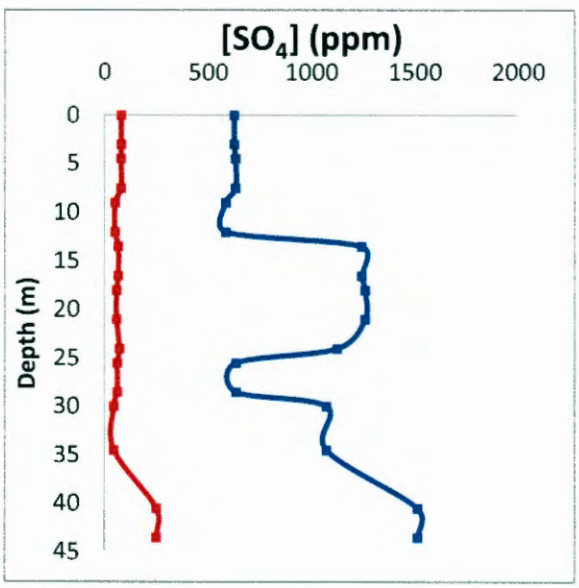

Figure 4.9 elemental concentration of SO_4 with depth for the first (blue) and last (red) leachate samples.

The main constituents of the first leachate collected correspond to those found for process waters in literature,[13] consisting mainly of SO_4, Na, Cl, K, Ca and B. There is however an additional alkaline component and the leachate is more enriched in trace elements Al Cr Se, Mo, Mn and V. This may be due to the weathering of the alkaline metal oxides, as mentioned in Section 4.2.1 and the continuous dissolution of the aluminiosilicate glass.

A higher concentration of alkaline species, Al, F, Si and Se was found in the 9 – 12 m section, whereas higher concentrations of Fe and Mn were found in the 25.5 – 28.5 m section compared to the other samples. Lower concentrations of Cl, Mn, B and Cu were found at 9 – 12 m, whereas Ca, Mg, Na, K, Cl, SO_4, F, Al, Ba, Si, Cr, Cu, Zn, Ni, B, Li, Mo, Co, Se and alkalinity concentrations were found at 25.5 – 28.5 m. The average concentration of the first and last leachate samples taken for the respective sections can be seen in Table 4.2.

Table 4.2 Average elemental concentrations of the first and last leachate samples collected.

Element	[Avg First] (ppm)	[Avg Last] (ppm)
SO4	9.7E+02	8.5E+01
Cl	4.0E+02	1.0E+01
MAlk	8.0E+01	4.9E+01
Palk	3.9E+01	2.4E+01
F	1.6E+00	1.0E+00
Na	5.6E+02	2.8E+01
Ca	1.5E+02	2.5E+01
K	5.1E+01	5.5E+00
Si	3.1E+00	3.2E+00
Al	1.3E+00	1.9E+00
B	5.2E+00	1.1E+00
Mg	1.6E+01	1.9E+00
Li	2.2E+00	1.2E-01
Cr	1.1E+00	4.3E-02
Mo	4.6E-01	1.6E-02
V	1.9E-01	1.4E-01
Ba	8.8E-02	7.3E-02
Se	8.1E-02	7.9E-03
Cu	7.2E-02	9.6E-03
Ni	7.0E-02	5.1E-03
Co	1.3E-02	9.9E-04
Fe	3.1E-02	1.5E-02
Mn	2.0E-02	8.0E-03
Zn	3.4E-02	1.1E-02

These results indicate that the elements can be classified into 4 groups based on their variation in concentration with relation to depth and leaching behaviour.

Group 1

Si, Al, F and (Alkalinity - hydroxyl (OH^-), bicarbonate (HCO_3^-) and carbonate (CO_3^{2-})) also showed a decrease in concentration with depth, although Si Al and F were found to be increasing during leaching. The decrease in of pH with depth may be due and interaction of the ash with the brine components over time, also favouring the mobility of elements encapsulated in the ash matrix, by continuous dissolution of the aluminosilicate glass components.[13] These components were also found to be enriched in the 9 – 12 m section and showed little to no difference in concentration, as can be seen in Figure 4.10.

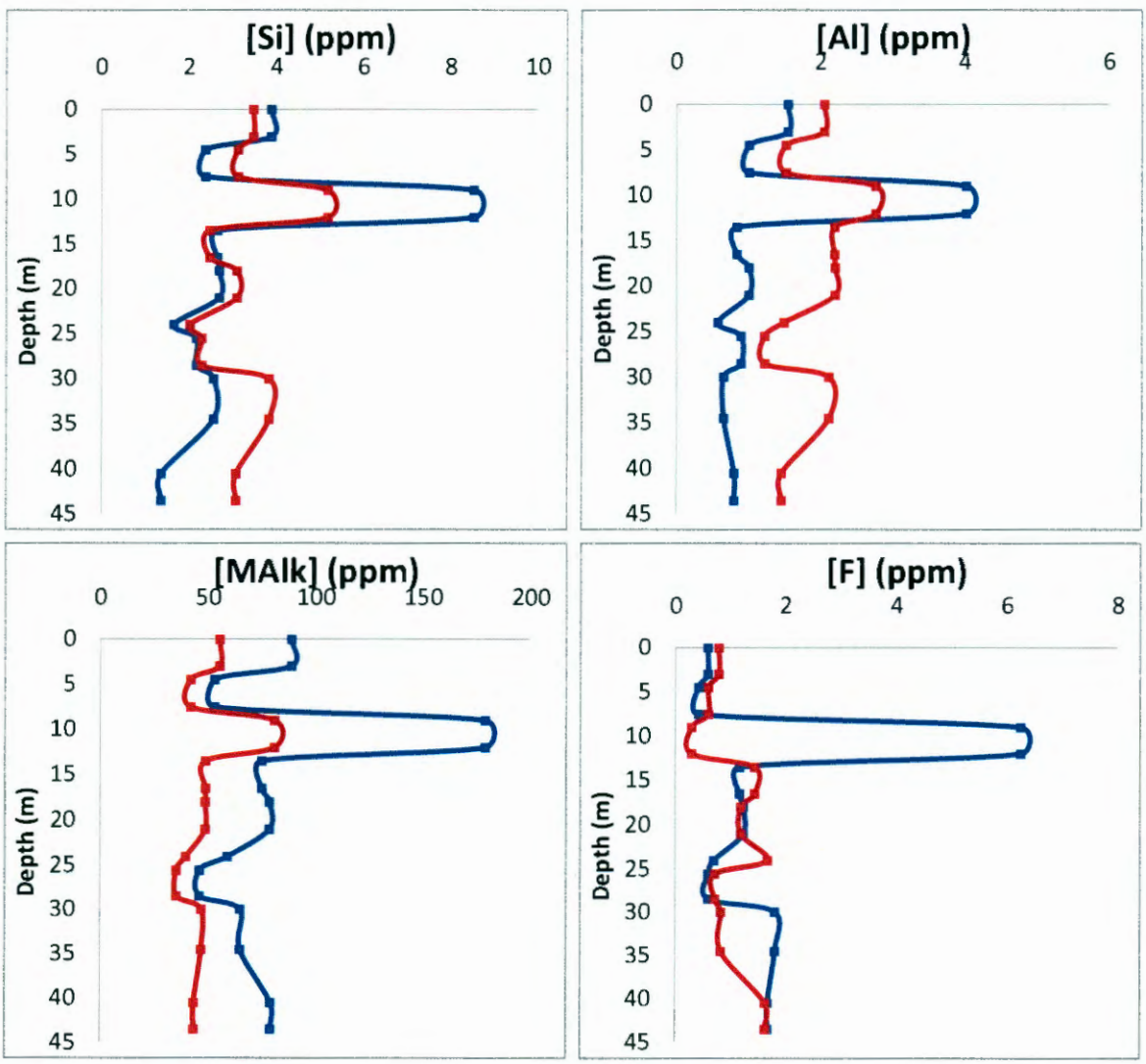

Figure 4.10 Elemental concentration variation with depth for Si, Al, M-Alkalinity and F.

Group 2

Observable trends also indicated an increase in the concentrations of SO_4, Ca, Na, K, Cl, Ni, Zn, B, Mo and Ba with depth. These elements were found to undergo rapid dissolution. Ca was found to be least concentrated in the 9 – 12 m section. Mg, Li and Fe also showed an increase in concentration with depth although Li and Mg were found to be most concentrated in the deepest sample section (40 – 43.5 m). Zn was found to be most concentrated in the section 18 – 21 m. The concentration profiles for Ca, Mg, Li and Fe can be seen in Figure 4.11.

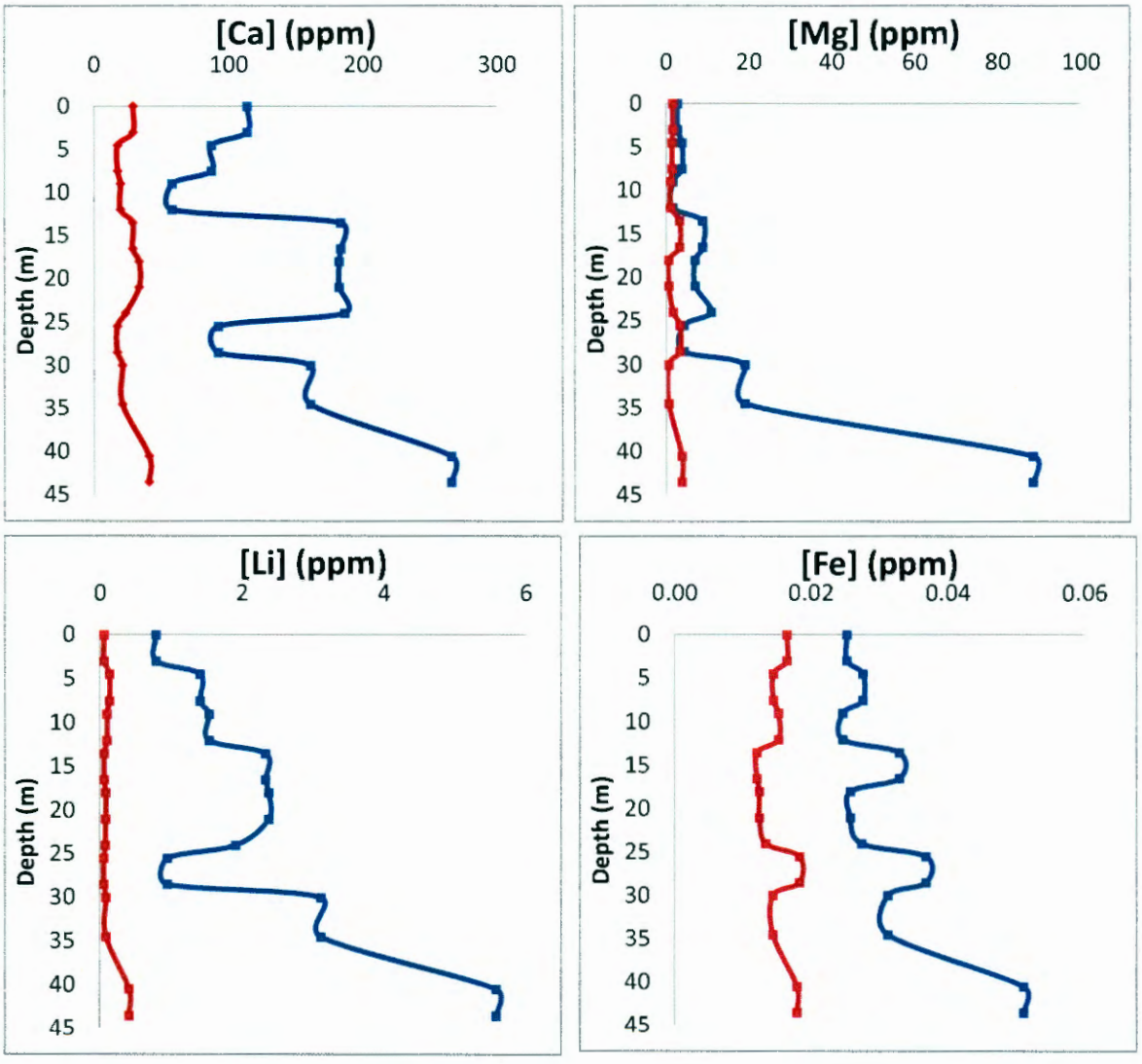

Figure 4.11 Concentration profiles for Ca, Mg, Li and Fe.

Group 3

An overall decrease in Cr, Co, V, Mn, Se and Cu concentration with increasing depth was distinguishable. Ba was also found to have increased in concentration in sections 18 – 21 and 21 – 24 m, whereas V was found to have increased in concentration in the sections 4.5 – 7.5 m and 13.5 – 16.5 m during leaching. Mn showed the general leaching behaviour, although its lowest concentration was found in the deepest sections 30 - 34.5 m and 40.5 - 43.5 m. The concentration profiles for Co, Mn, Ba and V with increasing depth can be seen in Figure 4.12.

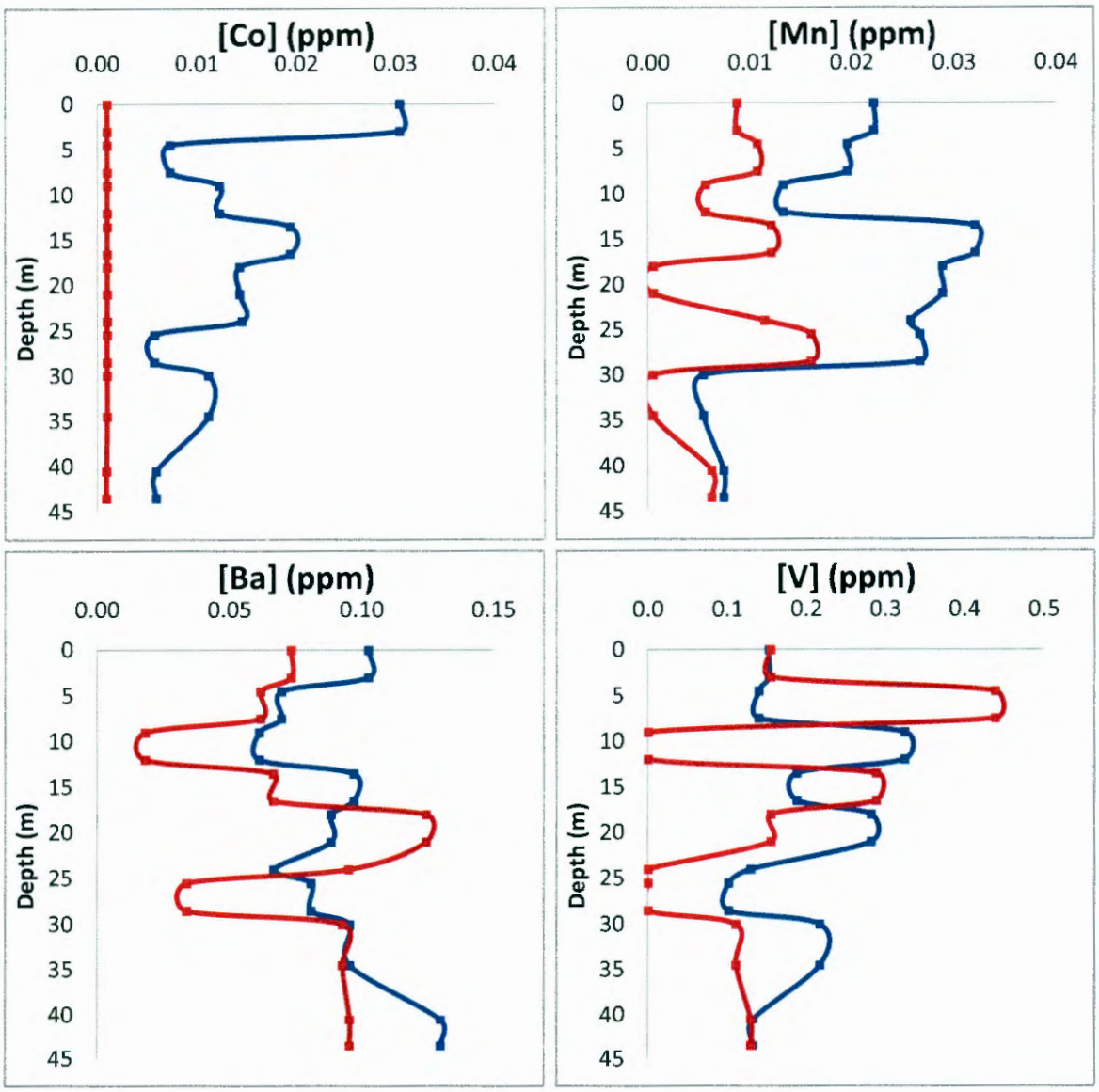

Figure 4.12 Concentration profiles for Co, Mn, Ba and V with increasing depth.

4.3.2.2 Change in leachate composition

In Figure 4.13 below the average concentration of elements of the first (left) and last leachate (right) collected for the major (top) and minor (bottom) components found in the 9 depth groups are illustrated. The line graphs on the subsequent page illustrate the change in composition of the various depth sections.

The first leachate solutions were found to be high in SO_4, Cl, Na and Ca, whereas the last leachate samples were much more alkaline and Ca rich. Thus, the initial contribution from chloride (Cl^-) and sodium (Na^+) is substituted by carbonates (HCO_3^-, CO_3^{2-}) and calcium (Ca^{2+}) respectively in the final leachate samples. This can be explained by the rapid release of the halide species from the system which are then replaced by calcium carbonate and sulphate species. As for the minor components, Li and Cr are dominant in the first leachate samples, after which Li and V becomes predominant.

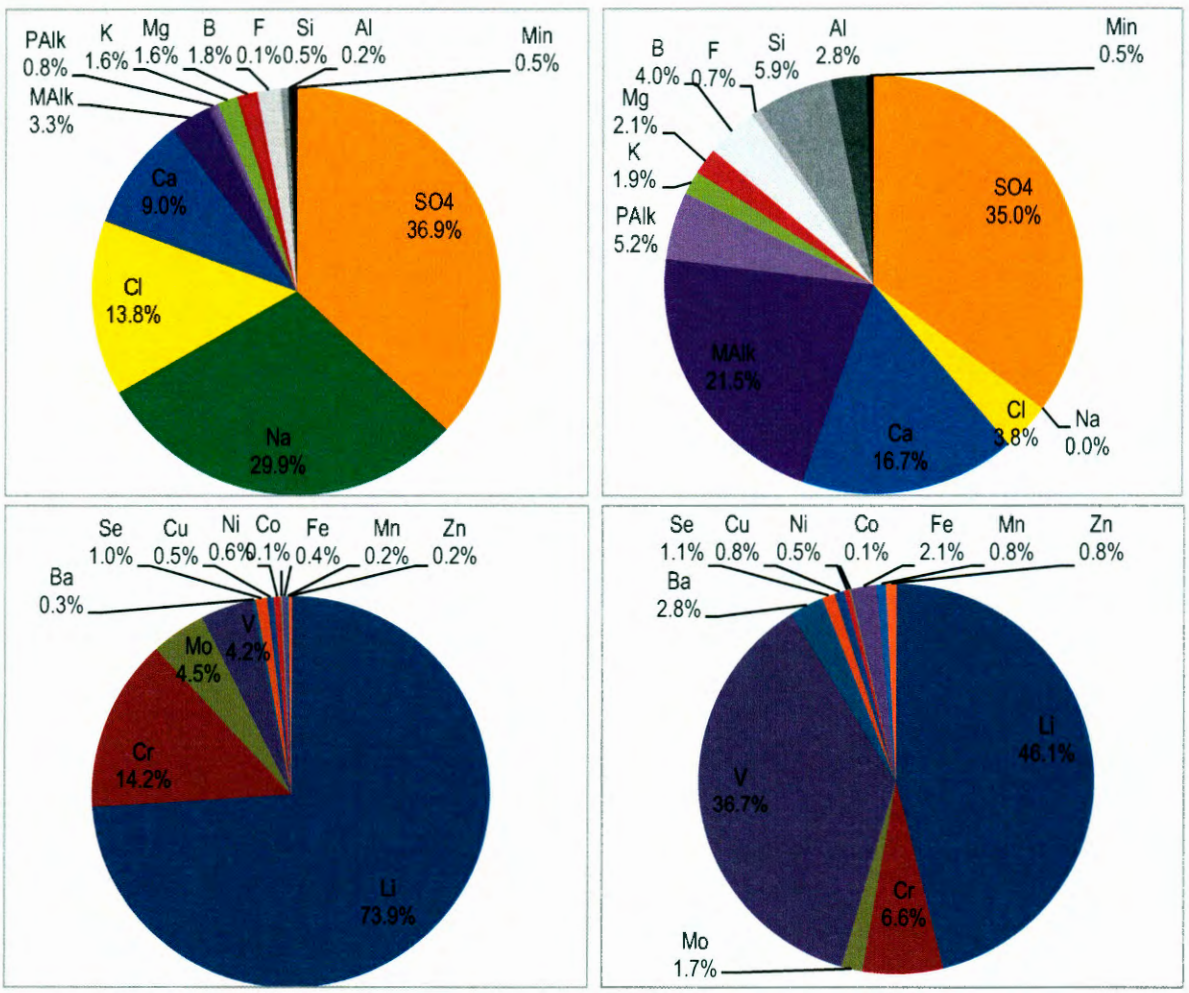

Figure 4.13 Change in average composition from the first (left) and last (right) leachate samples taken for the major (top) and minor (bottom) components.

The expanded durov diagram below (see Figure 4.14) illustrates that the produced leachate corresponds to that of effluent found at power stations and coal mines. It also shows the evolution of the leachate from Na, Cl, Ca and SO_4 rich water to Ca Alkaline rich water.

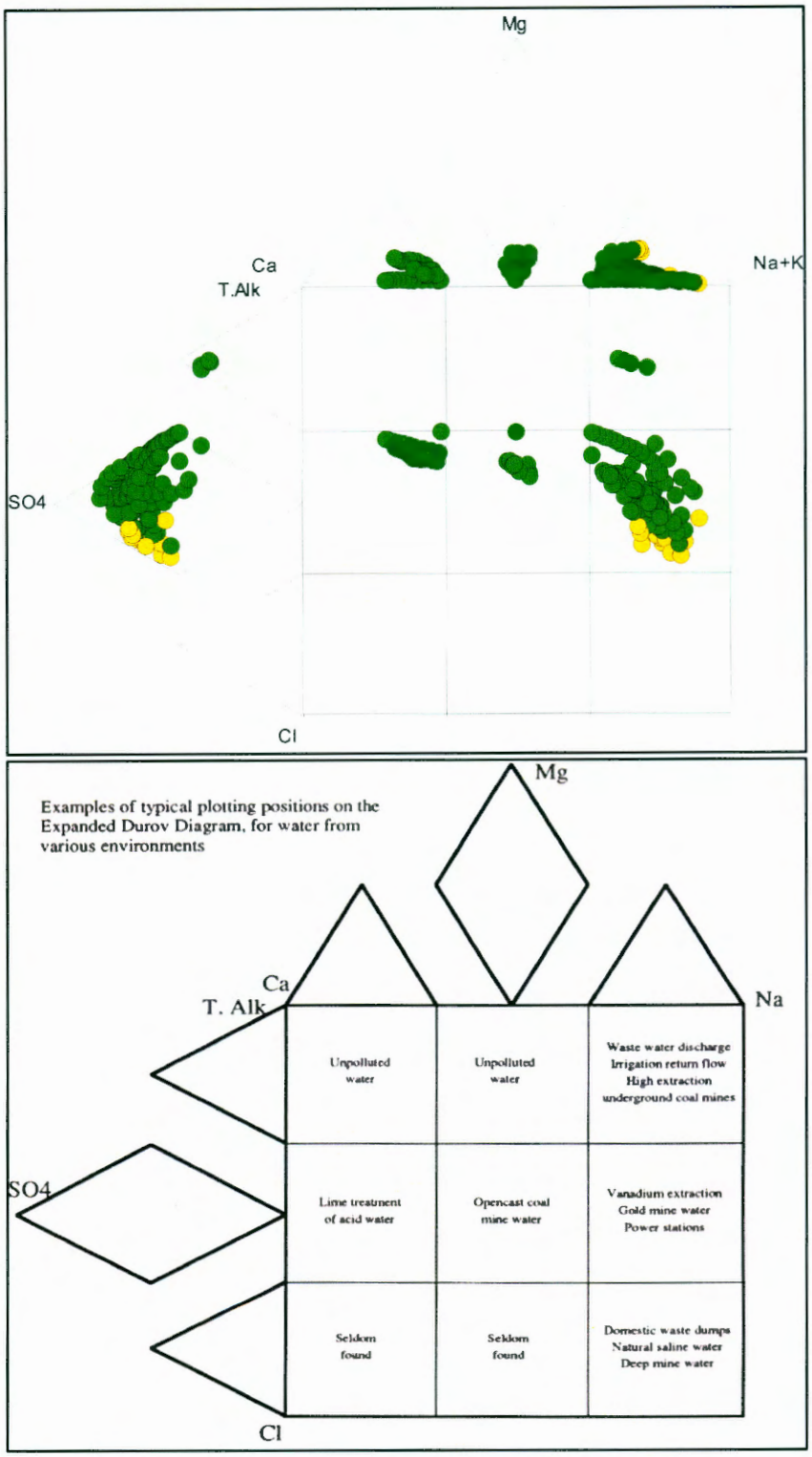

Figure 4.14 Expanded durov diagrams illustrating the change in leachate composition and related waters.[14]

4.3.2.3 Salt load and release rate

The load is a measure of the mass flux of a chemical and gives an indication of the degree to which the composition of water interacting with the fly ash can change. The load, L, is obtained by taking the product of the concentration, C (mg/l), and the flow rate, Q (l/s), thus giving the rate of release over time (mg/s):

$$L = C \cdot Q$$

The trends observed were that the load showed an exponential decrease over time, accompanied by a decrease in flow rate. Only the 30.5 - 34.5 m section showed an increase in flow rate over time. The salt load of the various depth sections over time (mg/s) can be seen in Figure 4.15.

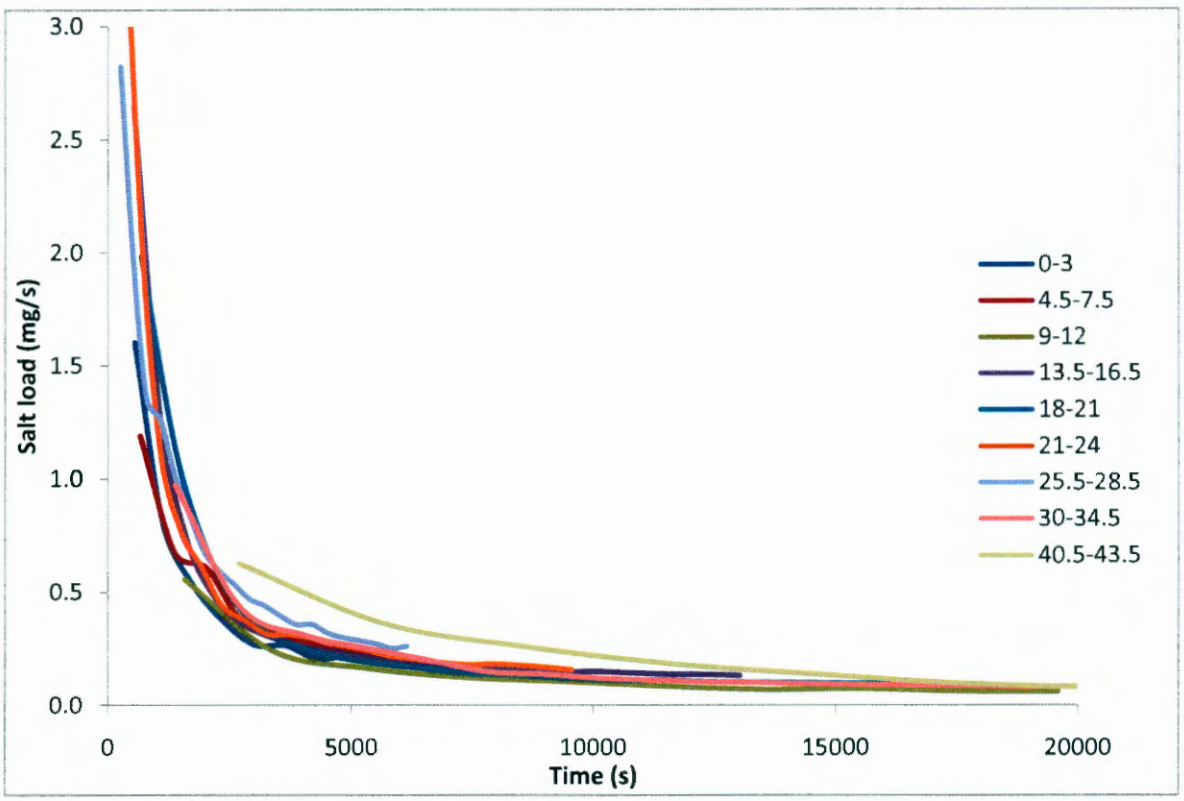

Figure 4.15 Salt loads of the various depth sections over time (mg/s).

The elements in selected sections showing the concentration of the first (blue) and last (red) leachate samples collected can be seen in Figures 4.17 – 4.19.

The average load (in tonnes per day) and TDS with increasing depth is illustrated in Figure 4.16 left and right respectively. By comparing the two graphs, the following may be deduced:

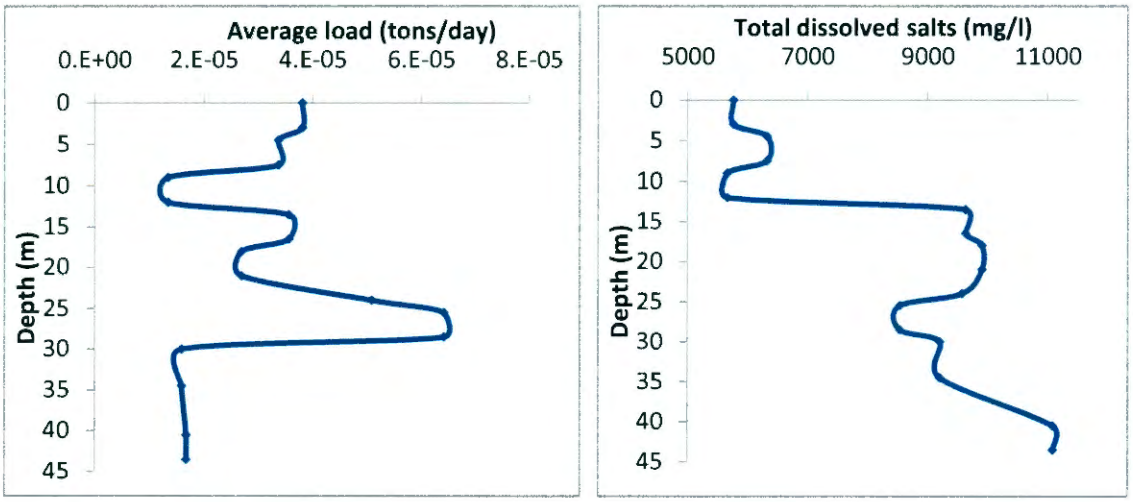

Figure 4.16 Average load (left) and TDS (right) with increasing depth.

The average load at the surface is moderate as less weathering has occurred (younger ash). This may be due to intermittent rainfall as there is a larger amount of alkaline species that may still be leached from this section, although more mobile elements such as Na and Cl have been leached alternatingly in the first 12 m. The leached upper part is followed by a water table or saturated section indicated by an increased concentration of the more mobile components.

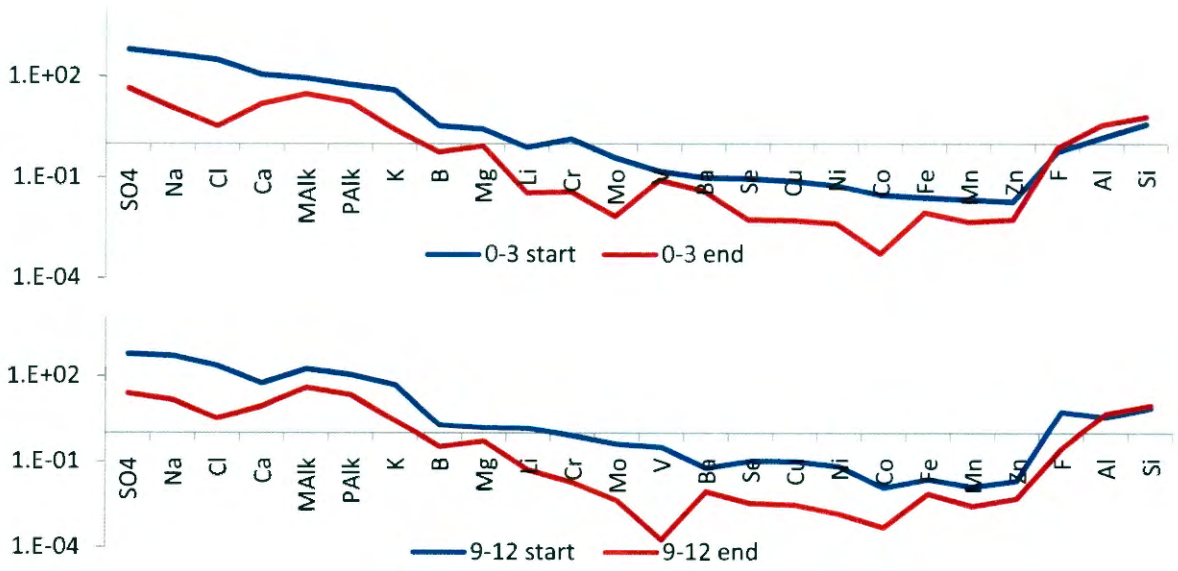

Figure 4.17 Concentration of elements for the sections 0 – 3 (top) and 9 – 12 m first (blue) and last (red) leachate.

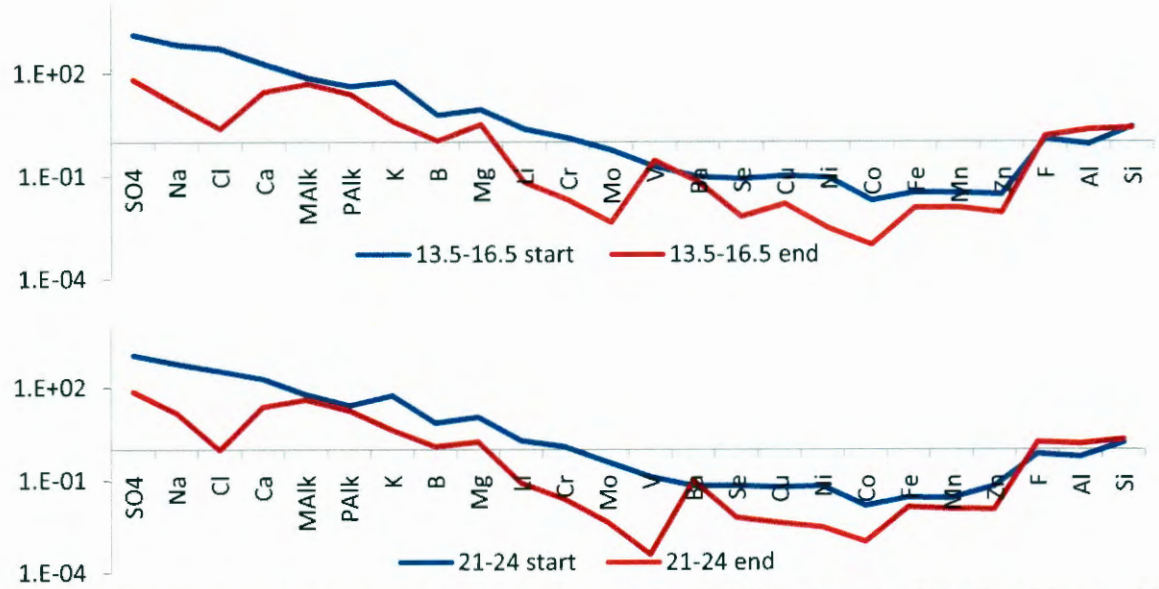

Figure 4.18 Concentration of elements for the sections 13.5 – 16.5 (top) and 21 – 24 m first (blue) and last (red) leachate.

A seepage face or area of high permeability found at 25 – 28.5 m may be the result of seasonal changes causing the formation of salt cracks as the section has a high release potential and small change in alkalinity, Si and Al, meaning a less reactive ash. Below the area of high permeability TDS increases at a low load, indicating a highly saturated ash. The same trends were observed for the leaching behaviour in the major and minor components of the collected leachate. The results of the average release rates of the major (left) and minor (right) components of the collected leachate can be seen in Figure 4.20.

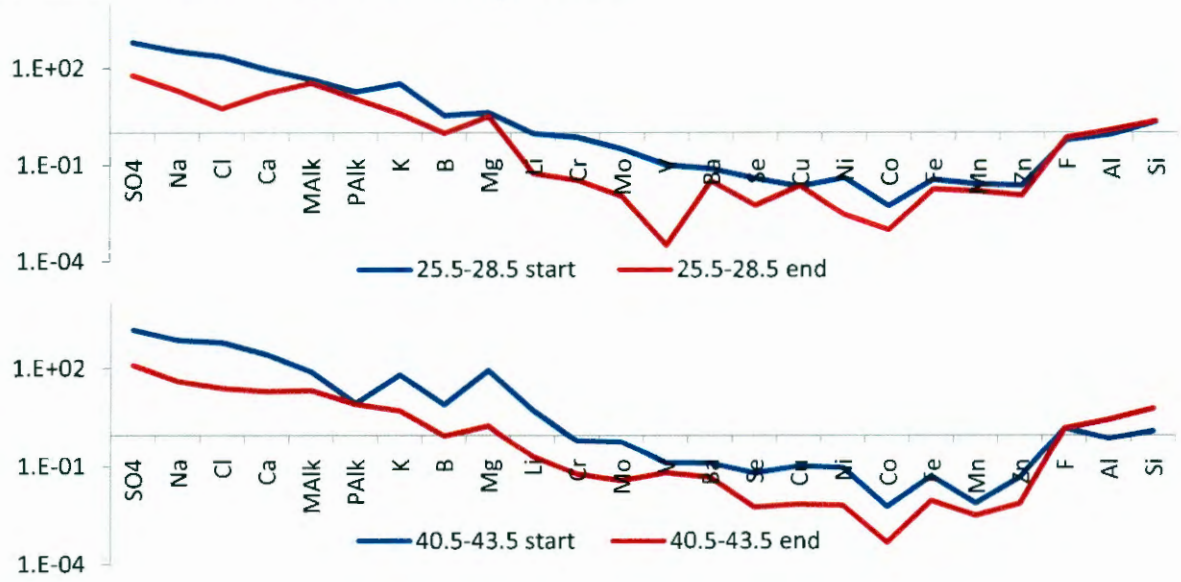

Figure 4.19 Concentration of elements for the sections 25.5 – 28.5 (top) and 40.5 – 43.5 m first (blue) and last (red) leachate.

The salt balance of the fly ash was calculated and the experimental data indicates that if water is allowed to infiltrate the system uninterrupted (constant head permeameter) that the fly ash would release the majority of its captured salt in a short period of time. The majority of ions released would be in the form of sodium, chloride and carbonates and to a lesser extend calcium, sulphate and potassium ions. Possible trace elements that could pose problems in the environment are fluoride, bromide, aluminium, chromium, molybdenum, barium, manganese and vanadium. A further cause for concern specifically is the presence of high levels of lithium and boron ions in the leachate as these are most concentrated in the deeper levels.

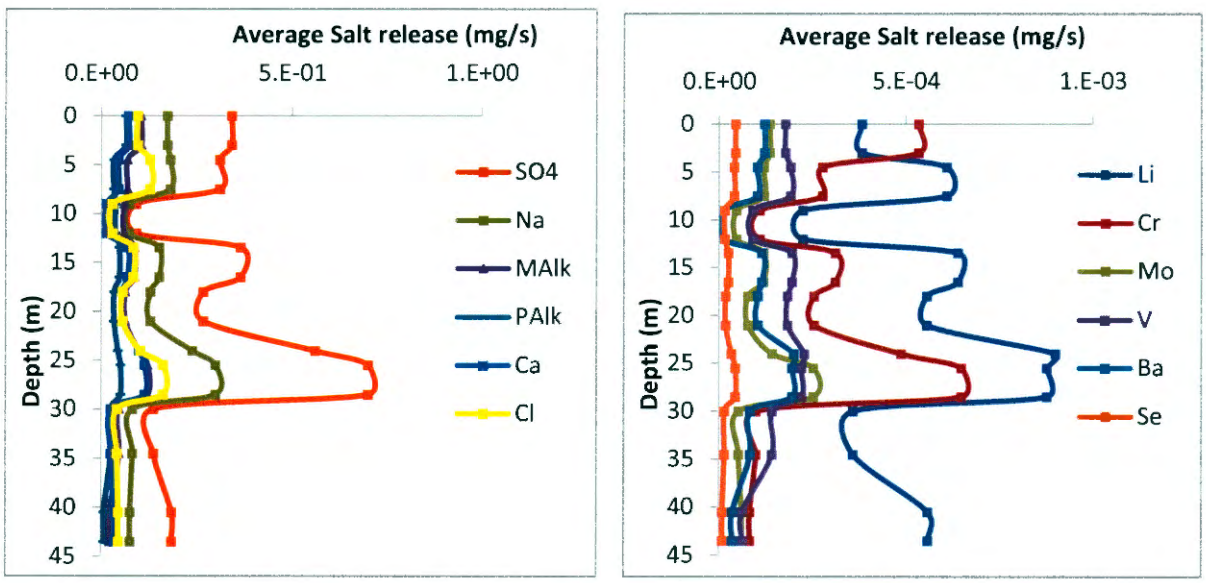

Figure 4.20 Average salt release of the major (left) and minor (right) components with increasing depth.

4.3.2.4. Elemental concentration variation over time

The elemental concentration variation with time, for the major constituents, during the leaching experiment is displayed in Figures 4.22 and 4.23. During the experiment, the majority of elements showed an exponential decrease in concentration. In most cases leaching of the samples yielded an increase in aluminium concentration, except for the sample series of 9 – 12 m which had higher aluminium and fluoride concentrations compared to the other sections and showed a decrease in concentration throughout the leaching process. Alkaline species were also relatively enriched in the 9 – 12 m section. Figure 4.21 illustrates the exponential decrease in SO_4 concentration during the leaching of the various samples of fly ash from the industrial complex.

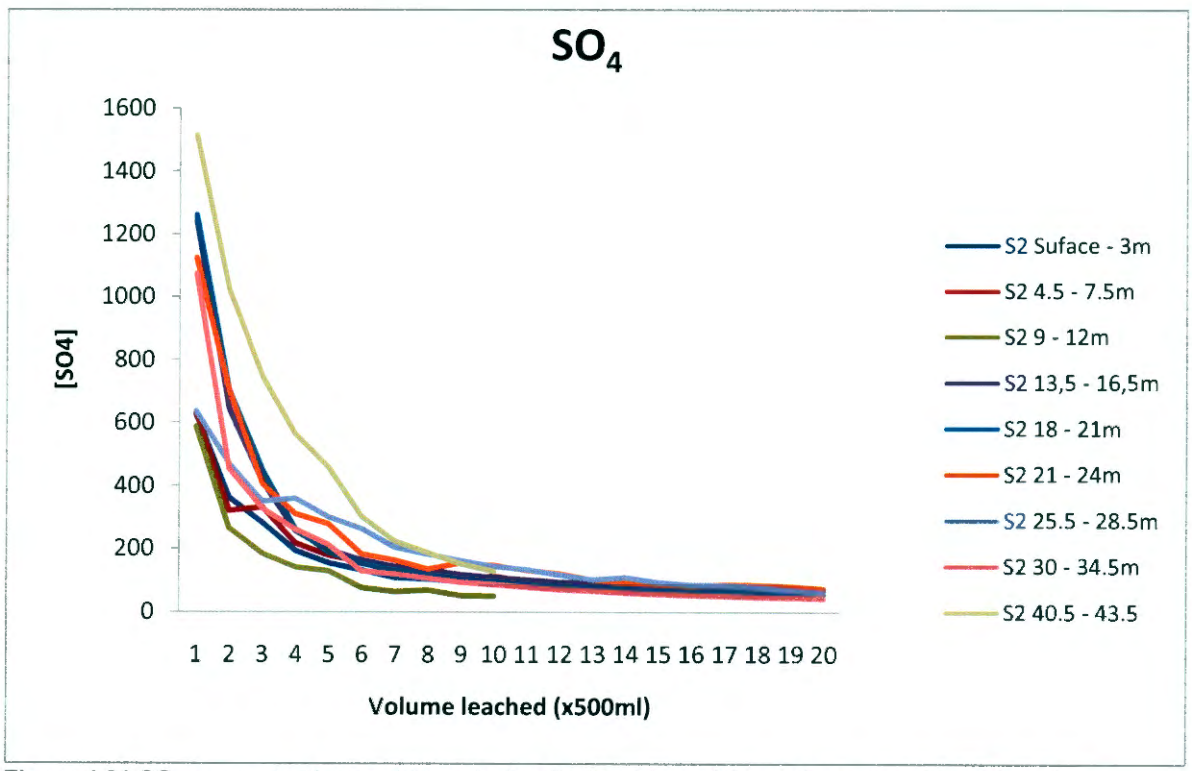

Figure 4.21 SO_4 concentration variation during the leaching of the various samples of fly ash.

The 9 – 12 m series was also found to have lower concentrations of many other elements such as: Ca, SO_4, Fe, B, Cr, Zn, Ni, Ba and Mo as can be seen in Figure 4.22 and 4.23. This corresponds to the change in leachate composition seen in Section 4.3.2.2, therefore indicating a more leached sample series.

Most elements were concentrated in the deepest sections (40.5 - 43.5 m), except Mn and chromium which were most concentrated in levels 18 – 21 m and 25.5 - 28.5 m respectively. There was also an unexpected increase in Ba concentration in the 18 – 21 m section accompanied by an increase in Mn. Those elements forming part of the minor constituents of the leachate (Li, Cr, Zn, Cu, Fe, Se, Co, Mo, Ni and V), displayed the same exponential decay as seen in Figure 4.23.

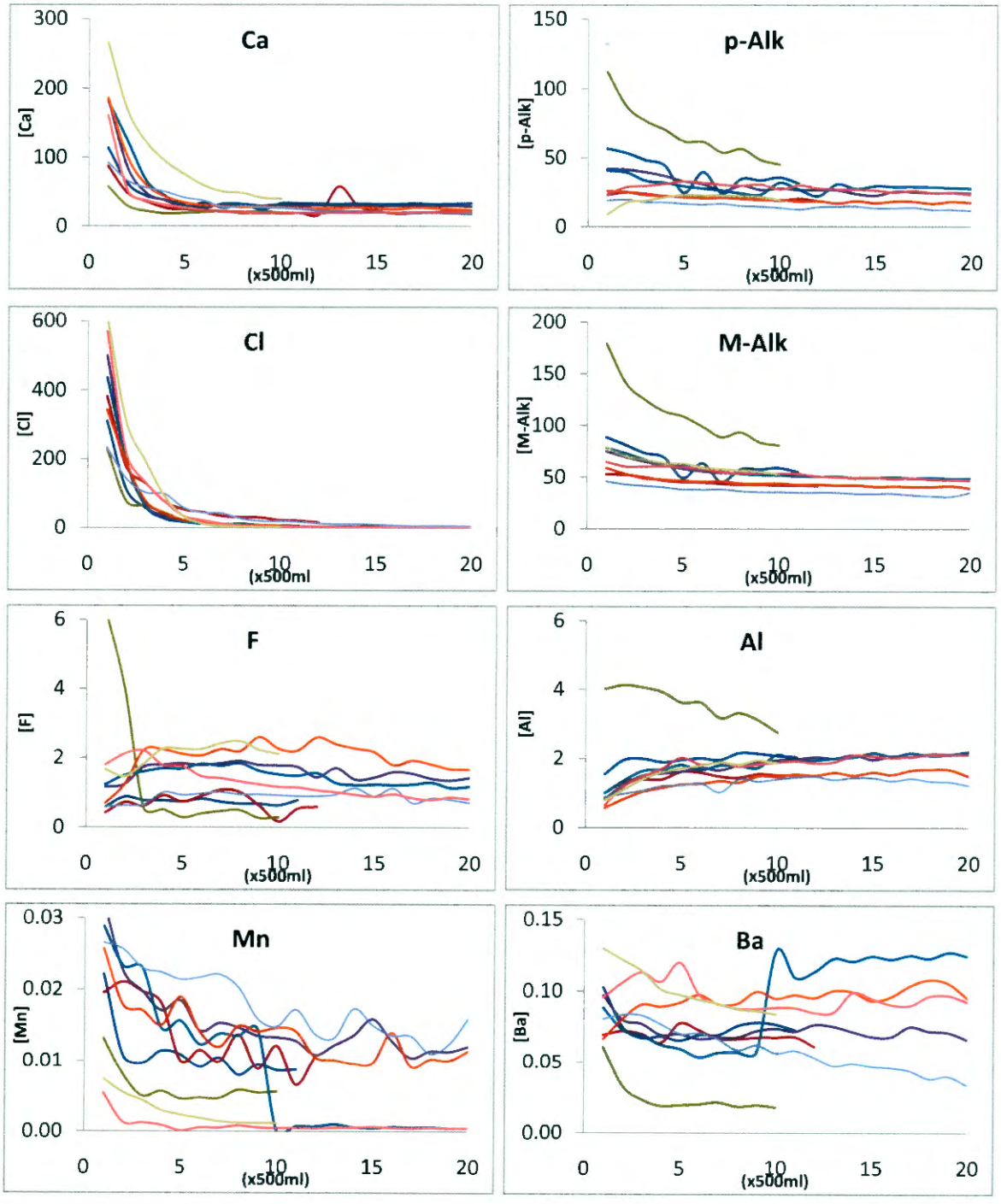

Figure 4.22 Elemental concentration variations over time with increasing leachate volume, for Ca, M-Alk, P-Alk, Cl, F, Al, Ba and Mn, of the different depth sections, during the leaching experiment.

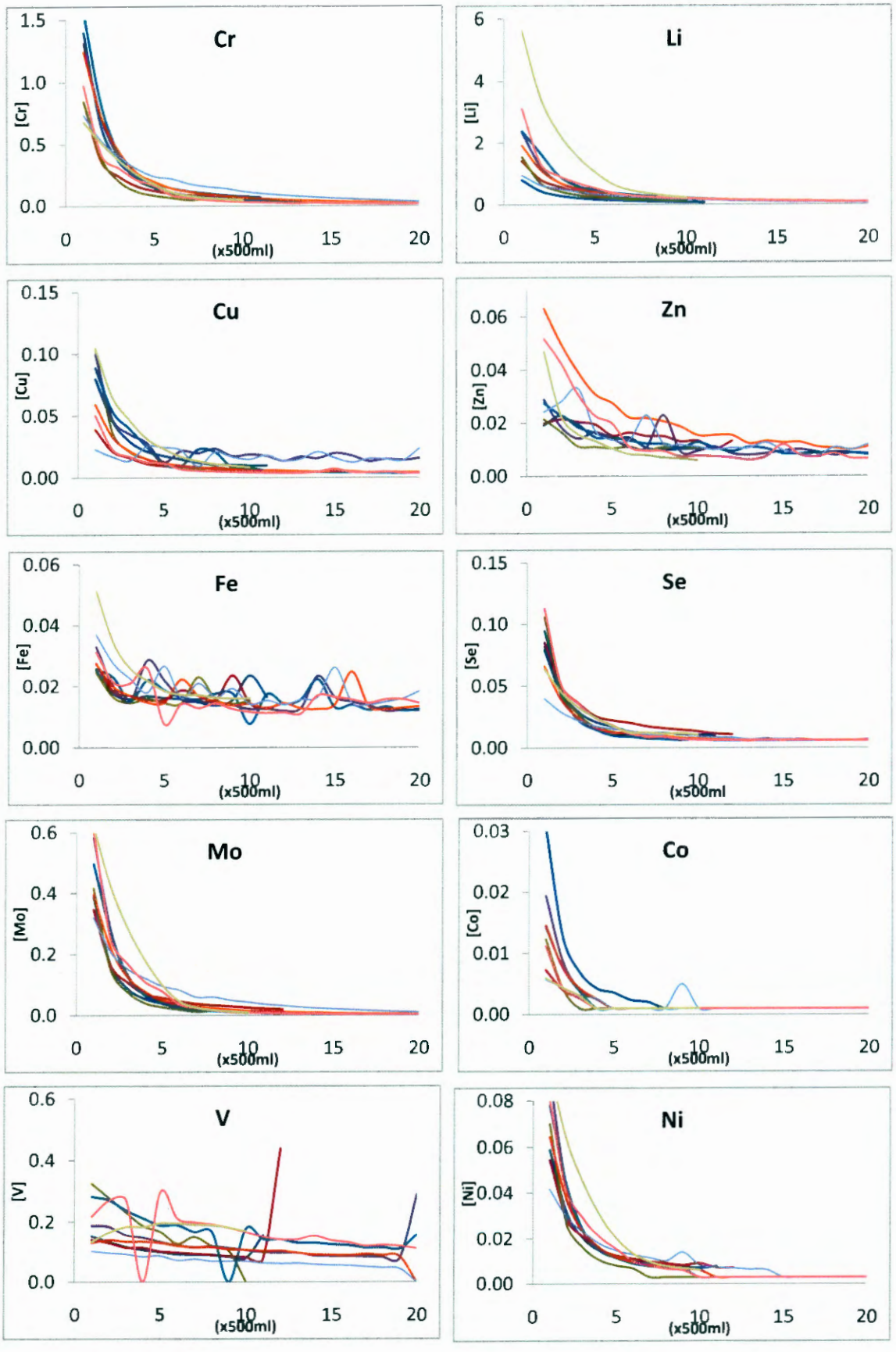

Figure 4.23 Elemental concentration variations over time with increasing leachate volume, for Li, Cr, Zn, Cu, Fe, Se, Co, Mo, Ni and V, of the different depth sections, during the leaching .experiment.

4.4 Transport parameters

The transport parameters were investigated during the leaching of the fly ash from the industrial complex, to determine if there was a large proportion of the matrix that goes into solution or cemented.

Laboratory scale tracer tests analysis were also performed to determine if any interesting transport phenomenon occurs and to evaluate the saturated hydraulic and transport parameters of the fly ash system. This was done by controlling factors that may influence the physical environment such as temperature, liquid density, and liquid viscosity. The initial leaching evolution of the samples was done until a suitable baseline for the system could be determined for a tracer test.

Darcy's law is commonly applied in laboratory column and tracer experiments to determine the saturated hydraulic conductivity coefficient using constant head hydraulic test data.

Darcy's law can be described as a simple proportional relationship between the instantaneous discharge rate through a porous medium, hydraulic conductivity (K), hydraulic gradient (I) and cross sectional area (A). Where q is the liquid flux (length/time), Q is the volumetric flow rate, i is the hydraulic gradient and h is the total head.[15]

$$q = \frac{Q}{A} = Ki = -K\frac{dh}{dl}$$

4.4.1 Hydraulic conductivity during constant head leaching

An overall decrease in hydraulic conductivity is observed over time, ultimately reaching a steady state. The change in flow rate can be due to physical changes from the presumably unsaturated dry ash to saturated ash. Also noted is that sample S2 30 – 34.5 m, which shows an increase in hydraulic conductivity over time, whereas there is a reversal in hydraulic conductivity in the 4.5 – 7.5 and 40.5 – 43.5 m sections. The moisture content is also a major factor during the compaction process as it does impact on the transport properties of the ash.

The results for the hydraulic conductivity with increasing volume leached (500ml intervals) can be seen in Figure 4.24.

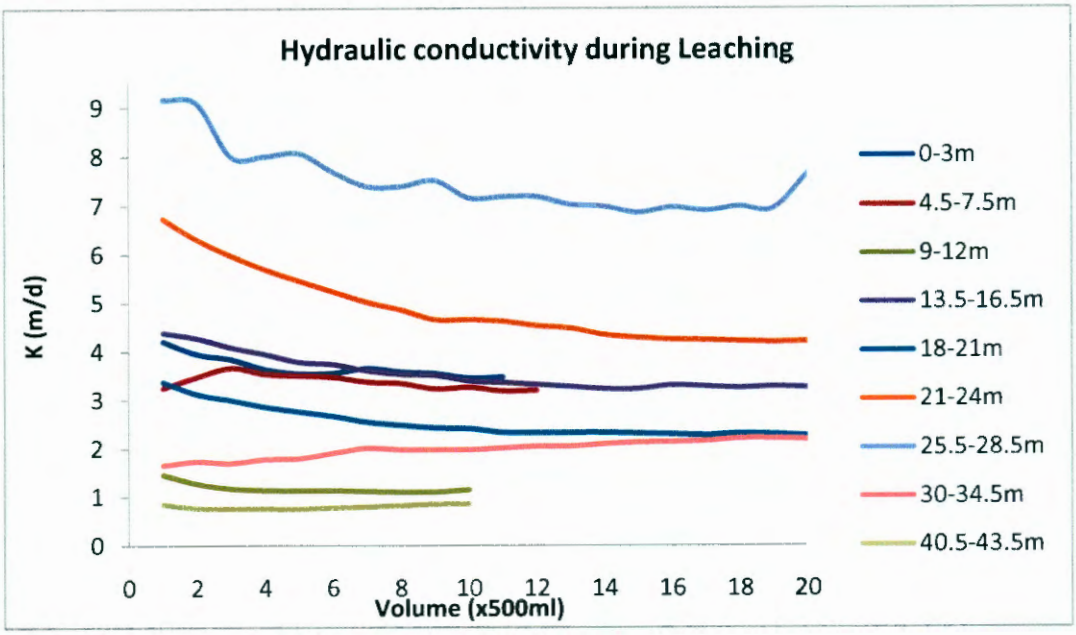

Figure 4.24 Hydraulic conductivity during leaching.

It was also found that there is a direct relationship between the salt load and hydraulic conductivity during leaching. Thus the higher the salt load, the higher the hydraulic conductivity. This may be due to the dissolved species creating a concentration gradient, influencing flow.[16] This relationship is illustrated in Figure 4.25 (right).

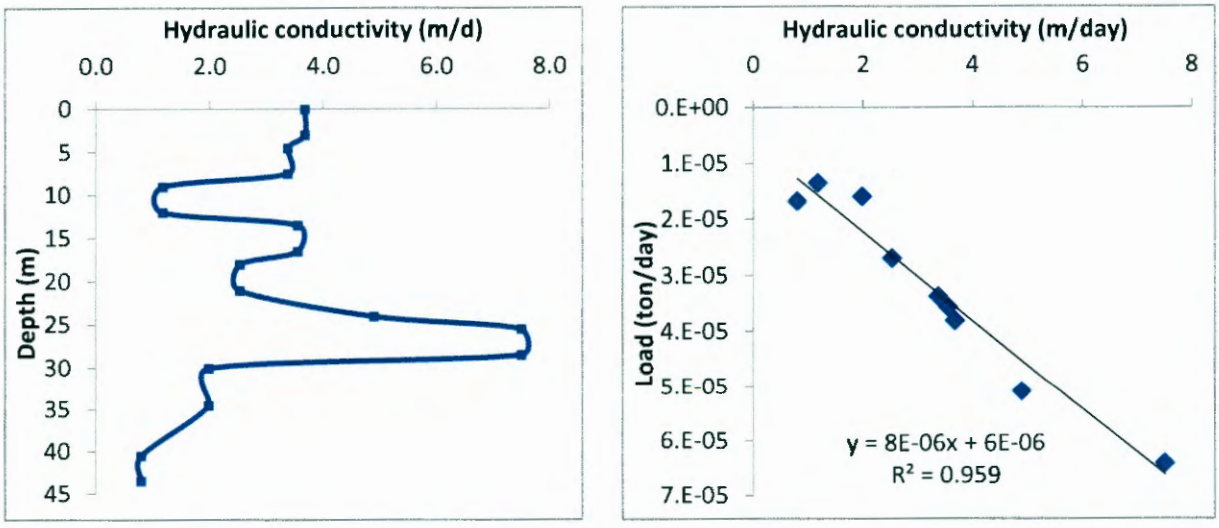

Figure 4.25 Average hydraulic conductivity of the fly ash samples (left) and the relationship between salt load and hydraulic conductivity during leaching.

4.4.2 Hydraulic and transport properties during tracer tests

2 ml of a mixture of 0.1 g / ml NaCl was injected into the tracer injection system at steady state conditions. The NaCl tracer solution was primarily used to create a highly concentrated spike into the flow system to observe a breakthrough curve of the concentration injected the constant head (SGLP) Darcy set up.

The electrical conductivity was monitored over time at constant volume intervals of 50 ml. The electrical conductivity over time was plotted to establish a breakthrough curve of the tracer experiment and used to calculate the velocity of the salt tracer through the ash. The tracer test experiment was performed in triplicate, i.e., Run 1, 2 and 3, followed by one of double and one of half the original concentration.

Breakthrough curves were plot of the electro conductivity over time. Similar to a hydrograph, which is a plot of stream flow with time, the breakthrough curves represent the time of travel from the injection point of a tracer to the point of observation in the leachate. An example of one of the breakthrough curves from this study can be seen in Figure 4.26.

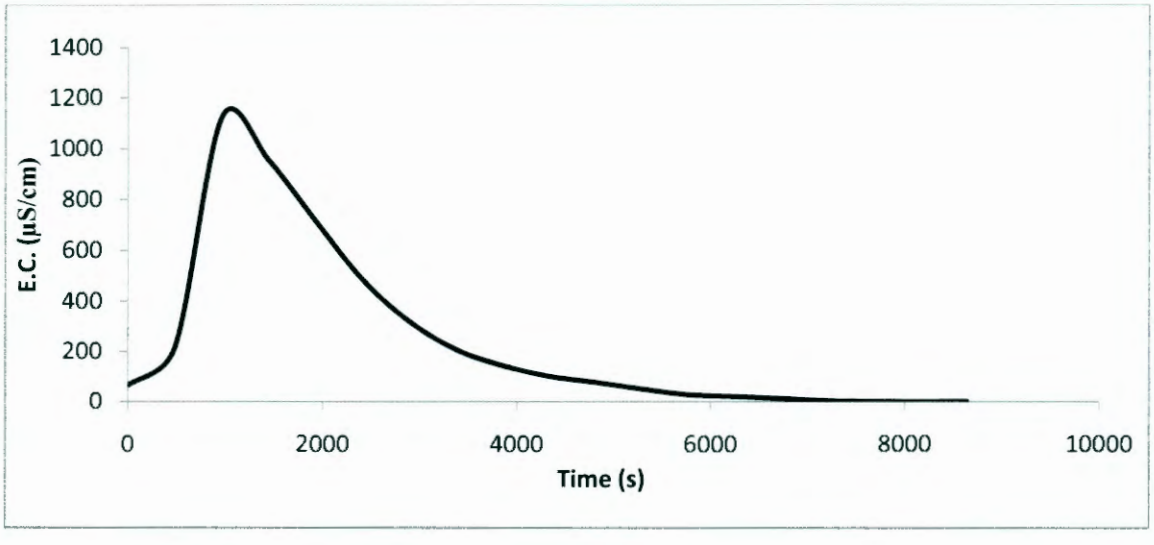

Figure 4.26 Breakthrough curve of electro conductivity over time.

When two distinct peaks were observed, as seen in Figure 4.27, a deconvolution algorithm was run in order to evaluate the system. The best fit using lognormal distributions was obtained (Figure 4.28).

Furthermore, the tracer data was fitted within a 90 % least squares fit value, to evaluate the average pore-water velocity (v) and dispersion coefficient (D) as can be seen in Figure 4.28. During the interpretation of these results the following data in Table 4.3 was obtained. The dispersivity (λ), an indication of how much the introduced tracer strays from the path of the carrier fluid, was also calculated from this data as:

$$\lambda = D/v$$

It seems that a delayed response occurs in the system. It should be noted that mass balance errors are likely to have an adverse effect on the estimation of all transport parameters. The average hydraulic conductivity during the tracer tests using sodium chloride by evaluating the electro conductivity can be seen in Figure 4.29.

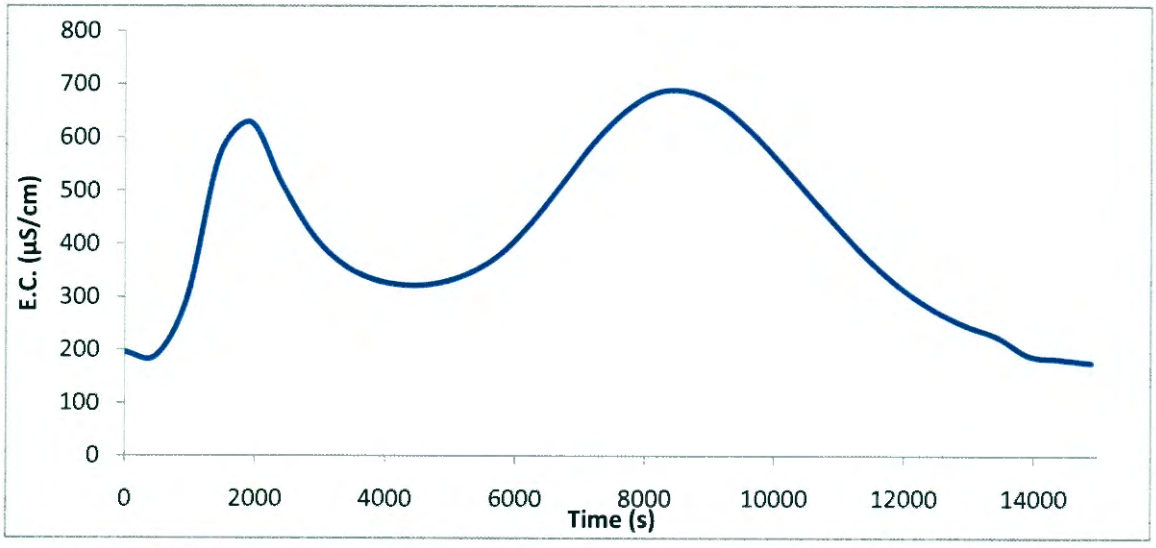

Figure 4.27 Fly ash tracer test data with two distinct peaks using NaCl.

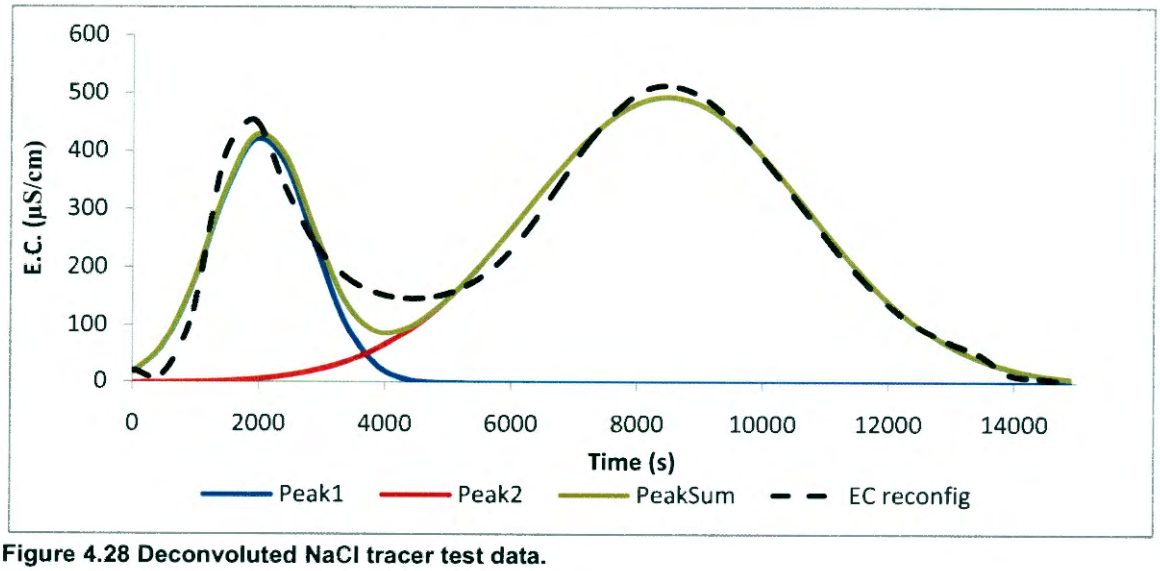

Figure 4.28 Deconvoluted NaCl tracer test data.

Table 4.3 Average pore water velocity (v) and dispersion coefficient (D) for the NaCl tracer test data.

Run no	1				2				3				4 (2X)			
	Peak1		Peak 2		Peak1		Peak 2		Peak1		Peak 2		Peak1		Peak 2	
Depth (m)	v1	D1	v2	D2	v3	D3	v4	D4	v5	D5	v6	D6	v7	D7	v8	D8
0-3	9.66E-03	1.04E-01	6.28E-03	1.05E-02	1.26E-02	1.66E-01	6.76E-03	1.05E-02	3.65E-03	1.29E-02	4.22E-03	3.24E-03	7.18E-03	6.01E-02	6.26E-03	1.22E-02
4.5-7.5	2.29E-03	2.89E-03	-	-	2.94E-03	5.63E-03	-	-	3.72E-03	6.01E-03	-	-	4.98E-03	2.04E-02	-	-
9-12	8.79E-05	4.11E-05	-	-	7.60E-05	3.88E-05	-	-	8.38E-05	7.49E-05	-	-	7.91E-05	4.05E-05	7.08E-05	6.23E-05
13.5-16.5	2.06E-03	1.18E-03	1.75E-03	9.52E-04	2.44E-03	1.01E-03	1.15E-03	7.41E-01	2.61E-03	8.00E-04	2.02E-03	2.91E-03	2.21E-03	5.45E-04	1.74E-03	3.42E-03
18-21	2.03E-03	1.46E-03	-	-	2.86E-03	3.82E-03	-	-	3.21E-03	3.85E-03	-	-	3.04E-03	5.45E-03	-	-
21-24	1.80E-03	2.93E-03	-	-	1.86E-03	4.96E-03	-	-	2.76E-03	7.33E-03	-	-	3.63E-03	8.54E-03	-	-
25.5-28.5	2.92E-03	3.55E-03	-	-	1.97E-03	4.18E-03	1.90E-03	1.32E-03	3.55E-03	2.90E-03	2.91E-03	8.63E-03	1.57E-03	3.14E-03	-	-
30-34.5	1.09E-03	3.27E-05	1.06E-03	2.12E-04	1.16E-03	5.76E-03	-	-	2.97E-03	1.67E-03	2.36E-03	9.01E-04	2.76E-03	9.07E-04	2.27E-03	1.29E-03
40.5-43.5	2.43E-02	1.18E-01	3.21E-03	9.80E-04	5.99E-03	9.82E-03	-	-	7.64E-03	1.87E-02	-	-	4.95E-03	2.93E-03	3.25E-03	1.45E-04

Run no	5 (0.5X)													
	Peak1		Peak 2											
Depth (m)	v9	D9	v10	D10	avg v1	avg v2	tot avg v	Std dev.	avg D1	avg D2	tot avg D	Std dev.	λ = D/v	
0-3	5.31E-03	1.10E-02	3.99E-03	2.80E-03	7.68E-03	5.50E-03	**6.59E-03**	2.76E-03	7.08E-02	7.85E-03	**3.93E-02**	5.50E-02	**5.97E+00**	
4.5-7.5	4.88E-03	6.30E-03	-	-	3.76E-03	-	**3.76E-03**	1.18E-03	8.25E-03	-	**8.25E-03**	6.93E-03	**2.19E+00**	
9-12	5.31E-05	8.90E-05	-	-	7.60E-05	7.08E-05	**7.51E-05**	1.23E-05	5.69E-05	6.23E-05	**5.78E-05**	2.11E-05	**7.69E-01**	
13.5-16.5	9.58E-04	6.64E-04	1.00E-03	1.07E-03	2.06E-03	1.53E-03	**1.79E-03**	5.89E-04	8.40E-04	1.50E-01	**7.54E-02**	2.34E-01	**4.20E+01**	
18-21	2.82E-03	3.04E-03	-	-	2.79E-03	-	**2.79E-03**	4.53E-04	3.52E-03	-	**3.52E-03**	1.45E-03	**1.26E+00**	
21-24	3.21E-03	5.15E-03	-	-	2.65E-03	-	**2.65E-03**	8.11E-04	5.78E-03	-	**5.78E-03**	2.19E-03	**2.18E+00**	
25.5-28.5	1.55E-03	3.59E-03	-	-	2.31E-03	2.41E-03	**2.34E-03**	7.82E-04	3.47E-03	4.98E-03	**3.90E-03**	2.27E-03	**1.67E+00**	
30-34.5	2.38E-03	1.88E-03	2.25E-03	1.89E-03	2.07E-03	1.99E-03	**2.03E-03**	7.36E-04	2.05E-03	1.07E-03	**1.62E-03**	1.69E-03	**7.95E-01**	
40.5-43.5	6.03E-03	4.86E-03	-	-	9.78E-03	3.23E-03	**7.91E-03**	7.40E-03	3.09E-02	5.63E-04	**2.22E-02**	4.27E-02	**2.81E+00**	

The results for the hydraulic conductivity calculated during the constant head tracer tests can be seen in Figure 4.29. A similar hydraulic behaviour was observed for the tracer tests, although the concentration of the tracer did not significantly influence hydraulic behaviour. This may in all likelihood be due to the relatively small salt load induced by the tracer and the fact that NaCl is native to the system. The comparison of the hydraulic conductivity for the leaching experiment and the tracer tests can be seen in Figure 4.30.

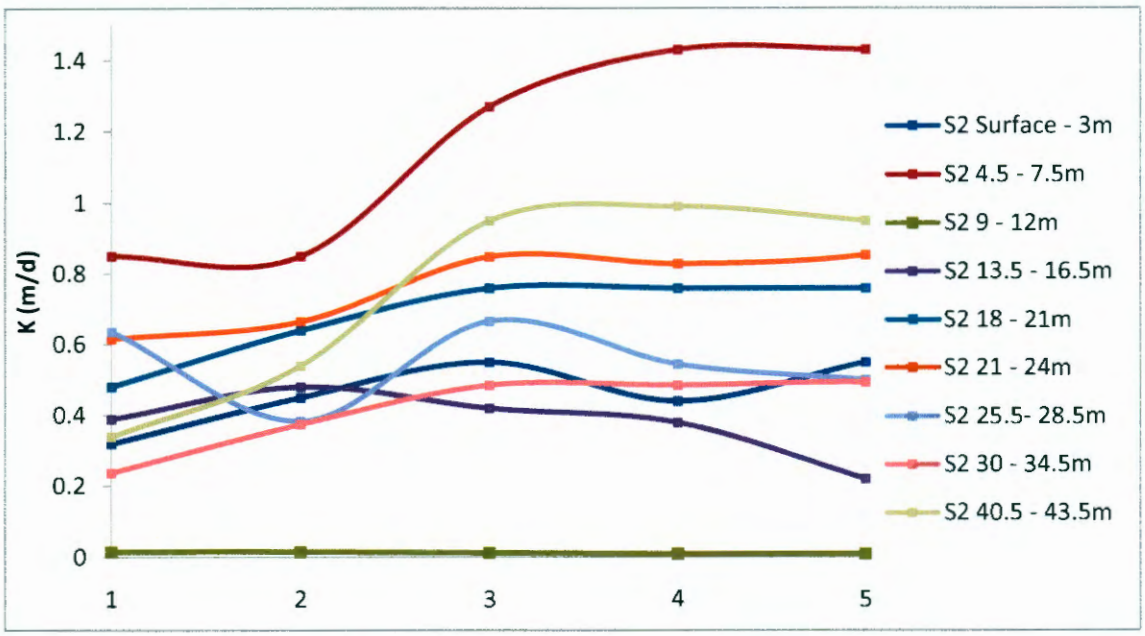

Figure4.29 Hydraulic conductivity observed during the NaCl tracer tests.

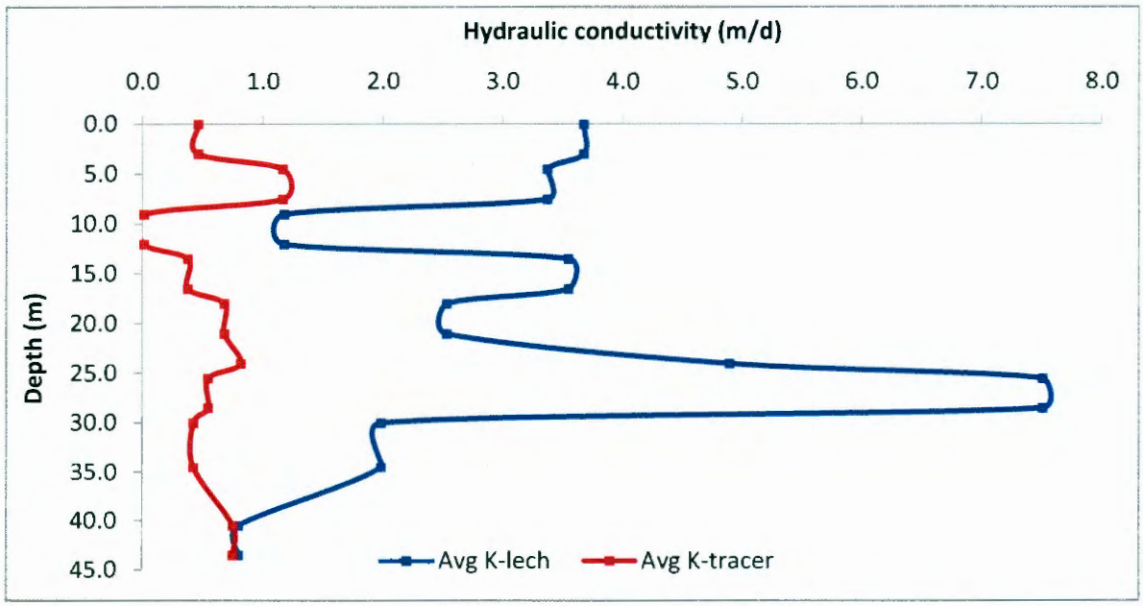

Figure 4.30 Comparison of hydraulic conductivity during the leaching (blue) and tracer (red) experiments.

In Figure 4.31, the dispersion coefficient *D* as function of the mean pore water velocity *v* obtained by inverse parameter estimation from analysis of steady-state data can be seen. From Figure 4.31 it is clear that the 13.5 - 16.5 m showed a relatively large dispersivity caused by a low diffusion coefficient.

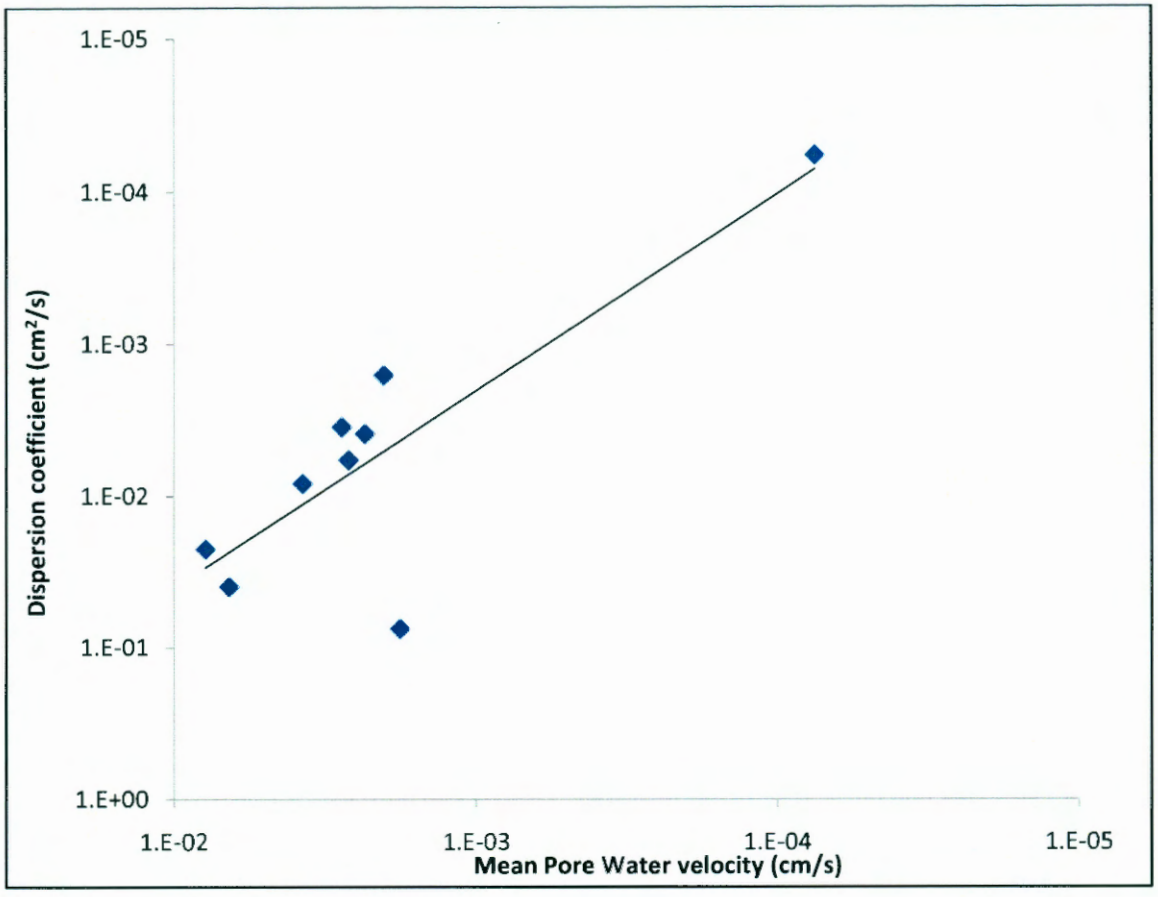

Figure 4.31 Dispersion coefficient (D) as function of the mean pore water velocity (*v*) obtained by inverse analysis of steady state data.

4.5 Time-lapse electrical resistivity tomography

The inverted resistivity models are shown and discussed in the following sections by illustrating the various phases of the infiltration study. These include the background, constant head injection and recovery phases. On both the west/east and north/south profiles, inversion of the recorded apparent resistivity data was done over seven iterations to yield least-squares errors ranging between 0.62 and 0.85 % on the west/east profiles and between 2.3 and 2.8 % on the north/south profiles. The maximum difference between any of the recorded and modelled apparent resistivities was less than 5 %. To assist in visualising the migration of the brine plume, as well as to remove possible artefacts in the contour maps of the resistivity models that are due to the contouring process, the background resistivity model was subtracted from the models of the injection and recovery phases.

4.5.1 West/East profiles

Figure 4.32 shows the background model. The modelled resistivity sections along the west/east profiles are presented as contour maps in Figure 4.33 to 4.36. From these figures, the following observations regarding the models and brine flow through the ash may be made:

Background phase

The initial bulk resistivity at the position of the injection pit (centre of the profile, 0 m) is very high. This is due to the presence of the empty pit itself with air being very resistive to electrical current flow.

The background resistivity model indicates the presence of a shallow resistive layer where resistivities ranged from approximately 35 to 110 mΩ, overlying a conductive layer with resistivities generally below 12 mΩ. These layers may be interpreted to be the unsaturated ash at surface overlying saturated ash. The saturated ash appears to occur at a depth of between 2 m and 2.75 m below surface.

This was in good agreement with field observations which suggested the presence of a perched water table near the survey area. The ash water used as brine during the investigations was from a nearby pond on the ash, the water level of which occurred approximately 3 m below the surface elevation of the ash at the position of the injection pit.

The results are shown in Figure 4.33 and 4.34 (beginning and end of Injection phase) and Figure 4.35 and 4.36 (beginning and end of recovery phase). These figures confirm that horizontal flow dominated over vertical flow and also show that flow was more pronounced in the western direction than the eastern direction. It is also seen that flow predominantly took place at the deeper level of the injection pit. This observation may be partly explained by the higher fluid pressures at the bottom of the pit, but may also be indicative of the presence of ash layers with higher permeabilities near the bottom of the pit.

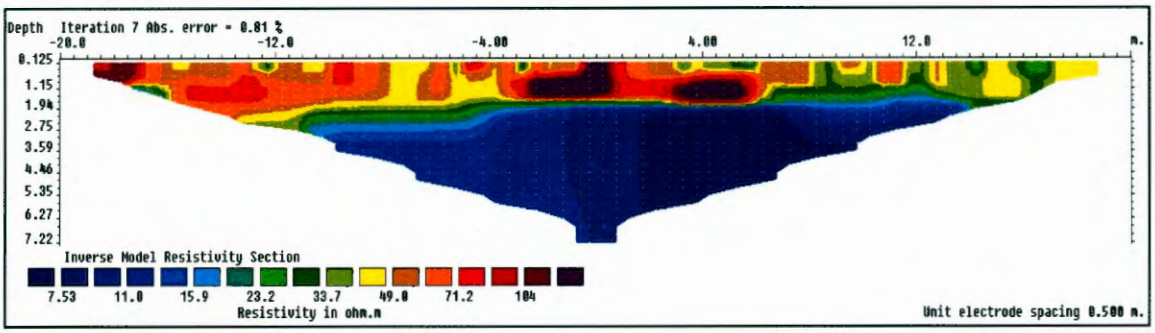

Figure 4.32 Modelled background resistivity section along the west/east profile prior to the injection of brine.

Constant head injection phase

Results for the Constant head injection phase are shown in Figures 4.33 and 4.34. Soon after brine injection commenced, the presence of the conductive brine is seen as a zone of low resistivity at the position of the injection pit. It should be noted that the resistivities of the material immediately below the pit also appear reduced as compared to the background resistivities. This is in all probability due to the inaccuracies inherent to the inversion and contouring processes and may give the false impression of rapid vertical flow of brine through the ash during early times.

As time progressed, the zone of reduced resistivities is seen to extend laterally, reducing the bulk resistivities of the material adjacent to the injection pit. It appears that the horizontal flow of the brine is more pronounced towards the west than the east. This is especially apparent in the near-surface material.

Horizontal flow seems to dominate over vertical flow during the injection phase with little evidence for vertical flow.

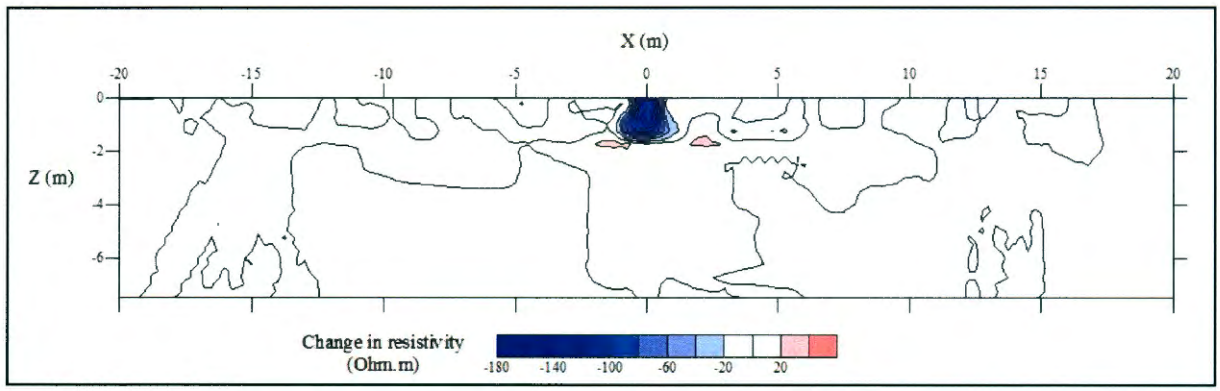

Figure 4.33 Changes in the modelled resistivity values (as compared to the background values) along the west/east profile 28 min after brine injection commenced.

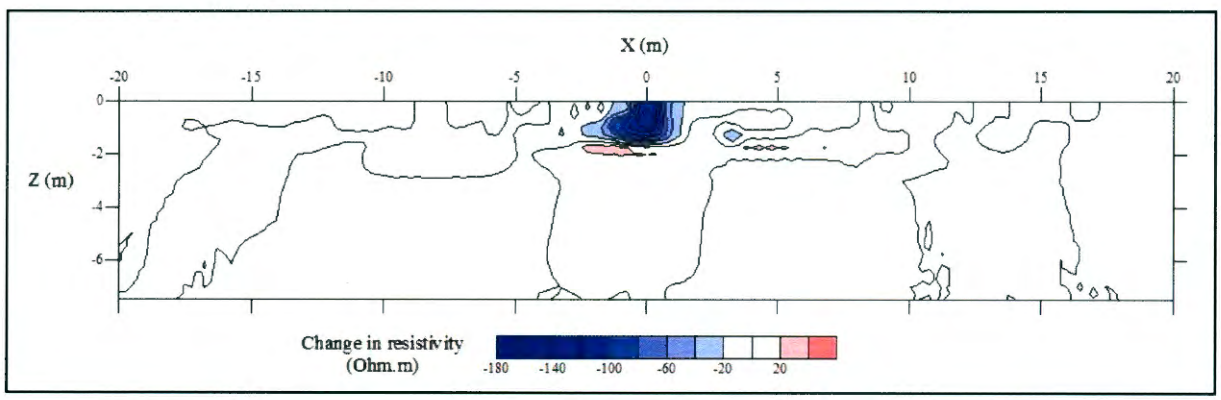

Figure 4.34 Changes in the modelled resistivity values (as compared to the background values) along the west/east profile 262 min (4 hr, 22 min) after brine injection commenced.

Recovery phase

Resistivity contour maps for the recovery phase are shown in Figures 4.35 and 4.36 (beginning and end of recovery phase). A large time gap (1,008 minutes, 16 hours 48 minutes) existed between the last measurements of the injection phase (Figure 4.34) and the first measurements of the recovery phase (Figure 4.35). The modelled resistivity sections indicate that during this time further horizontal brine migration occurred. A corresponding increase in the bulk resistivity at the position of the injection pit is noted as the brine saturation at this position decreased due to the spreading of the brine plume.

Although evidence for vertical flow can be seen in the reduced resistivities immediately below the injection pit (compare Figure 4.34 with 4.35) it again appears that horizontal flow dominates over vertical flow, in a westerly direction, especially in the shallow subsurface.

As time progressed and the brine plume extended, the resistivities in the vicinity of the injection pit are seen to increase gradually as the brine concentration at these

positions lowered. Comparing Figure 4.35 and 4.36 it can be seen how the resistivities immediately below the injection pit increased over a period of 24 hours as the migration of the brine plume continued.

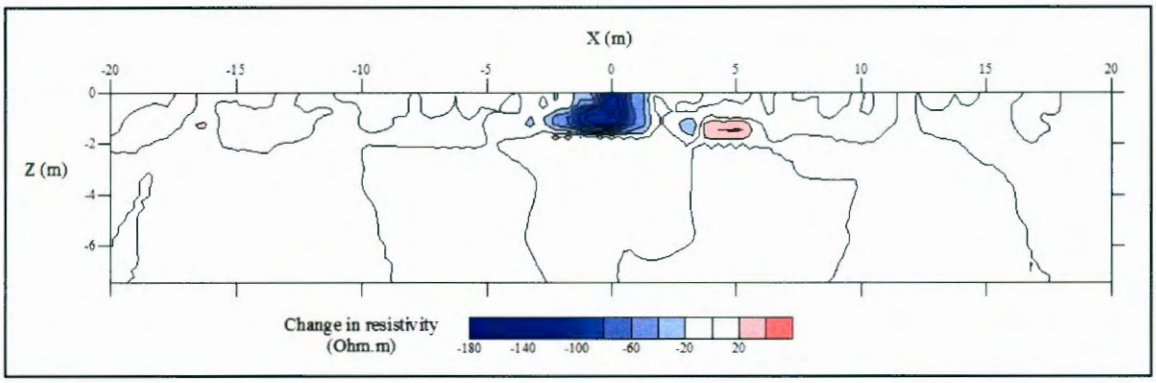

Figure 4.35 Changes in the modelled resistivity values (as compared to the background values) along the west/east profile 1,270 min (21 hr, 10 min) after brine injection commenced (990 min after removal of constant head).

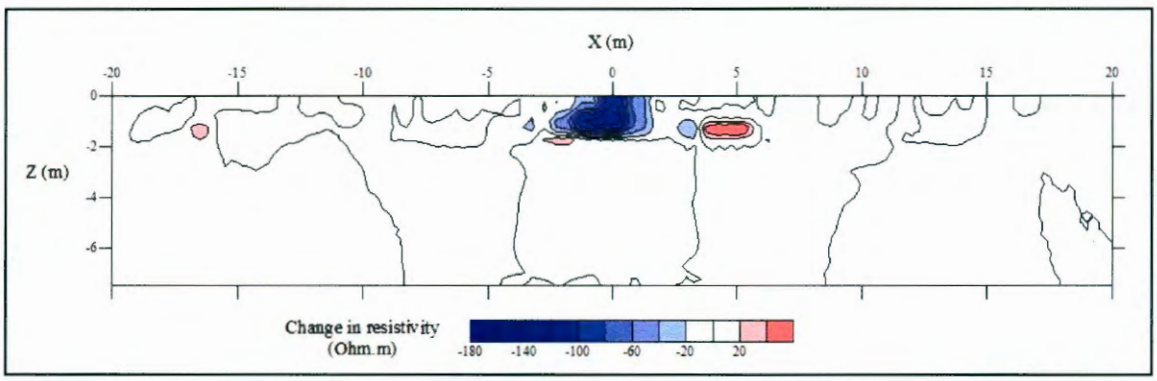

Figure 4.36 Changes in the modelled resistivity values (as compared to the background values) along the west/east profile 2,710 min (45 hr, 10 min) after brine injection commenced (2,430 min after removal of constant head).

4.5.2 North/South profiles

Figure 4.37 shows the background model. The modelled resistivity sections along the north/south profiles are presented as contour maps in Figure 4.38 to 4.41, with Figure 4.38 and 4.39 (beginning and end of injection phase) and Figure 4.40 and 4.41 (beginning and end of recovery phase). From these figures horizontal flow is again seen to dominate over vertical flow. This observation suggests that the apparent vertical flow observed in Figure 4.38 to 4.41 may to some extent be due to the smoothing effects of contouring.

Background phase

Background phase diagrams are depicted in Figure 4.37. As along the west/east profile, the initial bulk resistivity at the position of the injection pit is very high due to the presence of the empty pit itself.

The same two-layered model as along the west/east profile was observed. However, the depth to the saturated material appears smaller than along the background west/east profile. In addition, the resistivities of the saturated ash appear to be higher on the north/south profile. Since the two profiles occurred in close proximity and overlapped near the position of the injection pit, the depth to and the resistivity of the saturated material should be the same or very similar on the two profiles. It can be concluded that the differences are due to the non-uniqueness of the inversion process and the inaccuracies that result from the contouring process.

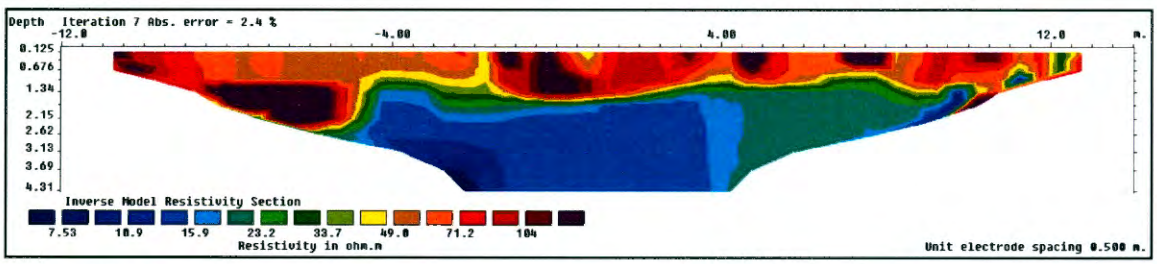

Figure 4.37 Modelled background resistivity section along the north/south profile prior to the injection of brine.

Constant head injection phase

Results for the constant head injection phase are shown in Figures 4.38 and 4.39. Soon after brine injection commenced, the presence of the conductive brine is seen as a zone of low resistivity at the position of the injection pit. In addition, the background model displays a shallow zone of high resistivities on the north-western side of the injection pit. This zone is absent in the resistivity models of the injection (and recovery) phase. These effects are in all likelihood artefacts due to the inaccuracies inherent to the inversion and contouring processes and should be taken into account when considering the horizontal and vertical flow rates.

As time progresses, the zone of reduced resistivities appear to not only extend laterally but also vertically, forming a continuous zone of low resistivities with the saturated ash soon after brine injection commenced.

As injection continued, the resistivities of the saturated material below the injection pit seem to have increased as compared to the earlier times. This suggests that the

brine (consisting of a mixture of ash water and tap water) has reached the ash saturated with highly saline ash water.

Although there is more evidence for vertical flow than along the west/east profiles, horizontal flow seems to dominate over vertical flow during the injection phase.

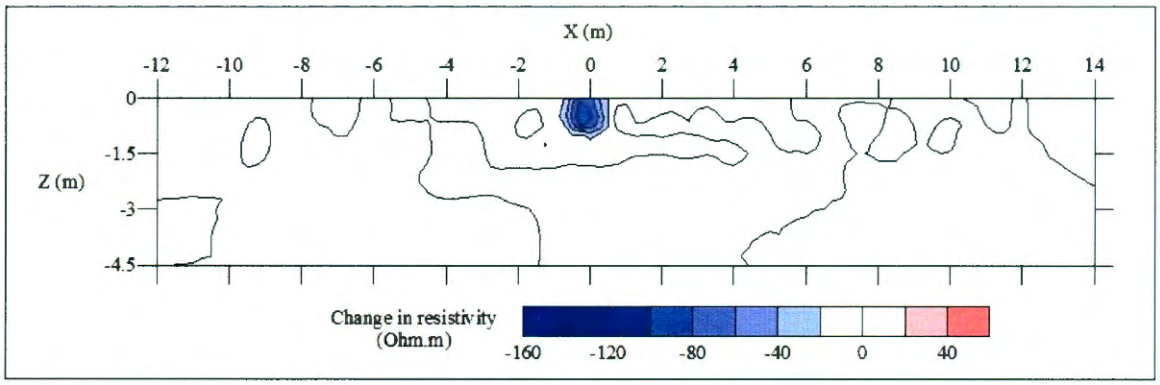

Figure 4.38 Changes in the modelled resistivity values (as compared to the background values) along the north/south profile 10 min after brine injection commenced.

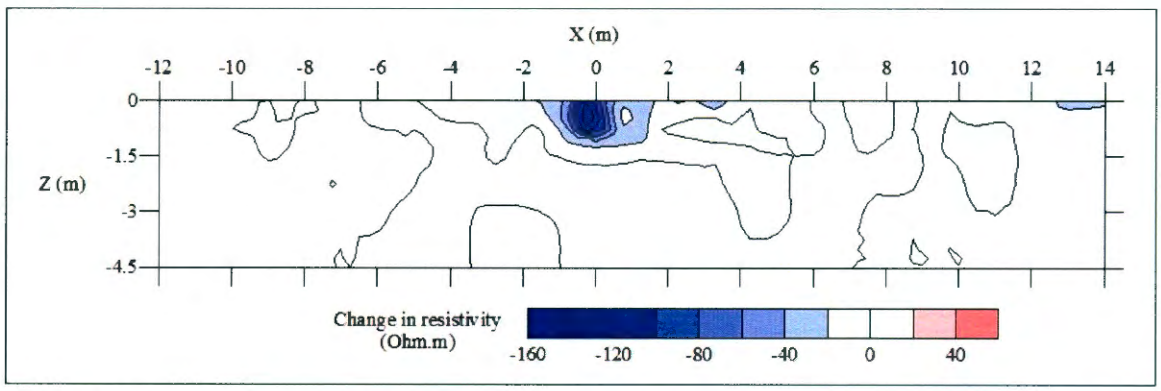

Figure 4.39 Changes in the modelled resistivity values (as compared to the background values) along the north/south profile 248 min (4 hr, 8 min) after brine injection commenced.

Recovery phase

Recovery phase diagrams are shown in Figure 4.40 and 4.41. A large time gap (1,052 minutes, 17 hours 32 minutes) existed between the last measurements of the injection phase (Figure 4.39) and the first measurements of the recovery phase (Figure 4.40). The modelled resistivity sections indicate that during this time further horizontal brine migration occurred. A corresponding increase in the bulk resistivity at the position of the injection pit is noted as the brine saturation at this position decreased due to the spreading of the brine plume. In addition, the resistivities of the saturated material on the southern side of the pit seem to have decreased slightly, possibly suggesting lateral flow of brine through the saturated zone.

Although evidence for vertical flow can be seen in the reduced resistivities immediately below the injection pit (compare Figure 4.40 with 4.41) it again appears that horizontal flow dominates over vertical flow.

Horizontal flow appears to preferentially take place in the northern direction, although there is also clear evidence for flow in the southern direction.

As time progresses and the brine plume extends, the resistivities in the vicinity of the injection pit are seen to increase gradually as the brine concentration at these positions is lowered.

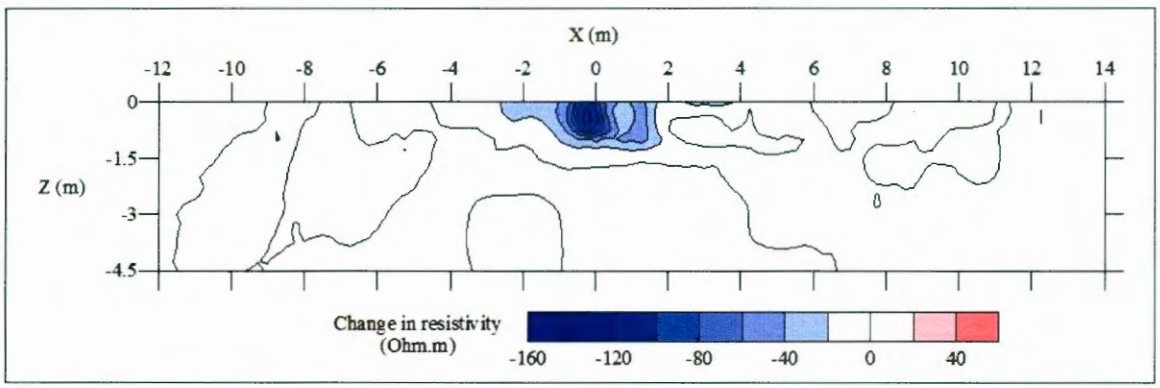

Figure 4.40 Changes in the modelled resistivity values (as compared to the background values) along the north/south profile 1,300 min (21 hr, 40 min) after brine injection commenced (1,020 min after removal of constant head).

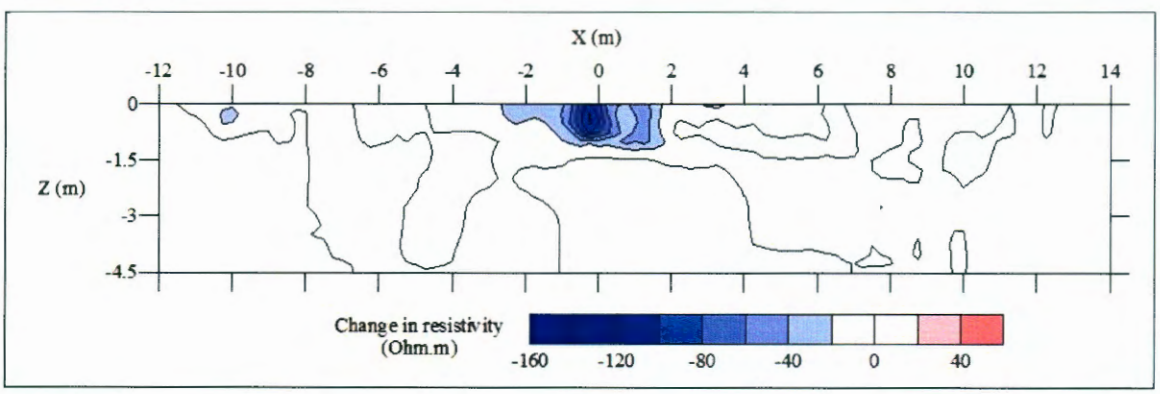

Figure 4.41 Changes in the modelled resistivity values (as compared to the background values) along the north/south profile 3,160 min (52 hr, 40 min) after brine injection commenced (2,880 min after removal of constant head).

4.5.3 Estimation of horizontal and vertical flow rates

4.5.3.1 Estimation based on flow distances

By considering the flow distance observed over the time period spanning the time-lapse ERT surveys, an upper estimate of the brine flow rates through the ash may be obtained. Since horizontal flow is seen to dominate over vertical flow, yielding measurable changes over distance and time, the estimation is only done for horizontal flow.

From Figure 4.36 and 4.41 the apparent maximum horizontal distances over which a modelled resistivity change of at least 20 Ωm is observed 2,850 and 2,880 minutes after injection commenced, vary between approximately 2.1 and 1.4 m. These values correspond to average flow rates of between 0.70 and 1.1 m/day. Since the flow rate can be expected to decrease with distance from the injection pit, these estimates of the flow rates may be considered as the upper estimates of the average horizontal flow rate.

It should be appreciated that the apparent horizontal distances travelled by the brine plume are to a larger extent dependent on the effects of contouring the resistivities at adjacent model cells with widths of 0.25 m. There is therefore much uncertainty as to the true distances travelled by the plume. The above estimated flow rates should therefore be seen as very crude estimates at best.

4.5.3.2 Flow rate estimation

Since the background resistivity models indicate that the saturated material occurs at a depth well in excess of the depth of the bottom of the injection pit, it is assumed that unsaturated conditions prevail in both the model cells laterally displaced from the injection pit and the cells immediately below the injection pit in early times after injection commences. The horizontal and vertical unsaturated flow rates through the ash are therefore estimated.

West/east profiles

The modelled resistivities in the model cells adjacent to the injection pit are shown in Figure 4.42 (left). The resistivities are seen to decrease rapidly after injection commences, but stabilise and display slight increases as the time after cessation of brine injection increases. A similar response is observed in the four cells

immediately below the injection pit (Figure 4.42 right). However, the resistivities in these cells increase much more rapidly after removal of the constant head than in the laterally displaced cells.

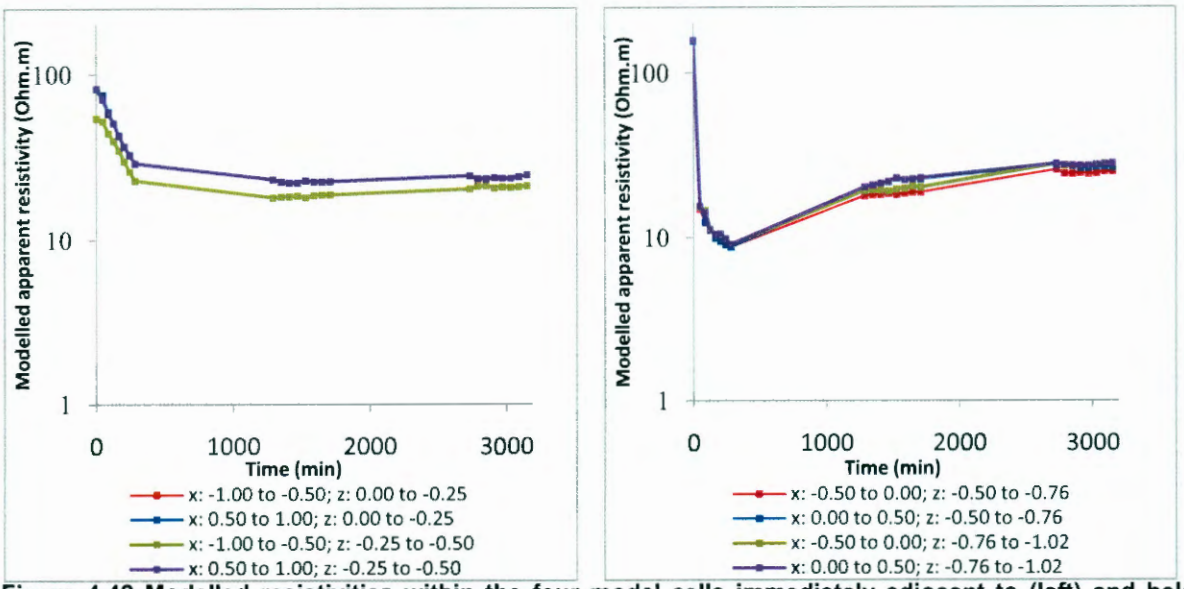

Figure 4.42 Modelled resistivities within the four model cells immediately adjacent to (left) and below (right) the injection pit (west/east profiles).

The horizontal unsaturated flow rates estimated from the modelled resistivity data displayed in Figure 4.42 (left) are shown in Figure 4.43 (left). This estimation is only applicable to unsaturated flow during brine injection. Thus only the modelled resistivities corresponding to those times when a constant head was maintained were used in the estimation. From Figure 4.43 (left) it can be seen that the horizontal flow rates are estimated to vary between 0.07 and 0.13 m/day.

The estimated vertical unsaturated flow rates within the model cells immediately below the injection pit are shown in Figure 4.43 (right). The estimated flow rates in the two shallower model cells display a gradual decrease over time, falling from flow rates in excess of 0.8 m/day in early times to approximately 0.05 m/day in later times. Due to model inaccuracies, the estimated flow rates in the two deeper model cells are seen to be more variable over time (even attaining negative values). At later times the flow rates in the deeper cells seem to settle on values of approximately 0.11 m/day.

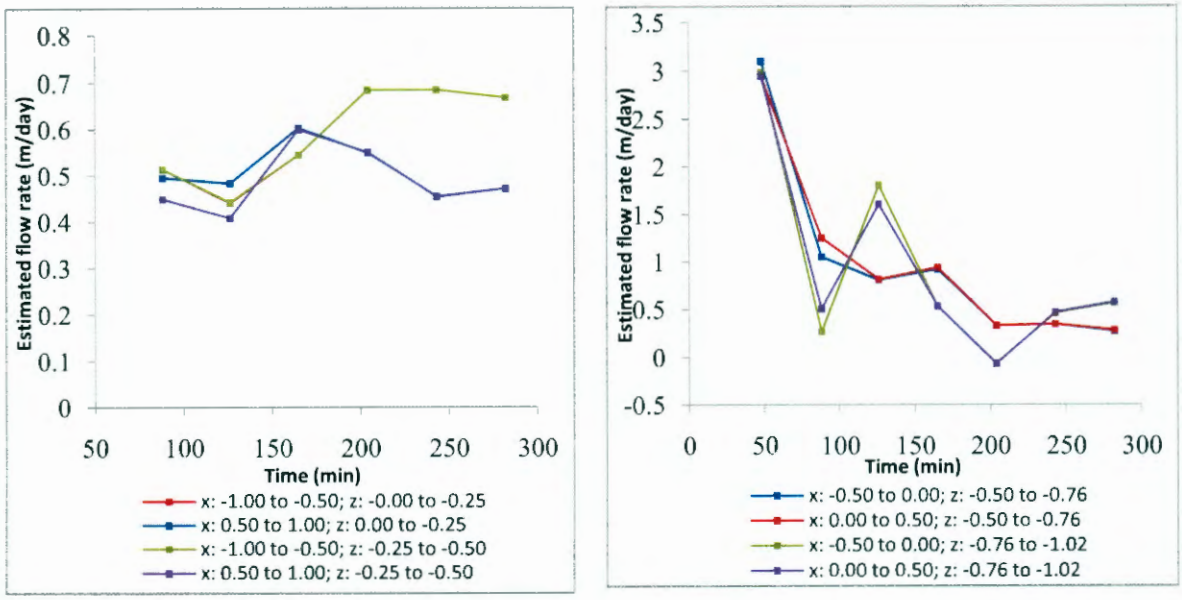

Figure 4.43 Estimated horizontal (left) and vertical (right) unsaturated flow rate within the four model cells immediately adjacent to the injection pit (west/east profiles).

North/south profiles

The modelled resistivity values in the four cells adjacent to the injection pit on the north/south profiles are shown in Figure 4.44 (left). The modelled resistivities of the two cells on the north-western side of the injection pit are seen to decrease monotonically during the injection phase of the investigations. During the recovery phase, gradual increases in the modelled resistivities are observed before the values seem to stabilise at late times. The model cells on the south-eastern side of the injection pit display similar behaviour, although more variability in the resistivities is observed during the early injection phase.

The modelled resistivity values in the four cells immediately below the injection pit are shown graphically in Figure 4.44 (right). The resistivity values in all four cells display the same behaviour, namely a monotonic decrease in early injection times followed by a gradual increase during the recovery phase.

The horizontal flow rates estimated from the modelled resistivity values shown in Figure 4.44 (left) may be obtained. These estimated flow rates are shown in Figure 4.45 (left). The temporal behaviours of the modelled flow rates in the cells on opposite sides of the injection pit seem to mirror one another. In early injection times, large variability (even negative flow rates) in the flow rate estimates are seen. This variability is probably due to model inaccuracies. At later injection times the estimated horizontal flow rates vary between 0.06 and 0.11 m/day.

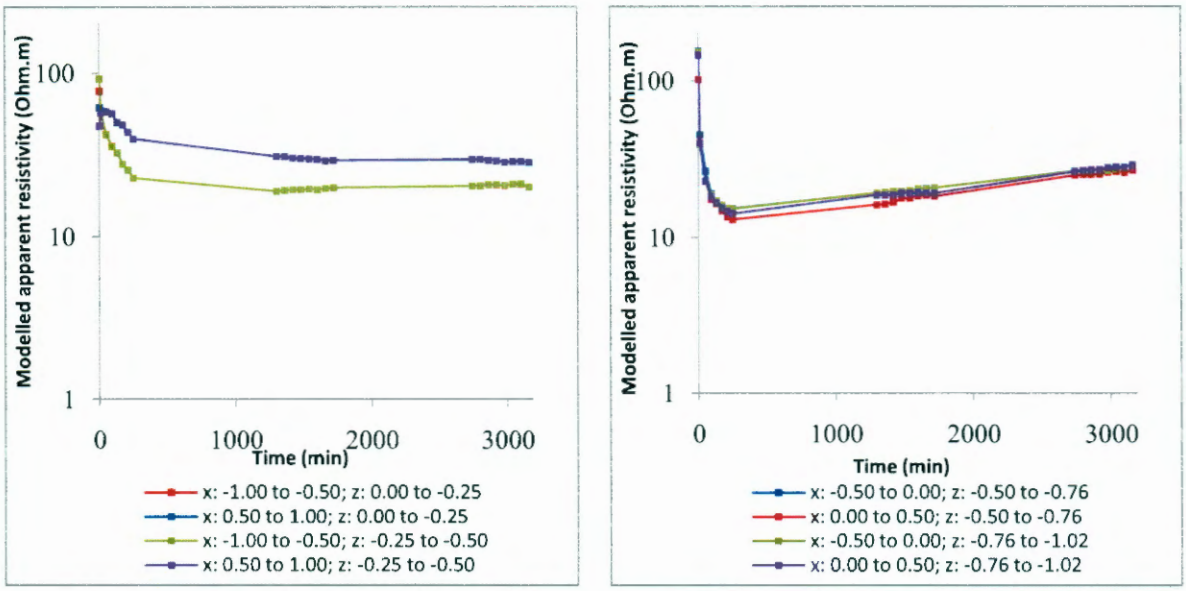

Figure 4.44 Modelled resistivities within the four model cells immediately adjacent to (left) and below (right) the injection pit (north/south profiles).

The estimated vertical flow rates in the four model cells immediately below the injection pit are shown in Figure 4.45 (right). The flow rates are seen to rapidly decrease during early injection times from values in excess of 0.70 m/day, before gradually decreasing to flow rates of less than 0.03 m/day after 248 minutes.

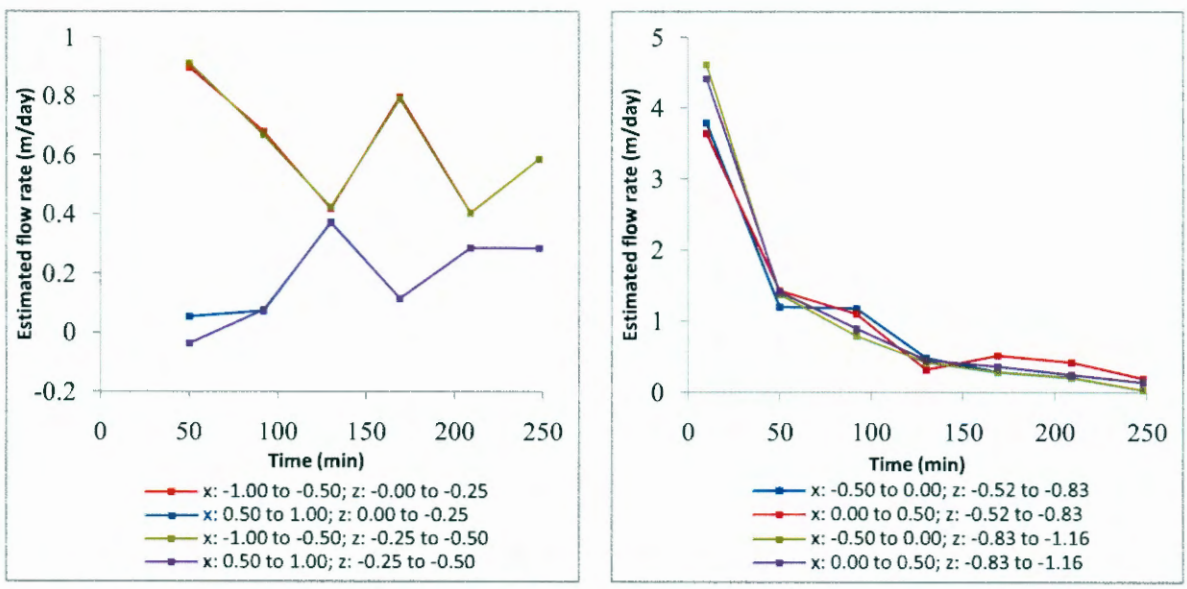

Figure 4.45 Estimated horizontal unsaturated flow rate within the four model cells immediately adjacent to (left) and below (right) the injection pit (north/south profiles).

4.6 Conclusion

In this section the hydraulic and chemical properties of the fine fly ash leachate experiments have been presented and the rates of salt load release to the environment were calculated. In every instance the chemical and hydrological properties of the various sections of the system under investigation differed.

4.6.1 Mineral identification

From these studies it was found that the chemical composition of the fly ash particles were similar to that found in literature, consisting mainly of the oxides of Si, Al, Ca, Mg, Fe, and minor P, Na, K and Ti. The crystalline fraction of the fly ash was found to consist of the mineral assemblages, mullite ($Al_{4.75}Si_{1.25}O_{9.63}$), alpha quartz ($SiO_2$), calcite ($Ca(CO_3)$), ferroan-dolomite ($Ca(Mg,Fe)(CO_3)_2$) and muscovite ($KAl_3Si_3O_{10}(OH)_2$).

It was clear that there is little to no change in the minerals the ash consists of during leaching and that it is fairly mature, consisting of species in equilibrium with the environment, thus those that are newly formed or remnants of minerals in the parent coal.

4.6.2 Constant head leaching experiment

The ash column laboratory experiments provided excellent controlled conditions which were used to describe site conditions and provide initial estimates of hydraulic and transport parameters. A parallel behaviour in the hydraulic conductivity with increasing depth of leached and unleached samples was found. These results do not however, take into account the effect of preferential pathways caused by bedding planes and areas of extensive leaching or weathering found in natural systems. The hydraulic properties of the column laboratory experiments also suggest that the ash properties change over time as water moves through the ash.

These results indicate that the profile at the sapling site may be alternatingly leached (0 - 12 m), followed by a water table or saturated section and a seepage face or area of high permeability at 25 – 28.5 m. This is correlated by the pH variation with an overall decrease in alkalinity with increasing depth, with the exception of the 9 – 12 m section which is highly alkaline and the 25.5 – 28.5 m section with little

variability. The change in pH values cannot solely be attributed to the drop in alkalinity, it can be assumed that it plays a significant role in the respective systems, since pH is a logarithmic function of proton concentration. Figure 4.46 illustrates the pH variation with depth of the first (blue) and last (red) leachate samples taken.

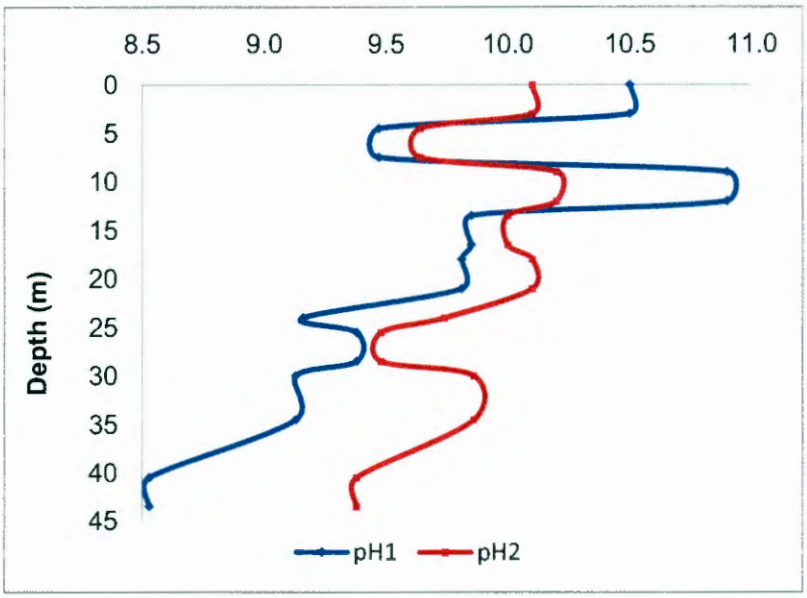

Figure 4.46 pH variations with depth of the first (blue) and last (red) leachate samples.

Chemical species released during the leaching process were analysed and it was determined that average salt load releases from the fly ash systems was approximately 4.6 g per day per ton of material. It was also found that there was a direct relationship between the salt load and hydraulic conductivity during leaching. (The values shown were calculated using real bulk densities for the respective material samples).

4.6.3 Transport properties

Hydraulic and transport properties of the ash have been evaluated both in the laboratory, using tracer tests and at field scale by time-lapse electrical resistivity tomography. Although similar results were obtained for the flow rates for the two methods, laboratory conditions seldom account for conditions in the field. There are also significant differences in the composition of fresh and weathered ash which may influence flow and element mobility.[5] The ability of ash dams to transmit fluid to the environment as surface and groundwater from a hydrological perspective is concerning, more so the unpredictability and variability thereof. The tracer tests

yielded flow rates of 0.0104 – 1.42 m/day at steady state conditions and showed similar hydraulic behaviour compared to that of leaching under constant head.

As part of the investigation into the flow patterns through an ash dam, the horizontal and vertical flow rates were investigated, by evaluating the resistivity changes in the subsurface over the time of the survey. The background ERT survey indicates the presence of a shallow resistive layer overlying a conductive layer. These layers are interpreted to be the unsaturated ash at surface overlying saturated ash. The saturated ash appears to occur at a depth of between 2 m and 2.75 m below surface.

The results of the time-lapse ERT survey show that horizontal flow through the ash strongly dominates over vertical flow. The flow rates through the ash were estimated by:

- Considering the rate of brine injection.
- Distance travelled by the brine plume over the time spanned by the investigations.
- Applying a modified Archie's law to the modelled resistivity values of model cells in the vicinity of the injection pit.

The rate of brine injection allowed a crude estimate of the average flow rate through the ash with a value of approximately 0.20 m/day at late injection times at a distance of 1 m from the centre of the injection pit. The horizontal distances travelled by the brine plume were used to calculate an upper estimate for the average horizontal flow rate of between 0.70 and 1.1 m/day.

Applying the modified Archie's law to the modelled resistivities suggested that horizontal flow rates may vary between 0.07 and 0.13 m/day. Due to model errors this method was less successful in estimating the vertical flow rates. However, there are indications that the initial vertical flow rate was very high (> 0.70 m/day), but that it rapidly decreased over time, falling off to values of less than 0.03 m/day approximately six hours after injection commenced.

The results discussed in the previous sections of this chapter were evaluated in an attempt to develop a conceptual understanding of the geochemical and flow characteristics of fluids moving through a fly ash dam. This was done in field and laboratory scale experiments as discussed in Chapter 3, producing an estimation of susceptibility to change. The mineral identification, mobility of elements in the ash and flow parameters was discussed. The results from the self potential tracers and subsequent matrix response will be discussed in the next chapter (Chapter 5).

4.7 References

[1] Rodriguez-Navarro, C., Cultrone, G., Sanchez-Navas, A., and Sebastian, E., 2003, *TEM study of mullite growth after muscovite breakdown, American Mineralogist,* 88, 713–724.

[2] White, S. C., and Case, E. D., 1990, *Characterization of fly ash from coal-fired power plants.* J. Mater. Sci. 25:5215–5219.

[3] Özbayoğlu, G. and Özbayoğlu, M.E., 2006, *A new approach for the prediction of ash fusion temperatures: A case study using Turkish lignites.,* Fuel, 85, 545-552.

[4] Soong, Y., Fauth, D. L., Howard, B. H., Jones, J. R., Harrison, D. K., Goodman, A. L., Gray, M. L., and Frommell, E. A., 2006, *CO2 sequestration with brine solution and fly ashes.*, Energy convers. manage. 47:1676–1685.

[5] Akinyemi, S. A., Akinlua, A., Gitari, W. M. and Petrik, L. F., 2011, *Mineralogy and mobility patterns of chemical species in weathered coal fly ash.*, Energy sources, Part A: Recovery, utilization, and environmental effects, 33:8, 768-784.

[6] Matjie, R. H., Ginster, M., van Alphen, C. and Sobiecki, A., 2005, *Detailed characterisation of Sasol ashes. In:* LTD., S. T. P. (ed.). Sasolburg, South Africa.

[7] Ward, C.R., French, D., 2006, *Determination of glass content and estimation of glass composition in fly ash using quantitative X-ray diffractometry.*, Fuel 85, 2268–2277.

[8] Ward, C.R., French, D., Jankowski, J., Riley, K. and Li, Z., 2006, *Use of coal ash in mine backfill and related applications.,* (Research report No. 62), CCSD, University of New South Wales.

[9] U.S. Department of Transportation, F. H. A., 1998, *Turner-fairbank highway research centre.* [Online]. Available: http://www.tfhrc.gov/hnr20/recycle/waste/cfa51.htm.

[10] Karayigit, A.I. and Gayer, R.A., 2001, *Characterisation of fly ash from the Kangal power plant, Eastern Turkey.*, International ash utilization symposium, Centre for applied energy research, University of Kentucky, Paper 4.

[11] Tripathy, S. and Praharaj, T., 2006, Delineation of water and sediment contamination in river near a coal ash pond in Orissa, India, *Coal combustion byproducts and environmental issues.*, Springer, NY, 241.

[12] Polic, P.S., Ilic, M.R. and Popovic, A.R., 2005, *Environmental impact assessment of lignite fly ash and its utilization products as recycled hazardous wastes on surface and ground water quality.*, Handb Environ Chem Vol. 5, Part F,Vol. 2.

[13] Fatoba, O.O., 2010, *Chemical interactions and mobility of species in fly ash-brine co-disposal systems*. UWC.

[14] Department of water affairs and forestry (DWA)., 1998, *Minimum requirements for the water monitoring at waste management facilities.*, CTP Book Printers., Capetown.

[15] Stevens, B., 1996, *Vadoze zone hydrology*, Florida: Lewis publishers.

[16] Rasmussen, T.C., 2013, *Chemical hydrology*, in: Quantitative hydrology, WASR 4500/6500. University of Georgia, Athens, p. 12.

Chapter 5

Self potential tracer tests and matrix response

5.1 Introduction

This chapter attempts to shed light on the effects of long term chemical interaction of the fly ash in the co-disposal system with constituents native to the ash and that of the natural environment. Saturated solutions of the halogen salts (NaCl, KCl, LiCl, LiBr, KBr and NaBr) were prepared and the electrical potential was compared with the chemical interaction in the resulting leachate during a tracer test on one of the fly ash samples.

This was done to determine whether the tracer could be followed using the self potential variation in the column as well as to monitor the long term chemical interaction of solutions with the sample matrix. The salts were chosen as they naturally occur in nature and in elevated concentrations in the leachate collected from the constant head synthetic groundwater leaching experiment as mentioned in Chapter 4. The salts are all monovalent with different atomic radii and standard potentials as can be seen in Table 5.1. The atomic radius and viscosity influences the diffusion of elements in solution.[1]

Table 5.1 Atomic radii of selected elements.

Element	Atomic radii (pm)	Standard Potential E(volts)
Mg^{2+}	145	-2.38
Li^{+}	167	-3.04
Na^{+}	190	-2.71
Ca^{2+}	194	-2.76
K^{+}	243	-2.92

Preferential adsorption of ions produces a self potential of ground water in motion under a pressure gradient through a porous media. This was confirmed by the cation exchange capacity as calculated in Chapter 4 (Section 4.3.1), indicating a net negative charge at the surface of the fly ash. Thus, the direction of flow is characterised by an overall increase of negative ions in the solution.[2]

The self potential is caused by the electric double layer of ions associated with the interface between the mineral grains and the pore fluid (ground water) in natural systems. Unoccupied sites (bonds) at the surface of mineral grains adsorb ions from solution, positive ions being attracted to the surface and negative ions being

repelled. This is caused by electrostatic interactions and surface complex formation.[1] This electrostatic force, which is effective over greater distances than purely chemical forces, affects surface complex formation and loosely binds other ions to the surface, effectively changing the surface charge.[1]

Figure 5.1 shows the SP range of the five equally spaced electrodes positioned along the permeameter sides from top to bottom (**SP1** – **SP5**) at equilibrium before and after the experiments. As in literature examples the net charge found over the material became increasingly negative in the direction of flow.[3,4] There was however a much larger negative self potential over the second probe which may be seen as **SP2** in Figure 5.1. This may be due to the relatively large pressure difference caused by diffusion along the flow path.

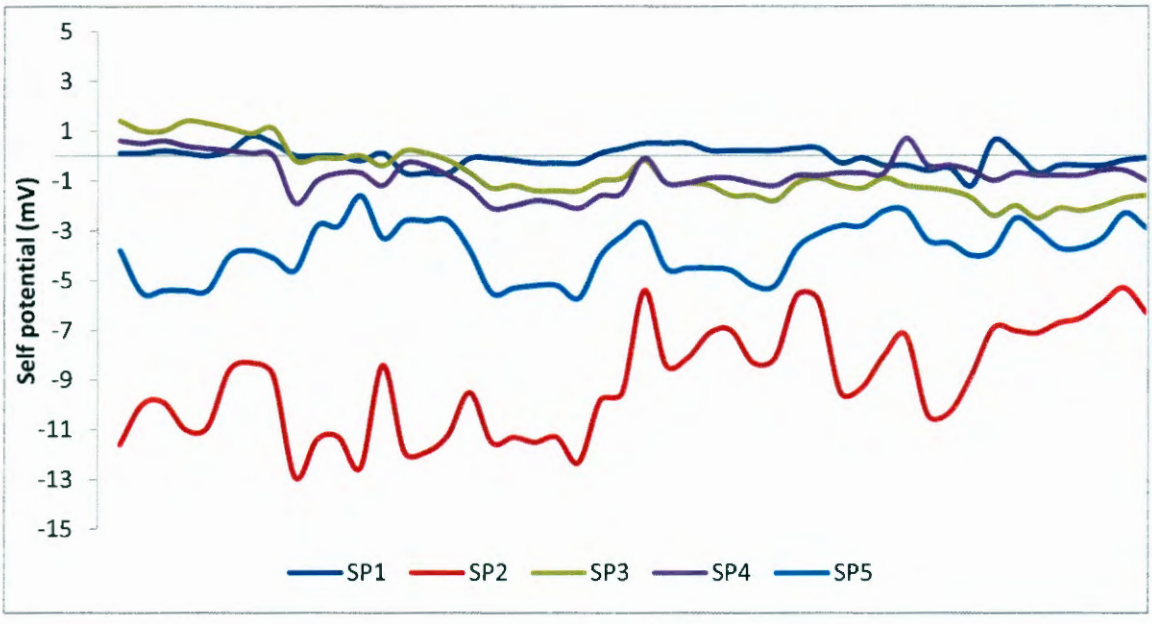

Figure 5.1 Self potential over the five equally spaced probes indicated by increasing depth with increasing probe number (SP1 - SP5).

From the analysis of SPT data, we can see that the arrival of the salt front corresponds to a sharp reduction in the measured self potential, which returns to initial values after the salt front passed each electrode as can be seen in Figure 5.2. Furthermore the SP anomaly decreases with the injection of the half concentration tracer.

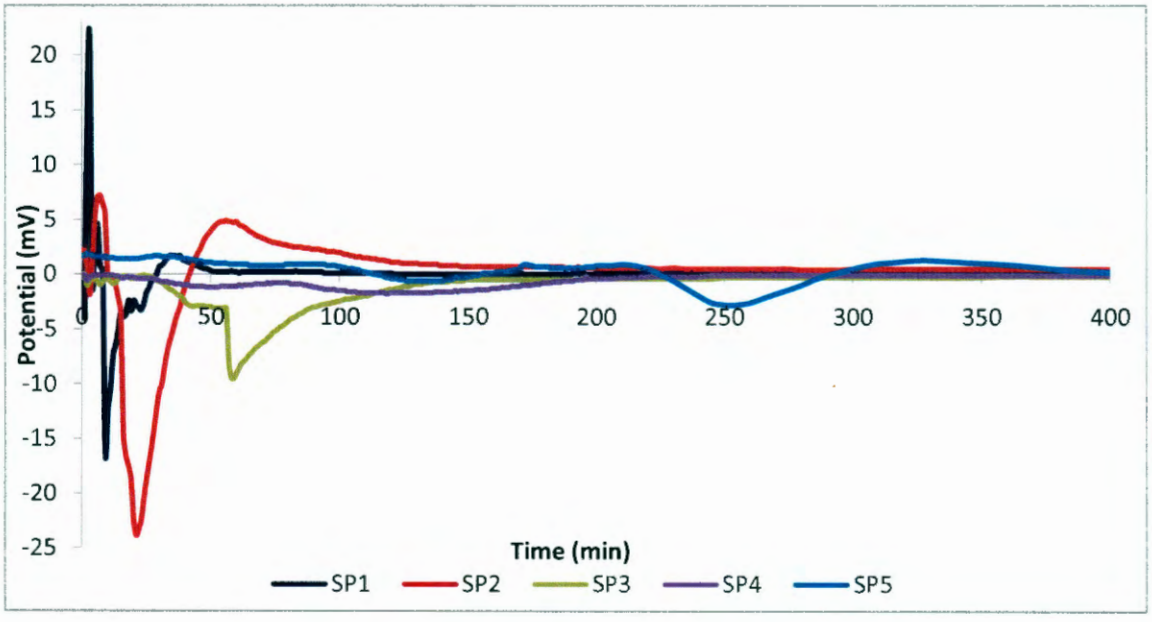

Figure 5.2 Self potential variation during the NaCl SPT over the 5 probes.

In the subsequent sections the water chemistry of the resulting leachate during the injection of the various salts are discussed.

5.2 NaCl SPT

The NaCl SPT was for the most part consistent, as seen in Figure 5.3, although there is a change in dominant cat- or an-ions in the resulting leachate, which may influence the resulting electro conductivity. During the NaCl self potential tracer it took approximately 35 minutes before the resulting increase in electro-conductivity could be noted. There was initially a decrease in chloride concentration resulting in a delay of 83 minutes when compared to other solute concentration increases. The Na concentration profile followed that of the electro-conductivity of the resulting leachate. At the same time there was also an increase in the concentration of Ca, K and Mg.

The half concentration NaCl SPT can be seen as having a lower self potential variation and also seems to be slower as seen in Figure 5.3. As the experiment is repeated, the release of those elements other than that of the injected salt that go into solution as a result of the tracer, diminishes. The half concentration NaCl SPT did however have K become the dominant cation over Ca more quickly (Approx. 200 min *vs.* 300 min) than the saturated NaCl SPT's as can be seen in Figure 5.6. The Na concentration is also higher in the half concentration NaCl SPT's leachate compared to the saturated solutions.

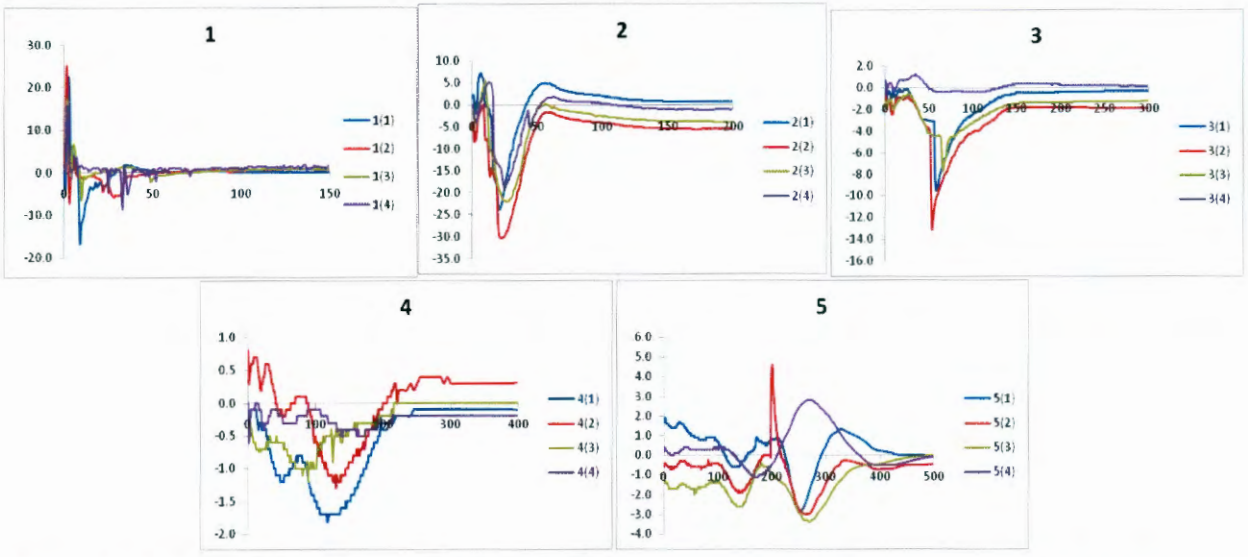

Figure 5.3 Self potential variation of fly ash indicated by the probes(1 Top – 5 Bottom) placed in equal increments along the length of the permeameter during the NaCl tracer test.

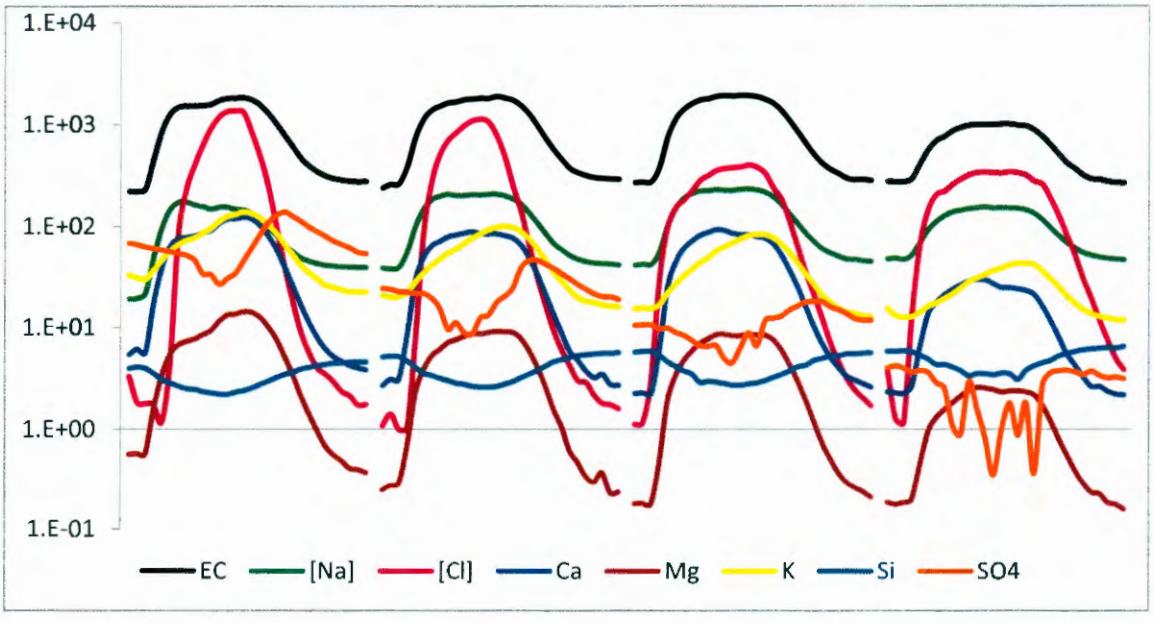

Figure 5.4 Water chemistry plots of the successive tracer experiments, indicating from left, the 3 saturated tracers followed by the half concentration experiment.

The graphs of the first experiment, using a saturated solution of the respective salt and subsequently that of the experiment using half the concentration of the saturated solution are illustrated in the respective sections. The axis on the left of the graphs, indicates the concentration of those elements monitored during the experiment (ppm or mg/l) as well as the electro conductivity (**solid black**) in micro Siemens per centimetre (µS/cm). The right axis indicates the corrected self potential observed in mill volts (mV). The normalised self potential data for the bottom probe (**SAT5 – dashed black**) is indicated on the chemistry plot, as it is the closest to the collected leachate.

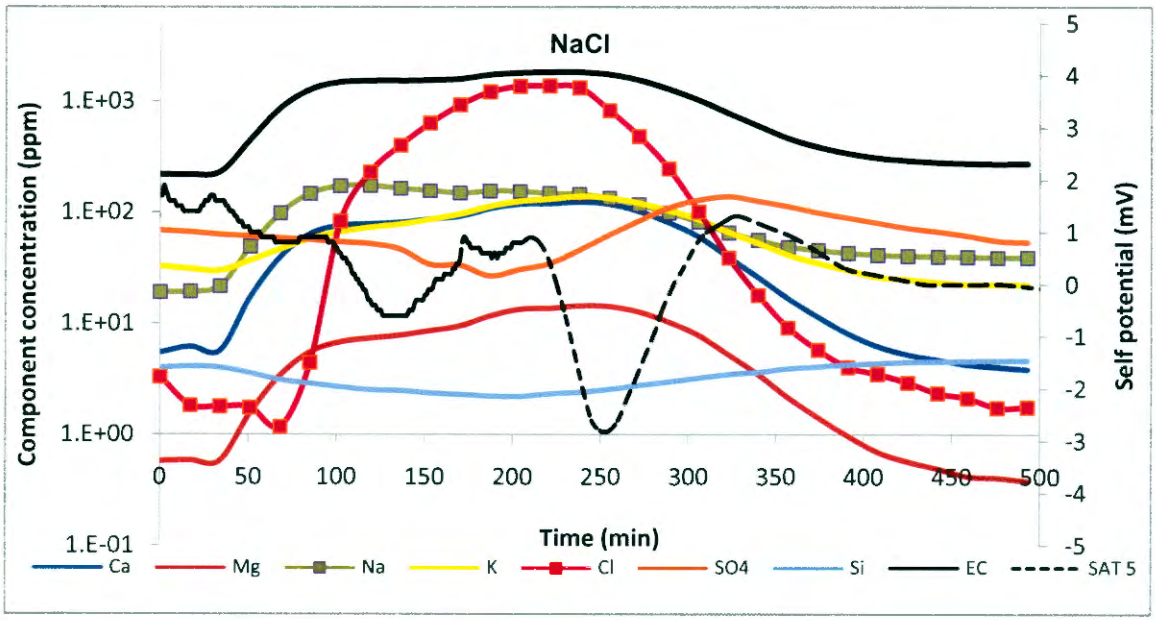

Figure 5.5 First NaCl SPT showing the chemical composition of the resulting leachate from a saturated solution injected as well as the self potential of the bottom probe.

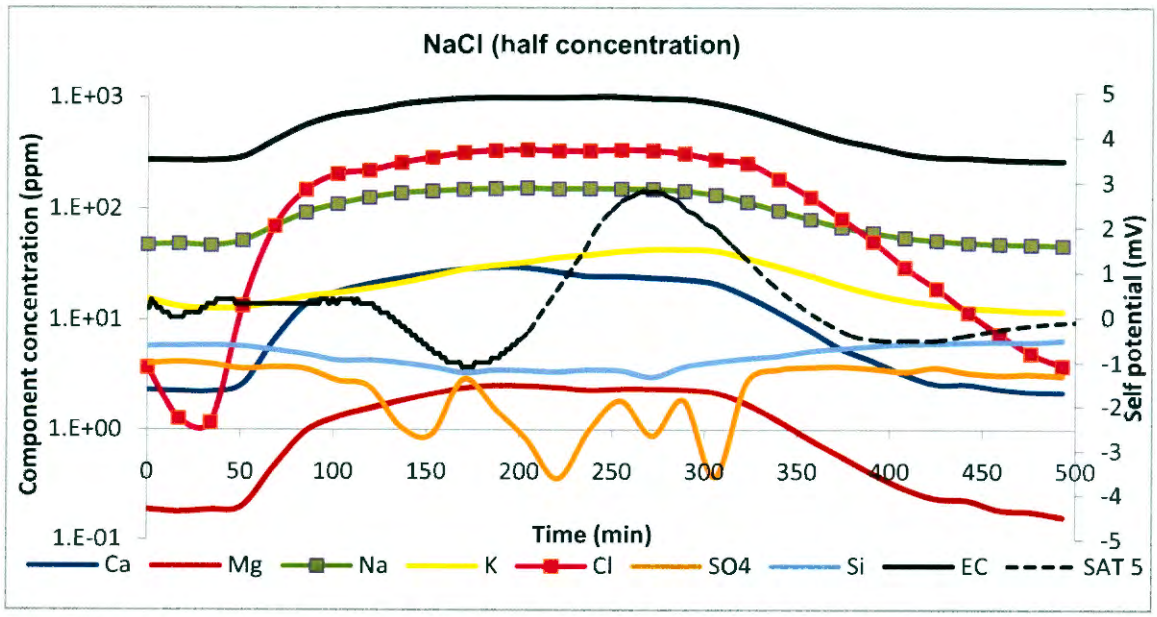

Figure 5.6 NaCl SPT showing the chemical composition of the resulting leachate from a half concentration solution injected as well as the self potential of the bottom probe.

5.3 KCl SPT

During the KCl SPT chloride concentration did not show the same initial decrease followed by an increase during the first experiment as it did for the NaCl SPT, as seen in Figure 5.7. This delayed increase was however observed for the two repeat runs, but not for the half concentration experiment when the chloride concentration was lower as seen in Figure 5.8. It should also be noted that the peak chloride concentration of the first saturated experiment is similar to that of the half concentration experiment. There was an increase in all element concentrations as well as the suppression of Si and SO_4 release from the matrix. The concentration of Ca released from the matrix, compared to that of the injected KCl, was also noticeably high. The Na from the previous experiment was systematically released showing an increase in the resulting leachate while the concentration of the other solutes was on the decline. This indicates a type of buffering or sorption effect as the experiments that followed also showed this behaviour.

The half concentration experiment also showed a sudden increase in the concentration of Ca, Na, K, and Mg at 187 minutes as well as a sudden increase of Na and decrease of Ca, K, and Mg concentrations at 262 - 275 mins. Electrical activity was over in less than 100 minutes, except for the first experiment which had activity in the bottom probe at approx. 240 minutes even though the electro-conductivity took in excess of 300 minutes to return to background levels. Thus there is a neutralising of the pore fluid.

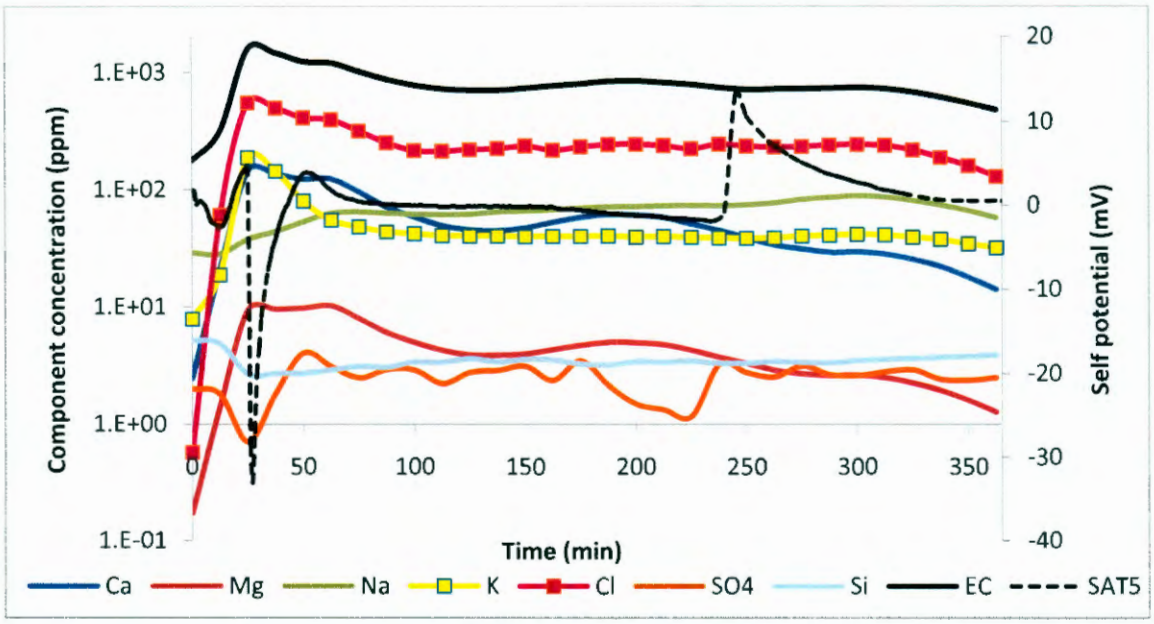

Figure 5.7 First KCl SPT showing the chemical composition of the resulting leachate from a saturated solution injected as well as the self potential of the bottom probe.

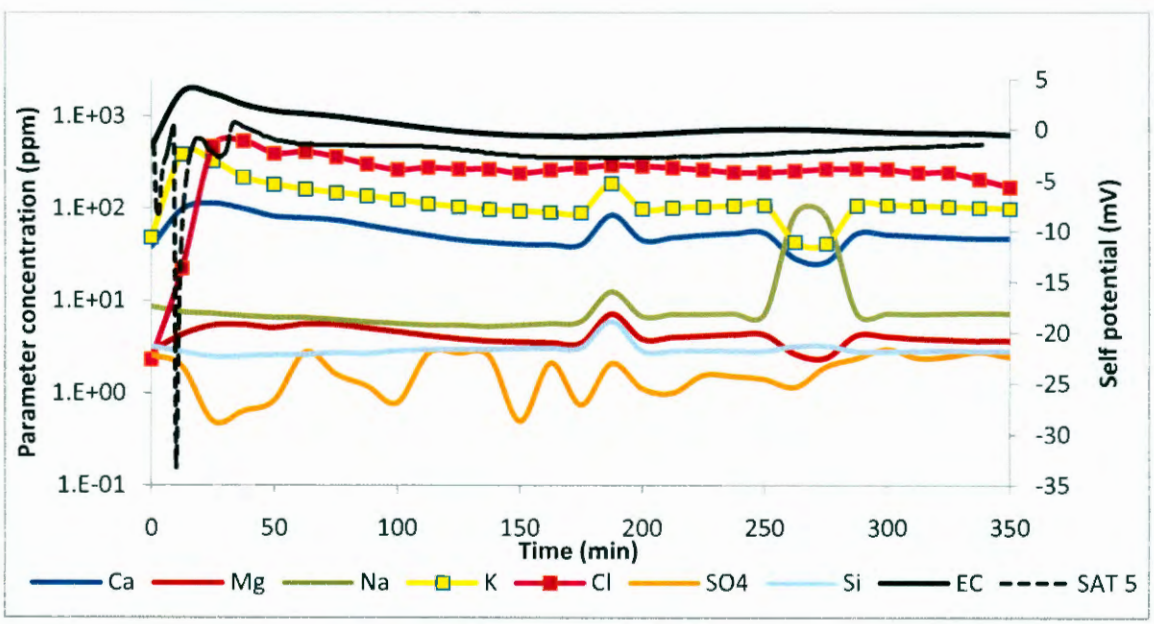

Figure 5.8 KCl SPT showing the chemical composition of the resulting leachate from a half concentration solution injected as well as the self potential of the bottom probe.

5.4 LiCl SPT

The LiCl SPT showed similar behaviour to that of the KCl SPT with Ca and the cation from the previous experiment (K) being the major elements released second to that of the anion of the injected salt during the first experiment. It did not however show the delay in chloride concentration as was found in the NaCl and KCl 'SPT's.

Ca and K became less prevalent as the saturated solution experiments continued and then again became major cations in the leachate during the half concentration experiment. This is contrary to the half concentration experiments of the other salts, where the ions of injected salt have the highest concentration. The water chemistry of the first experiment and that of the half concentration can be seen in Figure 5.9, 5.10 respectively. The electrical interaction also indicates a more rapid neutralisation.

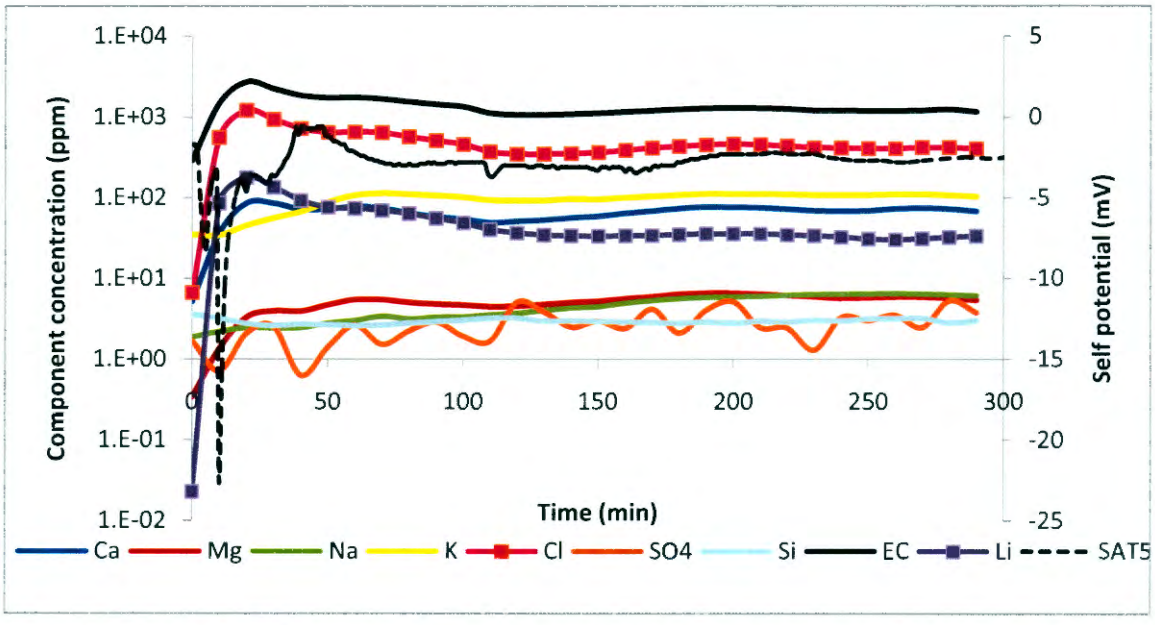

Figure 5.9 First LiCl SPT showing the chemical composition of the resulting leachate from a saturated solution injected as well as the self potential of the bottom probe.

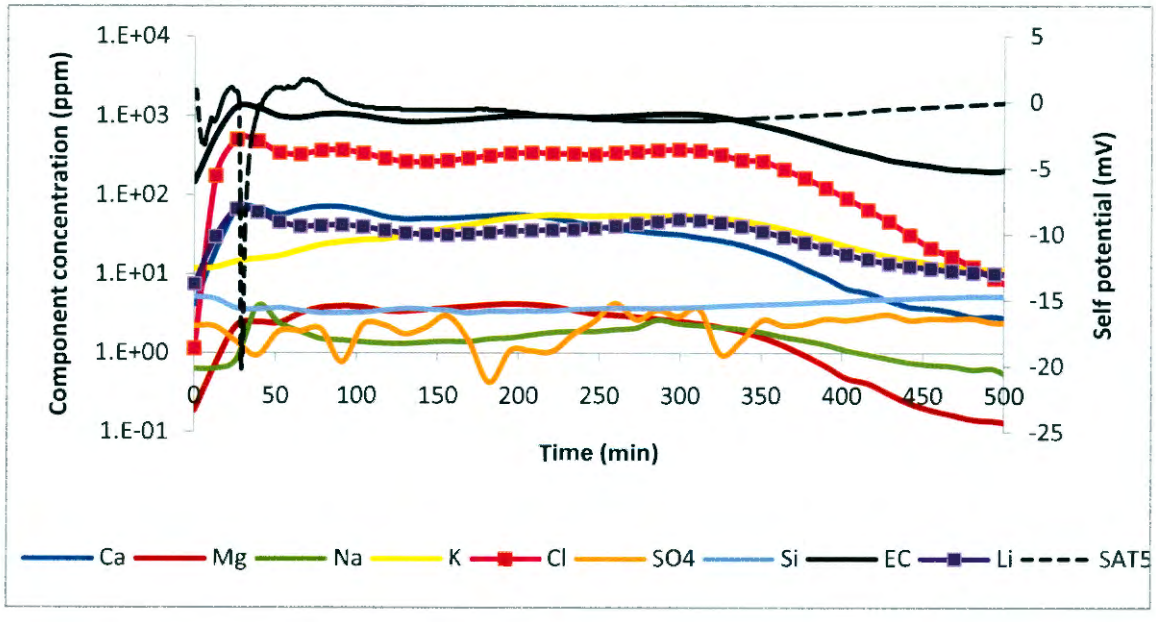

Figure 5.10 LiCl SPT showing the chemical composition of the resulting leachate from a half concentration solution injected as well as the self potential of the bottom probe.

5.5 LiBr SPT

During the first LiBr SPT a large drop in charge was detected at the top of the permeameter, which is later again observed in the bottom. Once again there is a large concentration of Ca and K during the first experiment. Li concentrations in the resulting leachate are seen to increase during the subsequent tracers, indicating that less of the cation is being adsorbed to the matrix. The water chemistry of the first experiment and that of the half concentration can be seen in Figure 5.11 and 5.12 respectively.

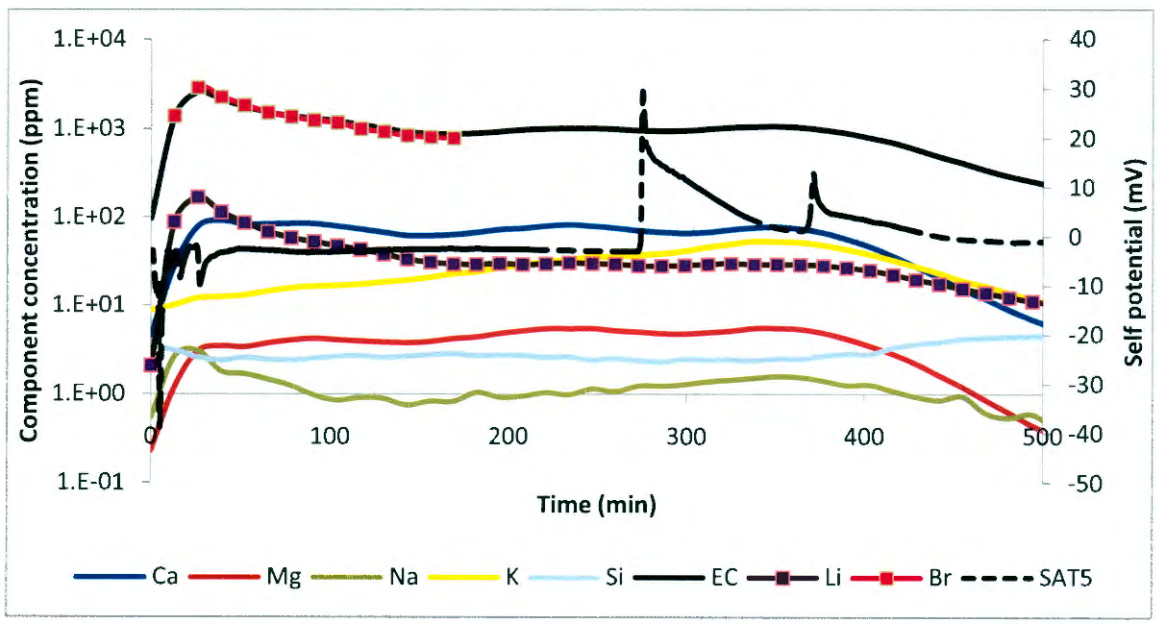

Figure 5.11 First LiBr SPT showing the chemical composition of the resulting leachate from a saturated solution injected as well as the self potential of the bottom probe.

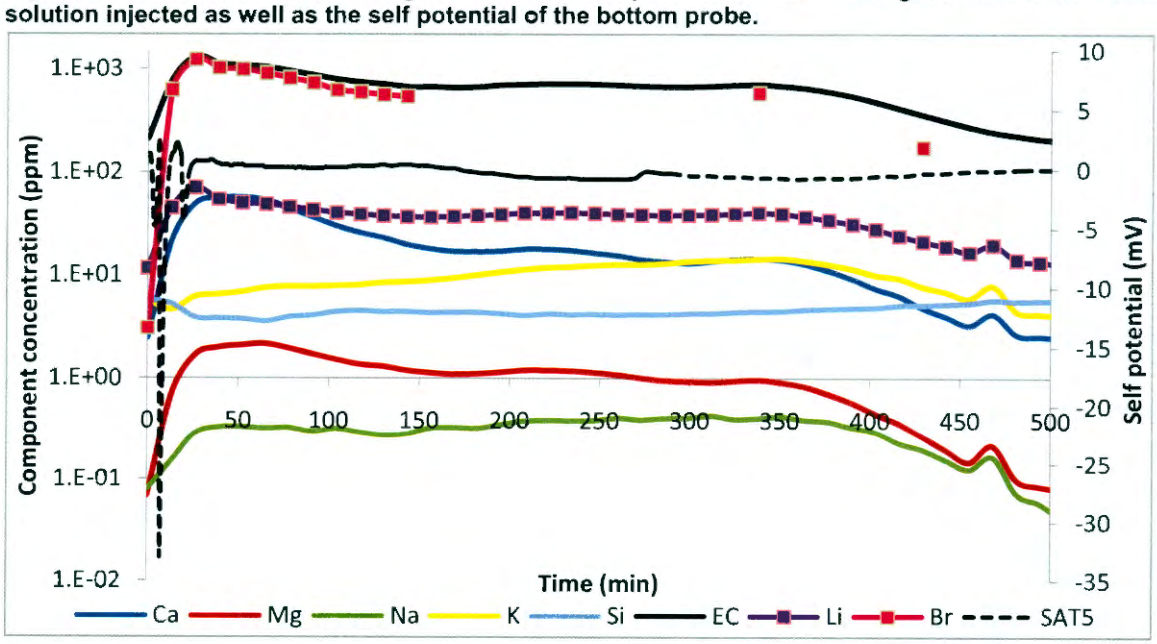

Figure 5.12 LiBr SPT showing the chemical composition of the resulting leachate from a half concentration solution injected as well as the self potential of the bottom probe.

5.6 KBr SPT

Similar trends were observed for the KBr SPT's. The tracer tests showed similar electrical activity as well as chemical interaction, with the previous cation (Li) being expelled systematically as well as decrease in concentration over the course of the experiments. The water chemistry of the first and that of the half concentration experiment for the KBr SPT's can be seen in Figure 5.13 and 5.14, showing once again, a large amount of Ca going into solution.

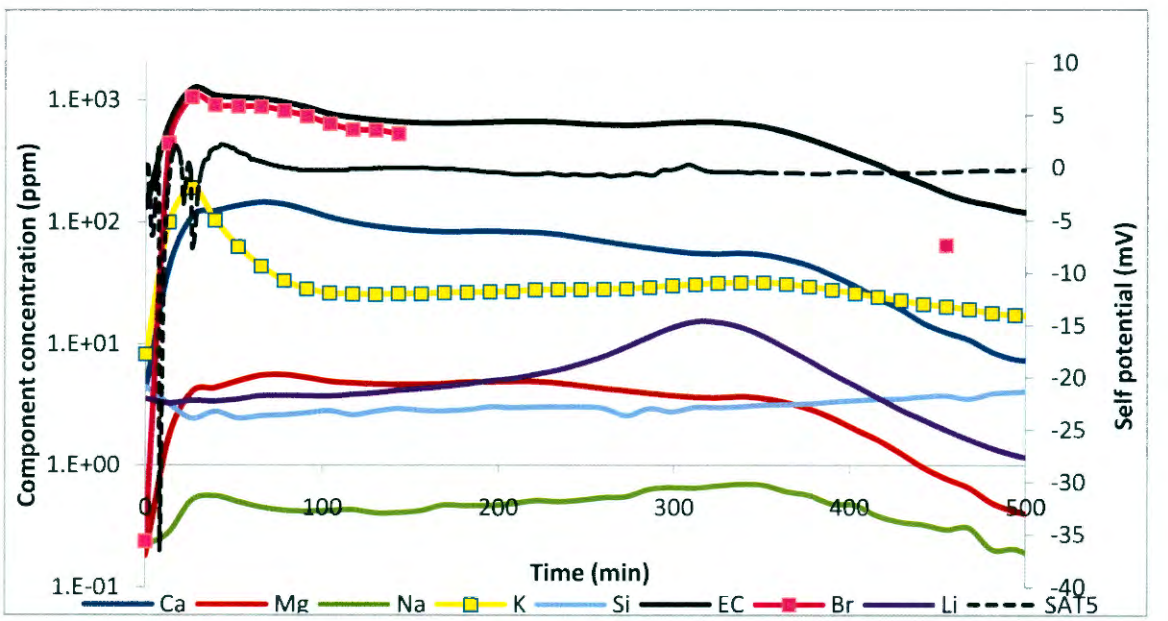

Figure 5.13 First KBr SPT showing the chemical composition of the resulting leachate from a saturated solution injected as well as the self potential of the bottom probe.

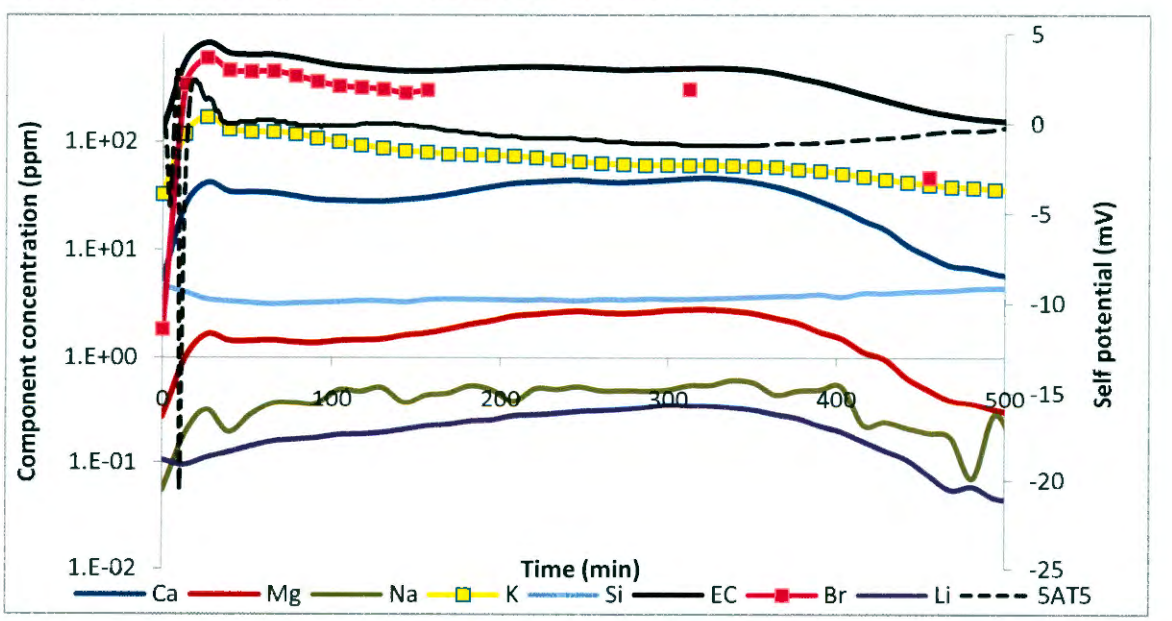

Figure 5.14 KBr SPT showing the chemical composition of the resulting leachate from a half concentration solution injected as well as the self potential of the bottom probe.

5.7 NaBr SPT

Similar trends were observed for the NaBr SPT's. The tracer tests showed similar electrical activity as well as chemical interaction, with the previous cation (K) being expelled systematically as well as decrease in concentration over the course of the experiments. The water chemistry of the first and that of the half concentration experiment for the NaBr SPT's can be seen in Figure 5.15 and 5.16 showing the suppression of silica release and increased release of Ca, K and Mg. Li is however found in very low concentrations.

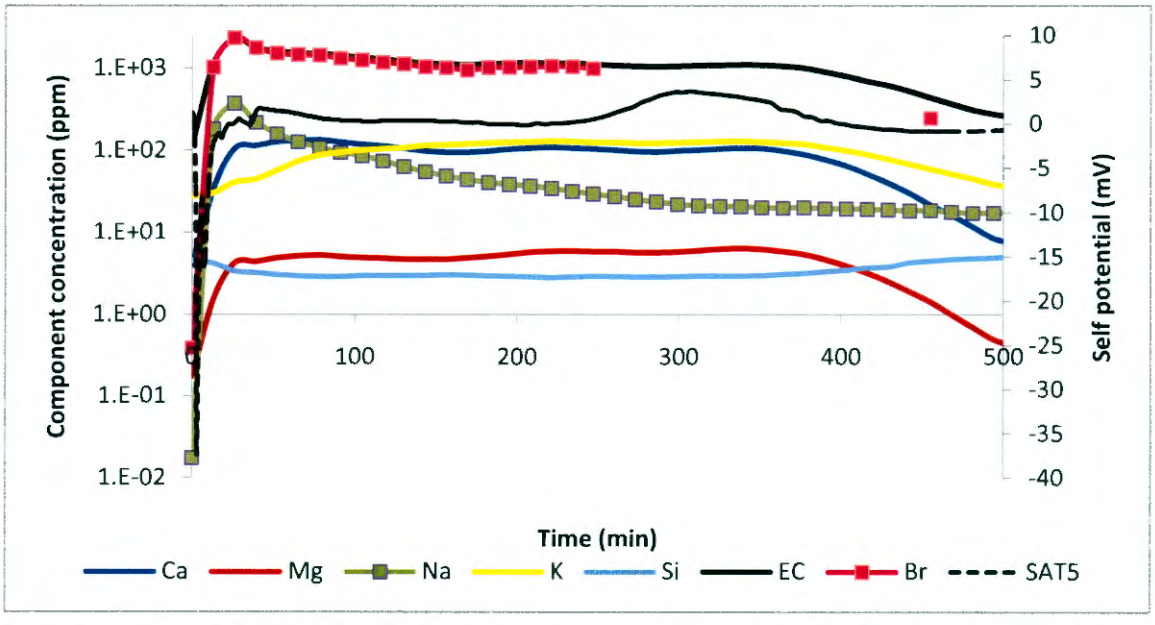

Figure 5.15 First NaBr SPT showing the chemical composition of the resulting leachate from a saturated solution injected as well as the self potential of the bottom probe.

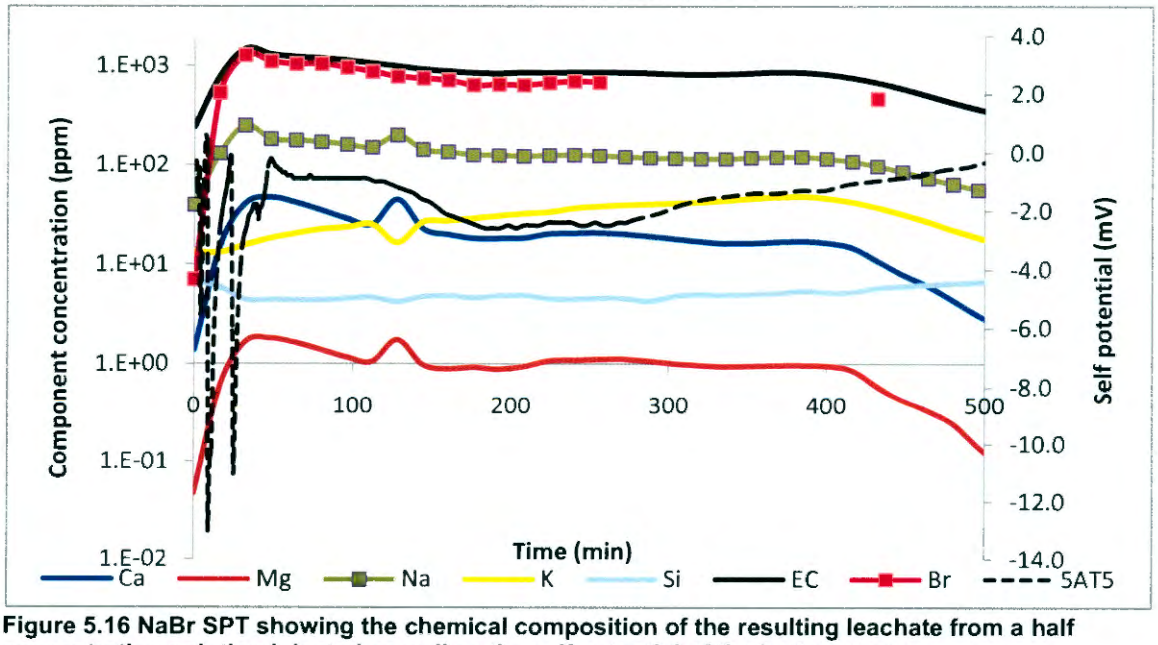

Figure 5.16 NaBr SPT showing the chemical composition of the resulting leachate from a half concentration solution injected as well as the self potential of the bottom probe.

5.8 Conclusion

The flow-through leaching test method was used to imitate the leaching process of the fly ash as the waste may have degraded under various environmental forces over time, exposing groundwater to the porosity system of the waste matrix.

Overall there is an increase in the concentration of the cat- and an-ion of the corresponding salt injected as well as suppression in the release of silica and a fluctuating sulphate concentration. The concurrent increase in the concentration of other ions can also be seen prior to returning to background levels. Thus there are some instances where the observed increase in electro-conductivity is the result of ions other than that of the injected salt. This may be due to a concentration gradient being created by the tracer, accelerating the leaching process and flow properties.[5] It also indicates that the interaction is between the carbonates in the system as the aluminosilicate glass dissolution is suppressed.

The concentration of Ca and K is higher than the injected cation in the first experiment except for the NaCl tracer which was previously used and these elements are also native to the ash. The concentration of Ca systematically decreases although Ca and K become the predominant cation in the LiCl half concentration experiment.

There was a temporary increase in the permeated volume after injection, considerably more than the injected volume. There is large amount of electrical potential variation in the top of the column where diffusion is lowest. The electrical signal also seems to register more rapidly at the deeper probes as the experiments continued, indicating the formation of preferential pathways throughout the column.

The successive interaction of the saturated solutions with the matrix thus strips it of Ca and K and adsorbs the cations from the salt to the matrix. These adsorbed cations are then again expelled from the matrix once a different cation passes through the matrix. Thus a tracer can only be used for transport parameter estimation if previously exposed to the system and should be monitored chemically instead of electrically when used on fly ash or soils with high cation exchange capacities. Table 5.2 illustrates the cumulative cations in the resulting leachate. The

concentration of the injected salt can be seen to increase during the successive injection of salts, indicating that less of the cations are adsorbed to the surface of the particles. The table also indicates the expulsion of the cations from the previous salt injected when a new cation is introduced.

Table 5.2 Concentration of introduced and expelled cations of injected salts.

Salt	NaCl	KCl	LiCl	LiBr	KBr	NaBr
Cation app (mg)	275.45	419.55	196.46	159.83	427.14	406.8
Anion app (mg)	424.55	380.42	1003.54	1840.17	872.86	1413.2
Tot Ca	75.9	81.6	86.7	102.1	115.5	137.3
	56.2	100.7	78.3	66.9	122.5	85.5
	54.5	83.8	65.4	60.2	106.5	66.5
0.5x	18.7	87.6	64.0	34.0	52.1	29.6
Tot Mg	8.3	6.6	6.6	6.3	5.9	6.9
	5.7	7.9	5.6	3.9	6.6	4.3
	5.3	6.2	4.5	3.4	5.7	3.2
0.5x	1.7	6.4	4.1	1.7	2.9	1.4
Tot Na	**136.2**	98.5	5.8	2.1	0.8	**105.0**
	167.5	51.6	4.9	1.4	0.8	**203.9**
	179.3	12.3	3.7	1.0	0.7	**257.6**
0.5x	**134.1**	18.3	2.8	0.5	0.7	**194.9**
Tot K	98.4	**73.4**	124.2	46.4	**64.8**	147.7
	66.6	**101.2**	102.2	30.3	**111.9**	118.3
	53.1	**142.7**	80.4	24.6	**158.9**	79.7
0.5x	32.3	**198.2**	59.1	16.2	**129.3**	46.6
Tot Li	-	-	**70.0**	**68.3**	9.7	0.4
	-	-	**123.9**	**90.1**	2.0	0.3
	-	-	**142.8**	**99.6**	0.8	0.2
0.5x	-	-	**60.1**	**62.8**	0.4	0.1
Tot Cl/Br	466.3	372.0	660.5	-	-	-
	400.3	448.0	893.3	-	-	-
	205.3	446.5	903.6	-	-	-
0.5x	223.2	410.9	458.3	-	-	-

5.9 References

[1] White, W.M., 1999, *Geochemistry*., Wiley-Blackwell.

[2]Erchul, R.A. and Slifer, D.W., 1989, *Geotechnical applications of the self potential (SP) method.*, (Technical Report REMR-GT-6 Report 2 of a series No. OMS p.0704-O188).Department of civil engenering, Virginia military institute Lexington, VA 24450.

[3] Cooper, S. S., Koester, J. P. and Franklin, A. G., 1982, *Geophysical investigation at Gathright dam*, Miscellaneous paper GL-82-2, US army engineer waterways experiment station, Vicksburg, MS.

[4] Ahmad, M., 1964, *Laboratory study of streaming potential*, Geophysical prospecting, 12, 49-64.

[5] Poon, C.S. and Chen, Z.Q., 1998, *Comparison of the characteristics of flow-through and flow-around leaching tests of solidified heavy metal wastes*. Chemosphere, 38.

Chapter 6

Conclusion

6.1 Introduction

This chapter summarises the discussions, significant findings and conclusions of the results presented in the previous chapters. The outline of the objectives set in Chapter 1 was:

- Interpret the results obtained from chemical analysis of a fly ash leaching experiment, concerning the mobility of water-soluble major and trace elements native to the weathered ash.
- Obtain information on the flow patterns through ash by evaluating solute transport through the heterogeneous medium at a laboratory and field scale.
- Evaluate the matrix response to the introduction of salts namely saturated solutions of NaCl, KCl, LiCl, LiBr, KBr and NaBr to emulate long term chemical interactions.
- Develop a conceptual understanding of the flow through a fly ash dam and the geochemical characteristics associated with it.

6.2 Overview

The aim of this study was to provide a detailed insight into the spatial and temporal mobility of major and trace elements from weathered fly ash from a disposal site. The system was evaluated to determine how the movement of fluid is influenced as a result of chemical interactions and long term exposure to the elements. In order to achieve the aims and objectives of this study, mineral identification, flow through constant head leaching, cation exchange capacity, tracer test, self potential tracer tests (SPT's) and matrix response as well as a geophysical study were carried out. The standard analytical modelling software, StanMod, was applied to calculate the saturated average pore water velocities (v) and dispersion coefficients (D). Several analytical techniques such as scanning electron microscopy-energy dispersion spectroscopy (SEM-EDS), powder X-ray diffraction (PXRD), and inductively coupled plasma-mass spectroscopy (ICP-MS) were applied to characterize the weathered and leached fly ash. The geophysical study was performed to estimate vertical and horizontal flow rates so as to compare to the finding of the laboratory study to

conditions in the field. The results of these tests and analyses were incorporated in order to give a decisive account of this study.

6.3 Characterisation of the weathered and leached fly ash

The characterisation of the fly ash used in this study is important in order to understand the physical, mineralogical and chemical composition of the samples. The characterisation was done to compare what was originally contained in the weathered samples with the residues after leaching the fly ash.

The PXRD analysis of the fly ash (Section 4.2.1) showed the complicated nature of the fly ash in terms of its mineralogical compositions. The major crystalline mineral assemblages of the fly ash are, mullite ($Al_{4.75}Si_{1.25}O_{9.63}$), alpha quartz ($SiO_2$), calcite ($Ca(CO_3)$), ferroan-dolomite ($Ca(Mg,Fe)(CO_3)_2$) and muscovite ($KAl_3Si_3O_{10}(OH)_2$). The fly ash may consist of a large component of amorphous glass (40 – 60 %), which cannot be characterised using XRD patterns.

There is little to no change in the composition of the crystalline fraction of the ash during leaching, indicating that it is fairly mature, consisting of species in equilibrium with the environment, thus those that are newly formed or remnants of minerals in the parent coal.

The scanning electron micrographs of fly ash (Section 4.2.2) showed the presence of solid spheres, cenospheres (Fe-Ca-Al silicate glass with trace amounts of Ti, K and Mg) as well as porous structures (coal remnants) and crystalline material (quartz and clay minerals). From these studies it was found that the chemical composition of the fly ash particles were the oxides of Si, Al, Ca, Mg, Fe, and to a lesser extent P, Na, K and Ti, indicating a class F ash due to the relatively low Alkalis and CaO (<20 %) and high SiO, Al_2O_3 and Fe_2O_3(>70 %). The relative change observed was an increase of SiO_2, Al_2O_3 and Fe_2O_3 accompanied by a decrease in CaO and MgO after leaching.

6.4 Constant Head Synthetic Groundwater Leaching experiment

This test was done to determine the leachability of species (Section 4.3.2) from the fly ash and the rate of release (Section 4.3.2.3) of species when water percolates through the fly ash dam over time. The experiments also provided excellent controlled conditions which were used to simulate the conditions after disposal at the industrial complex and to provide initial estimates of the hydraulic and transport parameters (Section 4.4.1).

The results do not, however, take into account the effect of preferential pathways caused by bedding planes and areas of extensive leaching or weathering found at the site. The hydraulic properties of the constant head synthetic groundwater leaching experiment also suggest that the ash properties change over time as water moves through the ash (Section 4.4.1).

The leachate solutions were found to initially be high in SO_4, Cl, Na and Ca, changing to a much more alkaline and Ca-rich composition (Section 4.3.2.2) as leaching continued. Thus, the initial contribution from chloride (Cl^-) and sodium (Na^+) is substituted by carbonates (HCO_3^-, CO_3^{2-}) and calcium (Ca^{2+}). This can be explained by the rapid release of the halide species from the system which are then replaced by calcium carbonate and sulphate species. There is also a systematic release of the more resistant elements Si, Al and F, indicating the dissolution of the aluminosilicate glass (Section 4.3.2.3).

The salt load showed an exponential decrease over time, accompanied by a decrease in flow rate (Section 4.3.2.3 and 4.4.1) The average load at the surface is moderate as less weathering has occurred (younger ash). This may be due to intermittent rainfall as there is a larger amount of alkaline species that may still be leached from this section, although more mobile elements such as Na and Cl have been found in lower concentrations. This indicates that if water is allowed to infiltrate the system without interruption, that the fly ash would release the majority of its captured salt in a short period of time. It also suggests that flow would not only be

driven by a difference in hydraulic head, but also by high concentration gradients in saturated areas of high salinity.

As for the minor components, F, Br, Al, Cr, Mo, Ba and Mn could pose problems to the environment, but in particular Li and B which are most concentrated in the deeper levels, closest to the water table. Li and Cr are the dominant trace elements, after which Li and V become predominant as leaching continues (Section 4.3.2.2).

6.5 Transport properties

Hydraulic and transport properties of the ash have been evaluated both in the laboratory, using tracer tests (Section 4.4.2) and at field scale by time-lapse electrical resistivity tomography (Section 4.5). The transport parameters investigated during the leaching of the fly ash from the industrial complex (Section 4.4.1) were to determine if there was a significant proportion of the matrix that goes into solution or cemented.

Laboratory scale tracer tests analysis were performed to evaluate the saturated hydraulic and transport parameters of the fly ash system. This was done by controlling factors that may influence the physical environment such as temperature, liquid density, and liquid viscosity.

Although similar results were obtained for the flow rates for the two methods, laboratory conditions seldom account for conditions in the field. There are also significant differences in the composition of fresh and weathered ash which may influence flow or element mobility and are highly dependent on the method of deposition. The ability of ash dams to transmit fluid to the environment as surface and groundwater from a hydrological perspective is concerning, more so the unpredictability and variability thereof.

The tracer tests yielded flow rates of 0.0104 – 1.42 m/day at steady state conditions and showed similar hydraulic behaviour compared to that of leaching under constant head with regards to the depth profile. The tracer data was fitted within a 90 % least squares fit value (Section 4.4.2), to evaluate the average pore-water velocity (v) and dispersion coefficient (D). The dispersivity (λ), an indication of how much the

introduced tracer strays from the path of the carrier fluid, was also calculated from this data.

As part of the investigation into the flow patterns through an ash dam, the horizontal and vertical flow rates were investigated, by evaluating the resistivity changes in the subsurface over the time of the geophysical survey at the site.

The background ERT survey indicates the presence of a shallow resistive layer overlying a conductive layer. These layers are interpreted to be the unsaturated ash at surface overlying saturated ash. The saturated ash appears to occur at a depth of between 2 m and 2.75 m below surface.

By considering the rate of brine injection, distance travelled by the brine plume and applying a modified Archie's law to the modelled resistivity values of model cells in the vicinity of the injection pit, the flow rates through the ash were estimated. The results of the survey show that horizontal flow through the ash dam strongly dominates over vertical flow.

The rate of brine injection allowed a crude estimate of the average flow rate through the ash with a value of approximately 0.20 m/day at late injection times at a distance of 1 m from the centre of the injection pit. The horizontal distances travelled by the brine plume were used to calculate an upper estimate for the average horizontal flow rate of between 0.70 and 1.1 m/day.

The modelled resistivities suggested that horizontal flow rates may vary between 0.07 and 0.13 m/day. Due to model errors this method was less successful in estimating the vertical flow rates. However, there are indications that the initial vertical flow rate was very high (> 0.70 m/day), but that it rapidly decreased over time, falling off to values of less than 0.03 m/day.

6.6 Matrix response to saturated solutions

There was a temporary increase in the permeated volume after injection, considerably more than the injected volume, once again confirming concentration gradient as a factor influencing the rate of flow. There is large amount of electrical potential variation in the top of the column where diffusion is lowest. The electrical signal also seems to register more rapidly at the deeper probes as the experiments continued, indicating the formation of preferential pathways throughout the column.

The concurrent increase in the concentration of other ions can also be seen prior to returning to background levels. Thus there are some instances where the observed increase in electro-conductivity is the result of ions other than that of the injected salt and confirms the acceleration of the leaching process.

The concentration of Ca and K is higher than the injected cation in the first experiment except for the NaCl tracer which was previously used and these elements are also native to the ash. The concentration of Ca systematically decreases although Ca and K become the predominant cation in the LiCl half concentration.

The successive interaction of the saturated solutions with the matrix thus strips it of Ca and K and adsorbs the cations from the injected salt to the matrix. These adsorbed cations are then again expelled from the matrix once a different cation passes through the matrix. The extent of adsorption and the rate of release of elements to the matrix may be influenced by the ionic charge as well as the atomic radii. Thus a tracer can only be used for transport parameter estimation if previously exposed to the system and should be monitored chemically instead of electrically when used on fly ash or soils with high cation exchange capacities.

6.7 Conceptual Model

By evaluating the results obtained from this study a conceptual understanding of the flow through a fly ash dam and the geochemical characteristics associated with it may be deduced.

When the ash is originally deposited at the disposal site, migration of the ponded co-disposal fluid will rapidly migrate vertically through the surface layer, after which it will mainly migrate horizontally through a multi-faceted structures formed by previously deposited ash. The fluid may then percolate through to seepage faces or be encapsulated in the matrix.

The encapsulated solutes may then lay dormant as perched water tables or saturated sections in wet months or form salt layers in the dryer moths. These salt layers may cause areas of increased permeability due to salt cracking. The salts may also increase the salt load of any additional fluid that passes it, whether it is from another deposition or rain water.

The layering of the subsurface zone or the lack thereof can play an important role in the hydraulic movement of water in the subsurface. The porosity of the medium can determine the absorption rate and transport through the medium. Considering only the porosity of a system, the movement will be much lower in fine grained media than in course media under saturated conditions. If preferential pathways exist, the infiltrating fluid will be transported to the surrounding environment at a significantly enhanced rate. Eventually those elements showing rapid release rates (Na, Cl and SO_4) will be exposed to the environment by reaching the regional water table or through the seepage faces.

The metal oxides and in particular CaO in the ash may react with ingressed CO_2 causing the formation of irregularly shaped carbonate and sulphates throughout the ash dam as dolomite and gypsum. These structures may then direct flow of those fluids of lower salinities. These carbonates are also susceptible to dissolution by fluids of high salinity, diminishing the buffering capacity of the ash. Considering the type and extend of no-flow boundaries and aquitards in an area can have a significant effect on the distribution of water and solutes in the subsurface.

Typically disposal sites are conceptualised in such a manner that the flow of water is assumed to be from the top to the bottom, with evaporation and return water systems removing excess water from the pond located on the structure of the dam or dump (Figure 6.1). However, there is a certain amount of uncertainty associated with this assumption since infiltration rates into the study waste disposal site presented does not seem to follow these general guidelines. Due to the layered structure of the dam and the particle size of fly ash, it is proposed that a heterogeneous system with high anisotropy would be expected.

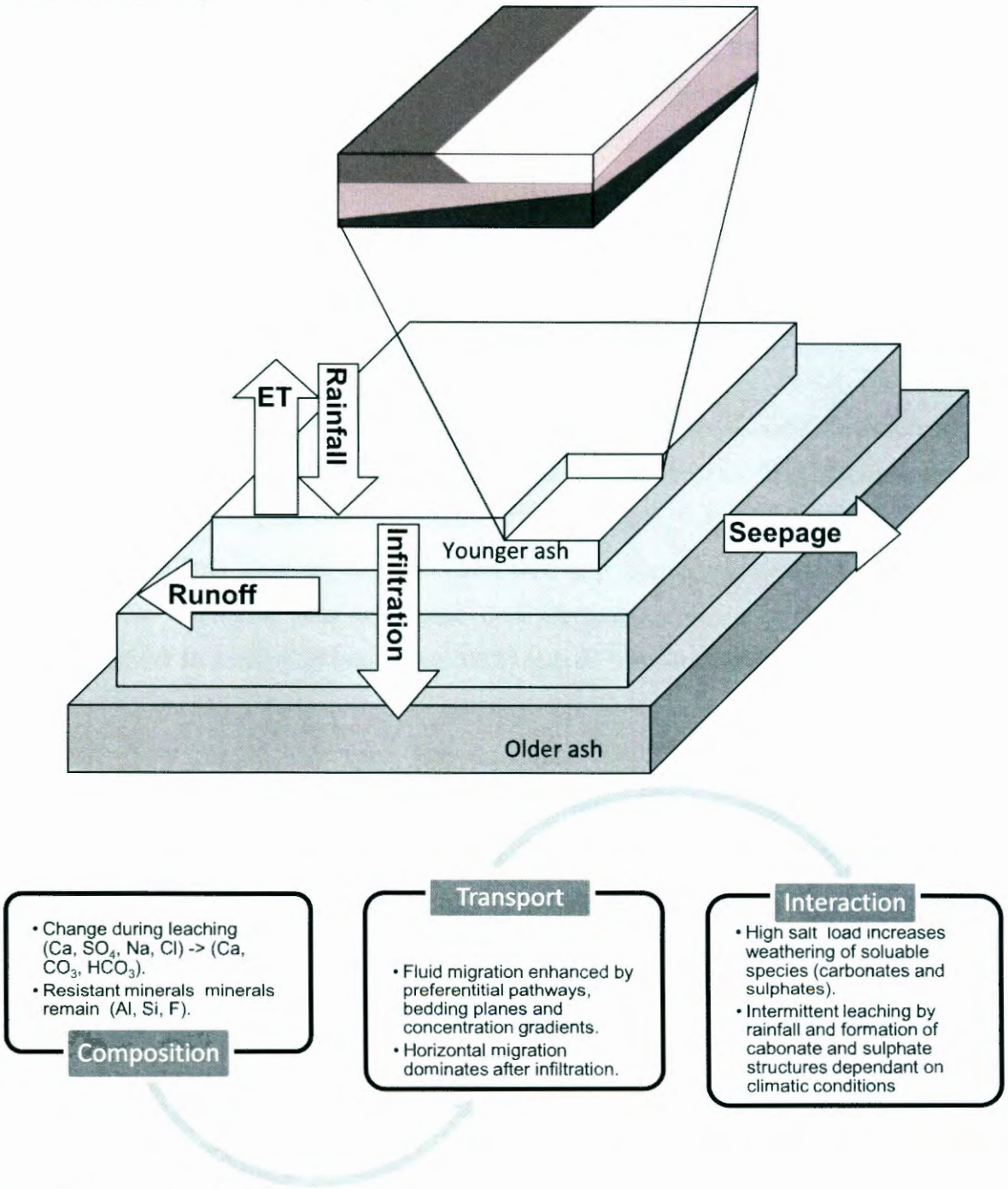

Figure 6.1 Conceptual model of site.

Opsomming

Vlieg as vorm deel van die verbranding oorblyfsels van minerale onsuiwerhede in steenkool en word tipies as 'n nat mengsel of droog gestort tydens die konstruksie van 'n steenkool as hoop of dam. Hierdie studie fokus hoofsaaklik op die ruimtelike en tydelike mobiliteit van elemente in 'n vlieg as hoop met die doel om logings eienskappe van verweerde as van 'n steenkool-stasie in die Mpumalanga Provinsie, Suid-Afrika te bepaal. Die vervoer van oplossings deur die heterogene medium is op laboratorium skaal deur sintetiese grondwater loging prosedure (SGLP) asook speurtoetse en op veld skaal deur tydsverloop elektriese weerstand tomografie (TEWT) geevalueer. Die vloeistof vervoer eienskappe en mobiliteit van geselekteerde elemente inheems aan die vlieg as word bespreek. Die chemiese en self potensiaal reaksie van die matriks op die versadigde oplossings van NaCl, KCl, LiCl, LiBr, KBr en NaBr word geevalueer om 'n konseptuele begrip te ontwikkel van die vloei deur die vlieg as dam en die geochemiese eienskappe wat daarmee gepaard gaan. Die geloogde oplossings word gevind om aanvanklik hoog wees in SO_4, Cl, Na en Ca. Die oplossings verander na 'n baie meer alkaliese en Ca-ryk samestelling soos loging voort gaan. Die aanvanklike bydrae van chloried (Cl^-) en natrium (Na^+) word vervang deur karbonate (HCO_3^-, CO_3^{2-}) en kalsium (Ca^{2+}). Onder die spoor elemente, kan F, Br, Al, Cr, Mo, Ba en Mn probleme inhou vir die omgewing, maar in besonder Li en B, wat die mees gekonsentreer in die dieper vlakke, naaste aan die watertafel aan getref word. Die speurtoetse lewer 'n vloei tempo van 0.010-1.42 m/dag by stabiele toestande op. Die TEWT opname toon dat horisontale vloei deur die dam sterk oorheers oor vertikale vloei. Die aanvanklike vertikale vloei tempo was baie hoog (> 0.70 m/dag), maar neem vinnig af met verloop van tyd, tot waardes minder as 0.03 m/dag. Die horisontale vloei van tussen 0.70 en 1,1 m / dag is geraam, hoewel die gemoduleerde weerstande voorstel dat die horisontale vloei tempo tussen 0.07 en 0.13 m/dag kan wissel. Die opeenvolgende interaksie van die versadigde oplossings met die matriks stroop dit van Ca asook K en adsorbeer die katione van die ingespuit sout aan die matriks. Die geadsorbeerde katione word dan weer vry gestel uit die matriks sodra 'n ander katioon deur die matriks geadsorbeer word. Speur toetse kan slegs gebruik word op vliegas of gronde met 'n hoë katioon uitruil kapasiteit, vir die beraming van vervoer eienskappe, mits dit voorheen aan die stelsel blootgestel word en moet chemies plaas van elektries gemonitor word. Die versadigde oplossings dui ook daarop dat konsentrasiegradiënt 'n belangrike rol in die migrasie van vloeistowwe in 'n stortings terein kan speel.